The effects of diagenetic overprint processes on the mineralogy and ultrastructure of biogenic calcium carbonates

vorgelegt von

Viola Julia Mages

Dissertation zur Erlangung des Grades
Doctor rerum naturalium

Ludwig-Maximlians-Universität
Fakultät für Geowissenschaften

München, 23.02.2021

Betreuer:	Prof. Dr. Wolfgang W. Schmahl
Erstgutachter:	Prof. Dr. Wolfgang W. Schmahl
Zweitgutachter:	Prof. Dr. Martin Dietzel
Promotionskommission:	Prof. Dr. Daniel Weidendorfer (Chairman) Prof. Dr. Wolfgang W. Schmahl Prof. Dr. Martin Dietzel Prof. Dr. Claudia Trepmann Prof. Dr. Bettina Reichenbacher Prof. Dr. Guntram Jordan
Tag der mündlichen Prüfung:	21.07.2021

für Hans Opa
für mich

Universitates studiorum sterquilina pulchra, in quae
quondam planta nobilis excrescit.
-Albert Einstein-

Hakuna matata
-Timon und Pumbaa-

Bald
-Viola Julia Mages-

Acknowledgements

Firstly of course, I want to say thanks to the *Deutsche Forschungsgesellschaft* (DFG) who generously sponsored this doctorate and hence enabled this immense learning curve. Also, my doctoral supervisor, Prof. Dr. Wolfgang W. Schmahl has to be thanked. Without him the project would not exist, and he aided to structure this work. Additionally the dean of the faculty of earth sciences, Prof. Dr. Ralf Ludwig, gave essential help.

Of course, my colleguages from the CHARON group project were a big part of this work, particularly my friend Dr. Dongmei Yu. They provided a lot of scientific insight and humor. Especially Prof. Dr. Adrian Immenhauser was an invaluable support and helped me out of many tight spots. For this I am truely very thankful.

My colleagues and the employees at the department of Earth Sciences of the LMU in Munich were of immeasurable value for this long time. We grew into a multi-cultural and funny group where advice could be asked on every topic. Thank you for this beautiful time, Dr. Xiaofei Yin, Dr. Martina Greiner, Dr. Mar Simonet Roda, Barbara Jäger, Stefanie Hoser, and Moritz Zenkert.

The essential foundation that helped me push through the many struggles was my family and friends. Especially my siblings, Dr. med. Laura Mages and Mr. Jonas Mages, provided support like no other, in particular in the last months of the doctorate. My parents, Dr. med. Valeria and Wolfgang Mages, always encouraged and enabled me to give everything on my course of education, archieve my highest performance possible. My friends, Dr. med. Sophie Riedemann, Khaing Sabai Mg, Thomas Freymüller, and Dr. Sebastian Zimmermann helped me to stay relatively sane. Not to be underestimated or even disregarded may be the strong emotional support of König Ludwig.

Abstract

This dissertation´s research is part of the DFG funded working group named CHARON, which is running since 2013, encompassing two phases with this work being part of the second phase. The aim of the CHARON working group is the collection of an extensive and diverse information pool on the diagenesis of calcium carbonates. The general goal was to make palaeoenvironmental reconstructions more precise and reliable.

The role of this subproject was the in-depth investigation of the individual steps of the diagenetic overprint process on calcium carbonate skeletal parts of biogenic origin. Along with XRD and AFM analyses, the most important method was electron backscatter diffraction (EBSD) coupled with scanning electron microscopy (SEM). This way comprehensive results on ultrastructure, mineralogy, crystallography, and textural features like the porosity, and the ultrastructure along with their alteration during diagenesis or the experimental hydrothermal treatments, respectively, were compiled.

For this, fossil material was utilized, as well as material which has been hydrothermally treated in a laboratory setting. The fossil material consisted of brachiopods from the extinct taxa *Afghanospirifer* sp., *Alispirifer middlemissi*, *Gigantoproductus* sp., *Gypospirifer* sp., *Hunzina electa*, *Terebratula scillae*, *Tetractinella trigonella*, *Trigonotreta larghii*, and *Trigonotreta lyonsensis*. The fossils originated from four geological basins: the Castell'Arquato Basin in northern Italy with a thermal gradient of up to 50 °C, the Pennine Basin in central northern England with a thermal gradient between 100 and 120 °C, the Lombardian Basin in northern Italy with a thermal gradient ranging from 150 to 200 °C, and the complex Karakoram Basin in the very north-east of Pakistan with a thermal gradient between 300 and 350 °C.

The recent materials that were utilized for the hydrothermal experiments were various extant marine organisms: the bivalves (mussels) *Aequipecten opercularis*, *Arctica islandica*, and *Mytilus edulis*, the sea snail *Haliotis ovina*, and the stony coral *Porites* sp.. Additionally, aragonitic as well as calcitic inorganic monocrystals were employed in the experiments. The experimental setup comprised one temperature of 175 °C, two alteration fluids: burial and meteoric, four time spans ranging from 4 to 28 days (pristine and, where available, fossil material has also been investigated), and the five different materials mentioned above.

Results from the naturally and laboratory altered samples reveal that the overprint process proceeds along a specific line of events, but presents small variances in the strength of the individual characteristics. All samples showed the sequence of 1) loss of the organic matter

leading to the formation of secondary porosity, enhancing the overall porosity, as well as mechanical disintegration along textural features, 2) amalgamation of singular ultrastructural units into larger clusters by merging and the adaptation of one common orientation, leading to the distortion of the characteristic shapes of the ultrastructural units into more rounded shapes while maintaining the existing mineralogy, and 3) nucleation of secondary calcite grains in the open cavital space and, with ongoing growth, the substitution of the pre-existing ultrastructure and mineralogy by secondary calcite.

The factors influencing the rapidity and strength of an overprint were determined and isolated. The external ones are the obvious ones, such as 1) the temperature or geothermal gradient. This naturally presents a positive correlation to the level of overprint. That means, the higher the temperature, the stronger the overprint. The same holds true for 2) the duration of the influence and the prevailing 3) pressure conditions: the longer the duration and the higher the pressure, the stronger the overprint. 4) The alteration fluid, through its contained inhibitors, influences the intensity of the dissolution and reprecipitation of the mineral matter. The influence of the internal factors is more complex. 5) The ultrastructure determines the amount and distribution of the organic matter as well as the mineralogy and interfacial energy. 6) The organic matter, through its disintegration, forms the network of the interconnected secondary porosity and determines the extent of the cavital space. 7) The porosity enables the percolation of the alteration fluid and presents open space for the nucleation of secondary calcite. 8) The mineralogy defines the solubility of the material and influences the extent and kinetics of the dissolution.

This research lies in the field of palaeoenvironmental reconstruction. This is primarily done with the aid of geochemical proxy carriers, such as the calcium carbonatic skeletal parts of the marine invertebrates investigated in this work. Such a geochemical proxy would, for example, be the oxygen isotopes. Measuring the ratio of the heavy ^{18}O isotope to the light ^{16}O isotope gives information on how much cryosphere, meaning ice matter, has been present at the time of life of the animal used for this hypothetical investigation. It is a common occurrence that during the formation of biogenic minerals, these minerals do not form in accordance with the environmental conditions surrounding the animal. This is made possible, because some animals can influence the conditions in the areas of growth at a small scale, so that phases that are metastable or instable can form regardless. This can only be upheld during the lifetime of the organism. But after the death of the organism, its sedimentation and through diagenesis comes an alteration of the skeletal hard parts. As will be shown in this dissertation, this alteration encompasses various processes of dissolution and reprecipitation. This leads to the ablation of primary, original matter and the addition of secondary, new material. With that the primary isotopes are exchanged by secondary isotopes and the measurements do not represent the isotopic signature of the time of life of the organism any more. As marine carbonates are most commonly used for palaeoenvironmental reconstructions, the findings of this research can, for example, be used to determine if and to which level the material at hand has been altered. The detailed investigations allow to pinpoint all specific occurrences individually for each area or ultrastructure. Furthermore, the specific reactions and susceptibilities of the various ultrastructures to develop certain features were worked out. These and further findings of this work allow to assess the suitability of the general material as well as specific areas of it as a geochemical proxy carrier.

Table of contents

1 Introduction

The research of this project was conducted as a subproject of the DFG funded group project called CHARON, standing for "marine **C**arbonate arc**H**ives: controls on c**AR**bonate precipitation and pathways of diagenetic alterati**ON**". At the time of this work, the CHARON project was in its second phase. Is was constituted of eight project groups from Germany, Austria, and Italy: Ruhr University Bochum (seat of coordinator Prof. Dr. Adrian Immenhauser and Dr. Chelsea Pederson), Graz University of Technology, Westphalian Wilhelms University in Münster, Ludwig-Maximilians University in Munich (location of this work), University of Milano, University Göttingen, and Helmholtz Centre for Ocean Reasearch (GEOMAR) in Kiel. Additionally, many further associate researchers were included in this group project (Ruhr-University Bochum 2020). It was a very interdisciplinary research group for a very interdisciplinary topic, covering the fields of geology, geobiology, palaeontology, mineralogy, crystallography, material science, and (isotope) geochemistry.

The general research aim of the CHARON project was to generate an information pool on marine carbonate archives filled with data from these different fields and to interconnect their output. The goal of CHARON was to make scientific studies and future prognoses on the evolution of the climate and the physio-chemical sphere of the earth´s continents and oceans more accurate and reliable.

There are many different kinds of marine carbonate archives. They can be of organic or inorganic origin. Organic calcium carbonates often utilized are the skeletons of marine organisms, such as the shells of brachiopods and bivalves, or the remains of stony corals for example in the form of reefs and build-ups which commonly occur in shallow water environments. Other carbonate accumulations that can be found in shallow water environments are sediments forming on the ocean floor through the build-up of particles (figure 1.1). Due to their frequency and versatility of occurrence in combination with the abundance of information they yield due to their role as „sink or source of carbon within the global carbon cycle", marine carbonates are one of the main elements in investigations and modellings that concern the function of the greenhouse gas CO_2 in connection with future global climate change (Schneider et al. 2006).

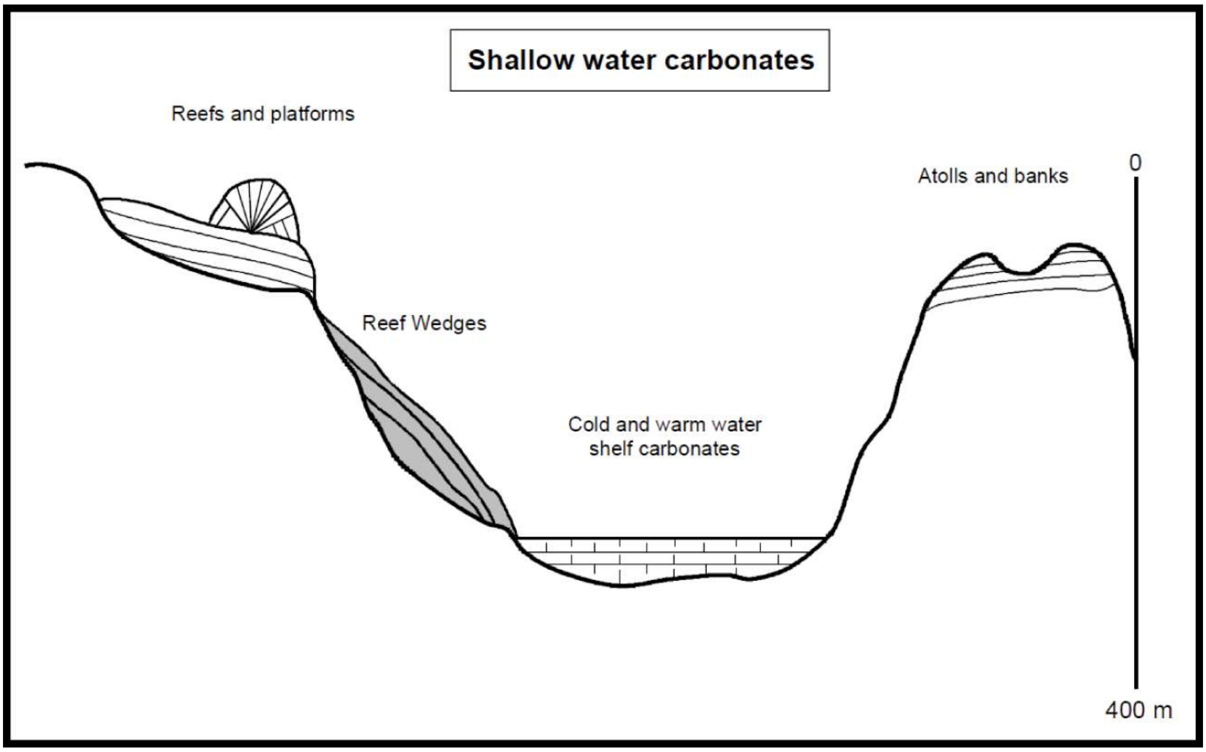

Figure 1.1: Schematic sketch of shallow water carbonates. Taken from Schneider et al. (2006) (slightly modified).

After their sedimentation, marine carbonates are being continuously altered through various environmental processes. Examples for such processes are compaction, elevated temperatures and elevated stress, change in chemical composition, and dissolution and reprecipitation induced by percolating fluids (i.g. Chapman 1987, Deming et al. 1990, Grotzinger et al. 2008, Krumbein 1942, Moore and Wade 2013, Serra 1986, Yamamoto et al. 2017). These processes manipulate the starting material, resulting in a corruption of the original isotope signals (Li et al. 2018, Tucker and Wright 1990). If not taken into account, the outcome of isotope analyses based on the marine carbonate archives are distorted and falsified. These alterations of the carbonate archives through the "overprint of environmental and metabolic signatures represents the single most significant obstacle in deep-time carbonate archive research" (Ruhr-University Bochum 2017).

Not enough research has been done on these influencing factors, so the CHARON working groups teamed up in this nearly decade long research to produce comprehensive data on different proxies, including geochemistry, fabrics, and mineralogy. This work is focussed on the fields of mineralogy, crystallography, and palaeontology.

More precisely, my part in this project is the assessment of diagenetic processes occurring in marine carbonatic skeletons. Thereby I examined fossil material from different provenances and basins with different ages and diagenetic histories. To get insight into the intermediate stages and for being able to assess the influence of various impact factors, I supplementary implemented laboratory based hydrothermal alterations on pristine materials. As a last step I set the results of the fossil and the laboratory altered materials into context with each other.

This assessment of the diagenetic overprint of fossil carbonatic hard tissues is the key to get insight into palaeoenvironmental dynamics. As mentioned above, the main hurdle that remains is the shift in the original isotope signatures through diagenesis. So in understanding the process of diagenetic overprint and in breaking it down into the intermediate stages, potentially previously made errors could be impeded and the precision could be enhanced.

1.1 Calcium carbonates

Although mostly only known as an undesired precipitate in the kitchen or bathroom by non-scientists, with more than 4 % in the earth´s crust – occurring as chalk, limestone, marble, marine sediments and biominerals – calcium carbonate constitutes one of the most important rock-forming minerals (Beck and Andreassen 20120, Sawada 1997). In their book Tucker and Wright (1990) give very comprehensive information on the general topic of carbonate sedimentology.

1.1.1 Polymorphs

Along with its abundance, calcium carbonate also possesses a wide variability of forms and characteristics: crystalline or amorphous, inorganically or organically grown, with a high content of substituting ions or very pure.

There are some crystallographically diverse forms, different minerals and mineraloids (amorphous mineral-like substance with no crystalline form) of the same elementary composition, termed polymorphs. In the case of calcium carbonate there are the three anhydrous minerals calcite, aragonite, and vaterite, as well as the mineraloid amorphous calcium carbonate, abbreviated ACC (Beck and Adreassen 2010).

Within the calcium carbonates, calcite is the most common representative found in nature (Lippmann 1973, Reeder 2018, Smyth and Ahrens 1997), due to the fact that it is the one polymorph stable at ambient conditions on the earth´s surface (Casella et al. 2017, Casella 2018, Frisia-Bruni and Wenk 1985, Kawano et al. 2009, Plummer and Bisenberg 1982, Radha and Navrotsky 2013). Calcite is an anhydrous calcium carbonate and has a rhombohedral unit cell, hence it is sorted into the trigonal crystal system (Tucker and Wright 1990). It has a density of 2.71 g/cm^3 (Northwood and Lewis 1968) and a solubility product of -8.48 at 25 °C (Sawada 1997, for detailed investigations see Ogino et al. 1987, and Plummer and Busenberg 1982). Calcite containing more than several mole % $MgCO_3$ (the separation line is not specified, but often set at 4 mole %) are assigned to the magnesian calcites (Tucker and Wright 1990). In marine environments many calcitic materials like calcareous skeletons and cements are build out of magnesian calcite. Investigations of modern marine skeletons and cements containing magnesian calcite present clear evidence for a positive correlation between the Mg content and the ambient temperature at the time of formation. However, data exists pointing likewise to a correlation of the Mg content in the forming calcite and the concentration of CO_3^{2-} in the surrounding seawater. Hence, thoughtful contemplation has to be applied when analyzing and interpreting these complex systems (Tucker and Wright 1990).

Aragonite is the anhydrous calcium carbonate polymorph stable at high pressure conditions and can be found in most marine cements (Frisia-Bruni and Wenk 1985). It also is a commonly known mineral built by organisms like bivalves, gastropods, or corals, formed through biomineralization (Frisia-Bruni and Wenk 1985). Aragonite is orthorhombic and has a density of 2.93 g/cm^3 (Northwood and Lewis 1968) and a solubility product of -8.34 at 25 °C (Sawada 1997).

A very rare anhydrous polymorph is vaterite. It can be formed through hydrothermal synthesis (Mukkamala et al. 2006, Zhang and Lin 2004), but also through biomimetic mineralization by bacteria (Rodriguez-Navarro et al. 2007, Xu et al. 2006). In this latter context it occurs within gallstones and kidney stones (Lee and Chen 2009, Sutor and Wooley 1968). Vaterite is hexagonal (Kamhi 1963, Xu et al. 2006), has a density of 2.56 g/cm^3 (Northwood and Lewis 1968) and a solubility product of -7.91 at 25 °C (Ogino et al. 1987).

Amorphous calcium carbonate, abbreviated ACC, is “isotropic in polarized light and does not diffract X-rays” and is hence described as amorphous (Addadi et al. 2003). Consequently, it is a very energetically unfavourable material and is “inherently unstable and relatively soluble in its pure state” (Weiner et al. 2003). However, there are different kinds of ACC. It can be inorganically or organically formed, and the most curious kinds are within the biogenic ACC. They can possess a “short-range order” and thereby become stable (Addadi et al. 2003, Weiner et al. 2003). Quite recently it has also been found that some organisms produce a “transient amorphous calcium carbonate phase” when forming their calcified skeletons (Wang et al. 2009, see also Aizenberg et al. 1996, Beniash et al. 1997, Ma et al. 2008, Politi et al. 2004, Politi et al. 2008, Raz et al. 2000, Weiss et al. 2002).

As already mentioned briefly, there are further polymorphs of calcium carbonate. Besides the anhydrous polymorphs there are various hydrous polymorphs, such as monohydrocalcite and ikaite (calcium carbonate hexahydrate) (Addadi et al. 2003). But for they are irrelevant for this work, they are disregarded herein.

1.1.2 Biogenic calcium carbonatic skeletons of marine organisms

The classical occurrences of these materials are hard parts of marine invertebrates, such as bivalves, gastropods, stony corals, or brachiopods. These hard parts are comprised of calcite and/or aragonite in various ultrastructures. After their time of life, the organisms sink onto the ocean ground and get buried during sedimentation. Following, they undergo the geological processes of subduction, diagenesis, and the re-emerging through orogenesis or another tectonic process. The material now presents an altered condition.

Biogenic carbonates have been utilized as high resolution archives for a very long time (e.g. Angiolini et al. 2011, Johnson et al. 2009, Schöne et al. 2005). They occur in strata at many localities all over the world, hiding within the stories of past times and past places. In their structures, such as growth lines in brachiopods, the organisms record the ambient conditions of the ancient oceans (Compston 1960, Grossman et al. 1993, Popp et al. 1986, Parkinson and Cusack 2007) through the "primary seawater isotope composition" (Angiolini et al. 2011). However, the information in the altered material needs to be decoded by considering the events and circumstances the pristine material went through since the time of death of the organism. For that it is inevitable to immerse oneself into the specifics of diagenesis.

1.2 Diagenesis

Diagenesis is one of the essential geological processes. It entails all processes after sedimentation that lead from a loose sediment to a solid rock (Grotzinger et al. 2008, Tucker and Wright 1990). Some occurring processes are compaction through the weight of overlying material or plate tectonics and mineralogical or chemical changes through the influence of fluid or ambient conditions such as heightened pressure and temperature. So diagenesis entails not only physical, but also chemical processes. Hence it leads to changes in the signatures of trace elements and isotopes (Tucker and Wright 1990).

Dissolution and reprecipitation processes during diagenesis follow the path to minimal Gibbs free energy under the current conditions (Altree-Williams et al. 2015, Casella 2018, Milke et al. 2013, Nakamura and Watson 2001, Putnis and Ruíz-Agudo 2013, Serra 1986). These processes are interactions between the solid mineral phase and the fluid phase. After the dissolution of the pre-existing mineral phase in contact with the fluid it becomes supersaturated with regard to the thermodynamically stable phase under the prevalent conditions, which leads to the nucleation of the new mineral phase onto the surface of the pre-existing mineral phase (Casella 2018, Dove and Hochella 1993, Giuffre et al. 2015, Lüttge and Arvidson 2010, Palmer and Wilson 2004, Pina et al. 1998, Ruíz-Agudo and Putnis 2012, Ruíz-Agudo et al. 2012, Ruíz-Agudo et al. 2014). These overprint processes (for in-depth discussion see chapter 5) lead to a falsification of the original isotope signature (Casella 2018, Li et al. 2018, Tucker and Wright 1990).

The end of diagenesis comes either with the elevation of the rock stratum to the earth´s surface, or, if the influencing parameters (e.g. temperature, pressure) are even more elevated, the process of diagenesis transacts to the process of metamorphosis (Tucker and Wright 1990). There is no strictly defined line between diagenesis and metamorphosis; the transition is fluent. However, while the fossil materials of this research all show the typical signs of diagenetic overprint, the defining characteristics of metamorphosis can not be found in the sample material of this research.

1.2.1 Carbonate diagenesis

Naturally, for the diagenesis of carbonatic material specifically the same conditions apply as described in the last chapter. However, carbonate minerals are known to be more susceptive to diagenetic alterations, such as dissolution, recrystallization, or replacement reactions, than other minerals (Boggs and Boggs 2009). Still it is important at this point to make the separation between geologic carbonates and biogenic carbonates. Geologic carbonates refer to strata made up of a carbonatic rock matrix, while biogenic carbonates are organically formed hard parts of organisms that are trapped in a rock matrix.

Geologic carbonate sediments are “intrabasinal deposits” (Boggs and Boggs 2009) and are largely formed in marine environments. They are comprised of comparably few main minerals: aragonite, calcite, and dolomite. At the time of their deposition these inorganic carbonate minerals stand in chemical equilibrium with the ambient fluids. There are specific diagenetic processes of carbonatic sediments that exhibit some substantial differences to other materials, such as siliclastic sediments. Also within the carbonate diagenesis itself differences can be found: often non-marine carbonate sediments are more resistant to the diagenetic alteration, because they are build up of the more stable low-magnesium calcite (Boggs and Boggs 2009). Talking about diagenesis of geologic carbonates it is important to mention the substitution of the original Ca^{2+} cation. In the course of dissolution-reprecipitation reactions during diagenetic alteration the original cation can be exchanged by Fe^{2+}, Mg^{2+}, Mn^{2+}, Na^{2+}, Pb^{2+}, Sr^{2+}, Zn^{2+} etc. that have been transported by the alteration fluid. The ions stand in complex correlations to each other, affecting the partition coefficient between the mineral phase and the solution (Bodine et al. 1965, Brand and Veizer 1980, Brand and Veizer 1981, Burke et al. 1982, Ichikuni 1973, Kinsman 1969, Peterman et al. 1970, Pingitore et al. 1988, Schroeder 1969). For example, some ions act as inhibitors that form a complex at the mineral surface in areas where dissolution would preferably take place (Arvidson et al. 2006, Brand 1994, Compton and Brown 1994, Lahann 1978, Morse 1983, Reddy and Wang 1980, Vinson et al. 2007). With the exchange of ions comes a change of the initial chemical imprint that is utilized for palaeoenvironmental reconstructions (Abdolmaleki and Tavakoli 2016, Finch et al. 2001, Fürsich et al. 2005). Apart from the fluid chemistry, the mineral phase is another important factor. Metastable mineral phases like aragonite or high-magnesium calcite react more easily to diagenetic alteration and transform into the thermodynamically stable low-magnesium calcite (Bathurst 1975, Bennett et al. 2011, Brand and Veizer 1980, Brand and Veizer 1981, James and Jones 2015, Land 1967, Morse 2003).

Biogenic carbonates are the main focus of this work for they are the working material comprised of fossil and recent skeletal parts of marine organisms. This material has been utilized very frequently for palaeoenvironmental reconstructions in fascinating detail, mostly by using chemical and isotopic signatures (Bauwens et al. 2009, Campbell et al. 2002, Frei et al. 2011, Frimmel 2009, Grossman et al. 1993, Guo et al. 2019, Khim et al. 2000a, Khim et al. 2000b, Rozanski et al. 1997). For example, it is possible to get insight into the seasonality through the growth increments of a bivalve (Poitevin et al. 2019, Schöne et al. 2005). During the formation process of the biogenic skeletal parts, the organisms are able to create tissue that is not in thermodynamic equilibrium with its surroundings. After death and enhanced through the prevalent conditions during diagenesis these metastable and instable phases are being transferred into an “inorganic equilibrium” through the formation of a phase that is thermodynamically stable under current conditions (Casella et al. 2017). In hydrothermal alteration experiments, mimicking natural diagenesis, it has been found that this replacement of the biogenic material by secondary calcite occurs at temperatures of roughly 175 °C and above in presence of burial fluid within the short time span of the experiments (Casella et al. 2017, Ritter et al. 2017). For this reason, all experiments of this work were carried out at this temperature (details see chapter 2.2). Furthermore, multiple experiments showed that the mineralogy and texture of the biogenic materials affect the course of the alteration. Possible factors for this are the surface area that is exposed to the alteration fluid, or the amount of organic matrices (Anderson et al. 1973, Casella et al. 2018a, Casella et al. 2018b, Perrin and Smith 2007). Of course, also within the biogenic carbonates the chemical and isotopic signatures become substituted in the course of dissolution-reprecipitation reactions and biogenic material becomes substituted by inorganic secondary calcite (Grossman et al. 1993, Immenhauser et al. 2005, Immenhauser et al. 2015, Korte et al. 2005, Müller et al. 2001, Pederson et al. 2019a, Pederson et al. 2019b, Richardson et al. 2001, Ritter et al. 2017).

1.2.2 Varying impact factors

The progression of diagenesis is determined by some various factors, such as temperature, pressure, material, time, and fluid chemistry. Obviously, all these factors are strongly determined by the geological setting and greatly interact with each other.

The temperature frames the borders of diagenesis and separates it from the subsequent metamorphosis. Obviously the temperature stands in positive correlation to the level of alteration. It is closely linked to the depth and the pressure conditions that prevail. And although the heat flow within sedimentary basins is generally governed by conduction, the fluid also plays an important role for it transports the heat (and dissolved material) through the masses (Bjørlykke 1994).

The mineralogy and texture of the material is another important factor. It encompasses features like porosity and grain size, which are impacting the dissolution process. One important feature for this work is the porosity. While compaction due to burial leads to a decrease in porosity, disintegration of the organic matter and dissolution result in an increase in porosity (Tucker and Wright 1990). The porosity and scope of fractures determine the permeability of the material and hence have a strong impact on the diagenetic alteration for it consequently also determines the flux of the pore water (Bjørlykke 1994).

It has been found that different textures react differently when altered under the same conditions (Casella 2018). For the mineralogical and crystallographic changes during alteration are determined by the pursue of equilibrium, the difference of solubility and density of the materials have a great influence. The discussion (chapter 5) gives detailed information on the different effects of diagenetic alteration on different ultrastructures of the material used in this work.

A complicated factor is time. Of course it is one of the main factors, but can not be reproduced by the scientists in laboratory experiments that aim to mimic the conditions occurring during natural diagenesis. After all, the geological time frames of hundreds of millions of years transcend the lifespan of any human, and most likely humanity itself, by a multitude. Still, as this work and many more before show, all stages of carbonate diagenesis up to the substitution of the pre-existing mineral matter by secondary calcite can be reproduced in experiments pending one month of duration (Casella 2018, see also chapter 4 within this work).

However, a factor that can easily be regulated by the scientists in the experiments is the fluid chemistry. The contained ions strongly determine the path of dissolution-reprecipitation processes, for it affects the equilibrium that the material strives for. In regards to the fluid three different diagenetic environments can be distinguished in the natural realm: marine, meteoric (near-surface), and burial. One could name a fourth diagenetic environment, which would be the mixing zone of marine and meteoric fluids (figure 1.2) (James and Jones 2015, Tucker and Wright 1990). Logically, diagenesis with marine pore fluid happens at the seafloor and immediately below. If the depositional region is close to the surface or shore, it can get from a marine to a meteoric diagenetic environment shortly after deposition; e.g. through being transported to a supratidal flat through a storm, or through the tides or the shift of the shore line (Tucker and Wright 1990). The presence of meteoric pore water leads to the dissolution of biominerals like aragonite and high-magnesium calcite for it is under-saturated with regard to these minerals, and it will cause the precipitation of low-magnesium calcite in return (Bjørlykke 1994). Although meteoric diagenesis generally takes place in near-surface realms like continental planes it also appears in greater depths in proximity to aquifers with a "strong hydraulic head and recharge descending into the deep subsurface" (Tucker and Wright 1990). The burial environment is a quite complex system and not easily understood. The burial realm starts underneath the meteoric realm in depths of ten to several thousand meters (Tucker and Wright 1990).

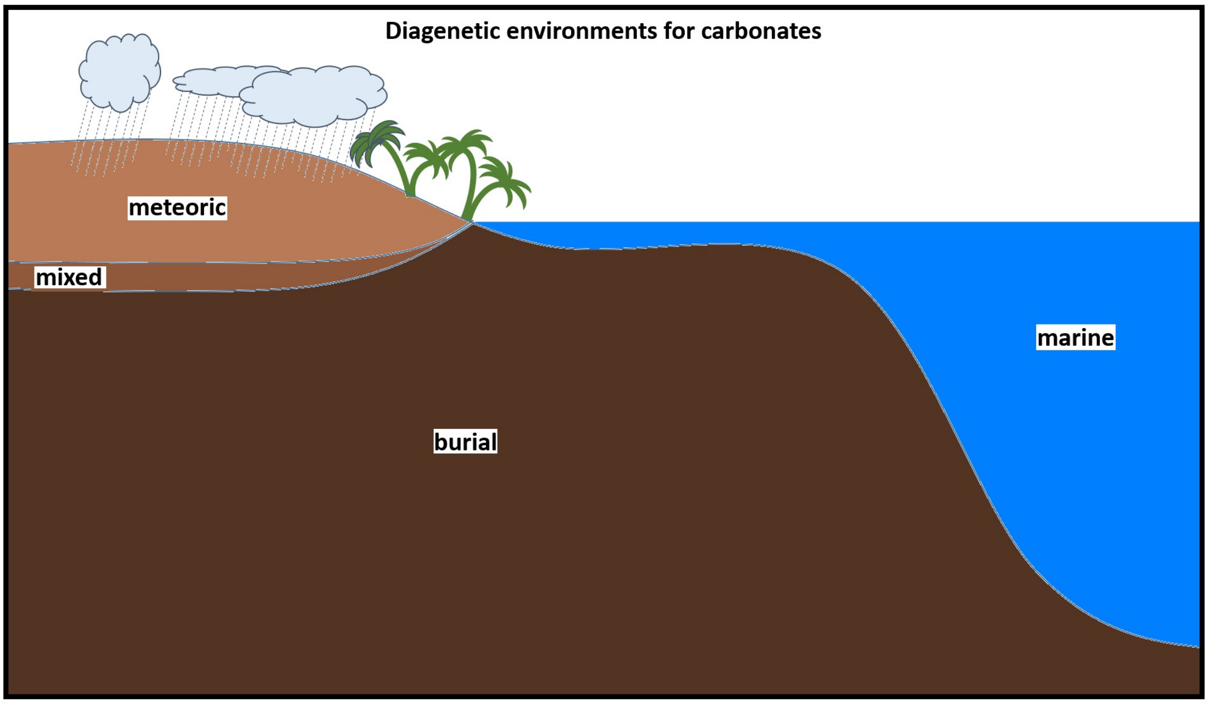

Figure 1.2: Schematic sketch of the diagenetic environments for carbonates. Created after James and Jones (2015).

1.3 Geological basins

There are different kinds of geological processes, which form different kinds of geological basins; a geological basin simply defined by being a depression in the earth´s crust where material congregates. Their sizes vary greatly, ranging from the large oceans' basins, like the Pacific basin, to small ponds. Among earth scientists, the term "sedimentary basin" is generally applied to basins with a scale of more than 100 kilometres and for which formation a "significant crustal deformation" was necessary (Helwig 1985). This definition of a basin is referred to in this work. Such depressions often act as a deposit for marine organisms after their death, which is also the beginning of the process of overprint for these organisms (see chapter 1.2.1).

There are different approaches when it comes to basin classification, and the most plausible definition comes from Helwig (1985): "A sedimentary basin is a domain of regional subsidence that can be characterized in space, time, and sedimentary fill". Helwig (1985) summarized and analyzed the older concepts and introduced a new classification. He reviews that the older suggestions (e.g. Klemme 1980, St. John et al. 1984) use too few and often not relevant characteristics. For instance, the one developed by Bally and Snelson (1980) "focus[es] [only] on the broader tectonic setting", while Kingston et al. (1983) only "focus on basin form and complex history". So Helwig proposed a characterization of sedimentary basins, based not only or mainly on plate tectonics, but simultaneously on the mechanisms of subsidence. In this "genetic (process) characterization" only the relevant features of sedimentary basins, which formed during the development of the basin, are identified. These would incorporate the form and fill of a basin, but also age, mechanics, and tectonics. Firstly, he organizes the basins into two types, determined by their shape: normal faulted "rift basins" with a "symmetrical, concave upward" shape, and thrust faulted "flextural basins" with an "asymmetrical, wedge-shape". Rift basins result from extensional stretching and thinning processes within the lithosphere. They can accumulate a maximal sedimentary load of 15 kilometres. This is limited due to the rifting of lithosphere creating oceanic crust which, under isostatic sediment loading, can sink to this deepness of roughly 15 kilometres. The thermal regime within a rift basin shows increasing heat flux directly proportional to the scope of the extension (McKenzie 1978). One example for the occurrence of rift basins are divergent plate boundaries. The second type of sedimentary basins, the flextural basin, results from the lithosphere being pushed down from a heavy load as a consequence of a compressional tectonic setting (Price 1973). Here, the maximal thickness of the accumulated sedimentary layer can rise up to several ten kilometres, which is determined by the material and the properties of the lithosphere (Beaumont et al. 1982). Flextural basins show no significant change in thermal regime. An example of the occurrence of flextural basins are convergent plate boundaries (Helwig 1985). In their comprehensive textbook “Basin Analysis: Principles and Application” Allen and Allen (2005) also applied this segmentation into “basins due to lithospheric stretching” and “basins due to flexure”.

The idea that basins are affected by a variety of geological events, not only one, was firstly introduced by Kingston et al. (1983), only shortly before Helwig´s publication. A much more modern approach for basin classification, from the 2000s, is by categorization of the basin-forming phases that are represented in so-called tectonostratigraphic megasequences, or TSMs. These TSMs are a rough segmentation of the sediment layers, each representing a different basin-forming geological process. The beginning and the end of each TSM, as well as the segmentation between them, is defined by unconformities (Hubbard et al. 1985, Roberts and Bally 2012). This seems a very good approach, because it considers the most variables and provides the most information on the basin, compared to other approaches. In his short review on basin classification Roberts (2012) described the details, in which the preferred approach of the use of TSMs exceeds other approaches, while also shedding light on the complexity of basin formation. Some of the elements of the TSM approach affecting only temperatures and palaeotemperatures in sedimentary basins are “variations in thermal conductivity, internal heat generation by radioactive decay and chemical reactions, convective / advective heat transfer within sediments, and surface temperature changes” (Allen and Allen 2005). It is the prevailing opinion among scientists that, as yet, there is no method that manages to considers all the influencing factors (Allen and Allen 2005, Roberts 2012). As Helwig (1985) put it: “Tectonic classification of basins is fraught with conceptual pitfalls, burdened with semantics, and crippled by the variety and complexity of basins”, but the “correct classification is fundamental for understanding basin history, constructing predictive models of basin development, and evaluating hydrocarbon potential”.

For the means of this work, it was no main objective to fully characterize each basin. It was, however, very important to ascertain specific details during the active phase of the basin as well as the following uplift during orogenesis: age, thermal gradient, and stress / strain. These values were directly compared to each other and helped to evaluate the features found in the fossils. Rock rheology was also an important feature, but for it is comparably similar within all basins of this work and hence was not of sufficient relevance, it was disregarded in the discussion.

One method to recalculate the maximal temperatures arisen within a basin is through the determination of thermal maturity by means of vitrinite reflectance, an optical parameter. It uses the predictability of the reaction of the reflectance of vitrinite to temperature (see Burnham and Sweeny 1989, Lopatin 1971, Sweeny and Burnham 1990). This technique is an old (popular guidances date back to Bostick and Alpern 1977, Bostick 1979, Dow and O´Connor 1982, Hunt 1979, Stach et al. 1982, Tissot and Welte 1984, and van Gijzel 1982) but still a very common method amongst the organic indicators. When plotted versus the depth, it can even function as a thermochronometer, giving the shift of temperature with time as well as the maximal palaeotemperature. Other renowned thermochronological methods are apatite fission track analysis and the diffusion of helium whilst U-Th decay (Allen and Allen 2005).

2 Materials and methods

2.1 Materials

There were two different types of specimens adduced for this study. Firstly, there were extant and recent species of a coral, a sea snail, and three bivalves, that were investigated in pristine and altered condition, and, if available, fossil condition. For basic comparison also inorganic aragonite and calcite monocrystals were altered and investigated. In the following these samples are combined into the alteration series project. Secondly, fossil brachiopod samples were taken from different geological basins; in the following referred to as fossil project. All fossil taxa are extinct and therefore have no extant comparison material. All taxa, from the alteration project as well as the fossil project, lived in solely marine environments. The following tables 2.1 and 2.2 list the specimen and the applied analytical methods in an overview.

Table 2.1: Overview of analytical methods applied on the materials of the alteration series project. Digits give the number of data sets acquired for the respective method.

alteration fluid	specimen (taxonomy)	condition (alteration duration)	XRD	AFM	SEM	EBSD	EDX
marine	*Arctica islandica*	pristine	1	18	-	-	-
		4 days	1	-	19	3	2
		7 days	1	30	18	-	-
		14 days	1	17	11	2	-
		28 days	1	-	9	1	-
		fossil	-	2	16	2	-
	Mytilus edulis	pristine	1	-	12	-	-
		4 days	1	23	35	8	1
		7 days	1	33	8	2	2
		14 days	1	24	4	4	-
		28 days	1	-	7	2	-
	Haliotis ovina	pristine	1	-	4	-	-
		4 days	1	24	37	2	-
		7 days	1	39	4	2	-
		14 days	1	118	13	3	-
		28 days	1	-	20	10	-
	Haliotis tuberculata	fossil	1	-	18	8	7
	Porites sp.	pristine	-	-	-	-	-
		4 days	1	10	17	2	2
		7 days	1	6	5	-	-
		14 days	1	9	12	3	-
		28 days	1	-	28	2	-
	Porites pusilla	fossil	1	-	4	2	1
	inorganic aragonite	28 days	1	-	7	1	1
	inorganic calcite		1	-	8	1	1
burial	inorganic aragonite		1	-	6	2	1
	inorganic calcite		1	-	3	1	1
	Aequipecten opercularis	pristine	1	-	29	8	-
		4 days	1	33	13	-	-
		7 days	1	16	-	1	-
		14 days	1	74	4	1	-
		28 days	3	-	29	3	-
		fossil	1	-	32	2	-

Table 2.2: Overview of analytical methods applied on the materials of the fossil project. Digits give the number of data sets acquired for the respective method.

sedimentary basin	thermal gradient	specimen (taxonomy)		specimen number	SEM	EBSD	EDX
Castell'Arquato Basin	up to 50 °C	*Terebratula scillae*		V14b	2	3	-
Pennine Basin	100 – 120 °C	*Gigantoproductus* sp.		V2b	4	2	-
Lombardian Basin	150 – 200 °C	*Tetractinella trigonella*		V1a	2	2	-
Karakoram Basin	300 – 350 °C	Baroghil Pass, Lashkargaz Formation	*Hunzina electa*	V3a1	2	2	-
			Hunzina electa	V6a	6	1	1
		Karambar Pass, Gircha Formation	*Trigonotreta lyonsensis*	V41	17	1	-
		Chapursan Valley, Gircha Formation	*Trigonotreta lyonsensis*	V47	8	2	-
			Trigonotreta larghii	V49	24	7	-
		Karambar Pass, Twin Valleys Section	*Gypospirifer* sp.	V42	5	5	-
			Afghanospirifer sp.	V46	14	3	-
		Lashkargaz Gulley	*Alispirifer* cf. *middlemissi*	V50	13	2	-

2.1.1 Alteration series project

The compilation of the recent specimen comprises eight different aragonitic and calcitic ultrastructures (acicular araognite, prismatic aragonite, cross-lamellar aragonite, fibrous calcite, foliated calcite), including three different layers of nacre: sheet nacre, columnar nacre, and nacre in brick-and-mortar arrangement. With this the most commonly used ultrastructures utilized for palaeoecological research are covered.

2.1.1.1 *Aequipecten opercularis*

The bivalve *Aequipecten opercularis* (Linnaeus 1758) (figure 2.1) belongs to the family Pectinidae. Since the Miocene, approximately 20.43 Ma ago, the species exists in the northeast Atlantic as a "facultatively mobile epifaunal suspension feeder" (Dhond 1971, Linnaeus 1758, Marquet and Dijkstra 2000, Wood 1848, Woodring 1982, recorded in the Paleobiology Database Fossilworks, accessed 13.03.2019).

The shell consists predominantly of foliated calcite, while aragonite can only be found on the shell inside in areas of muscle insertions and in thin layers within the pallial line showing a crossed lamellar microstructure (Checa et al. 2007). The foliated calcitic ultrastructure is made up of interlacing mineral units with a gradiently shifting inner orientation. These calcite grains have a great variation in size and shape, but the crystallographic orientation is quite alike. At the interface to the aragonitic layer on the inside, the calcite is arranged in thin elongate mineral units of very small size.

The specimens were collected by and received from Prof. Dr. Antonio Checa, working at the University of Granada, Spain. The valves had a size of approximately 4 x 4 cm and originated from adult specimens. The pieces that were cut out and utilized in the experiments were from different specimen, but the same section in the middle of each respective shell, where the aragonite layer of the muscle insertions was present.

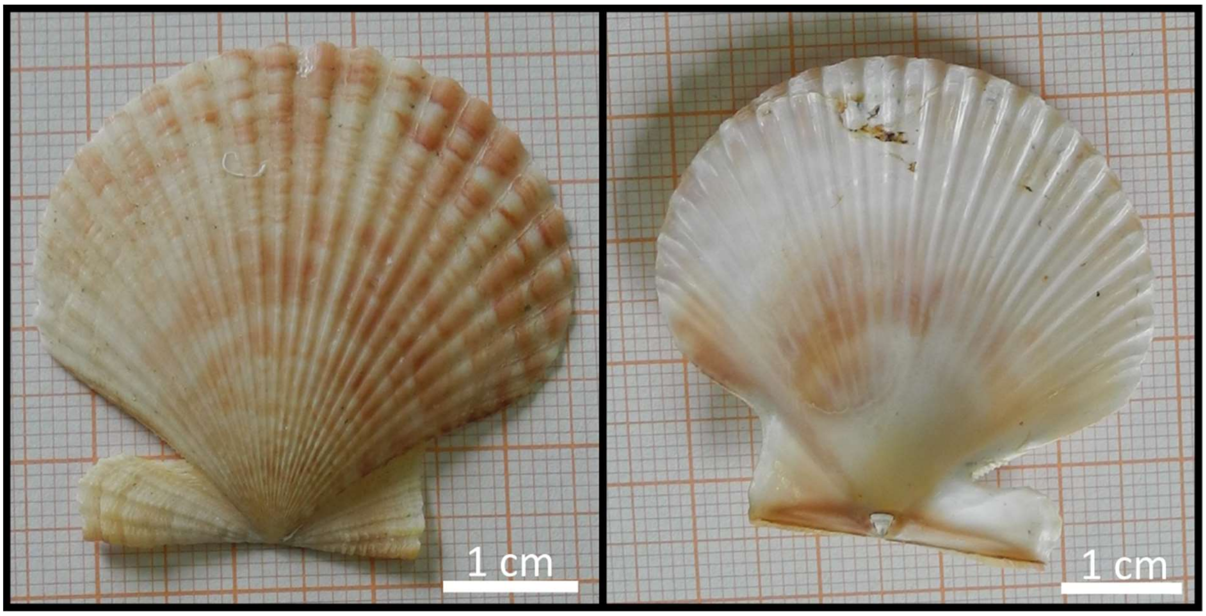

Figure 2.1: Overview of pristine *Aequipecten opercularis* (own material).

2.1.1.2 *Arctica islandica*

Arctica islandica (Linnaeus 1767) (figure 2.2), belonging to the family Arcticidae of the bivalves, is a very widely spread species, distributed from the coasts of North America to the Baltic sea. The species emerged 28.4 Ma ago and lives as a "facultatively mobile infaunal suspension feeder" (Woods 1848, recorded in the Paleobiology Database Fossilworks, accessed 13.03.2019).

Arctica islandica shows only one type of ultrastructure, that is comprised of cross-lamellar aragonitic mineral units of varying sizes containing a high organic content (Casella et al. 2017, Greiner et al. 2018).

The material from this species was collected from Loch Etive waters in Scotland and from a fishing company in northern Iceland. All pristine and altered pieces were cut from two large valves with the size of approximately 10 x 10 cm. It was seen to that the individual pieces were cut in closest possible proximity to ensure maximal comparability.

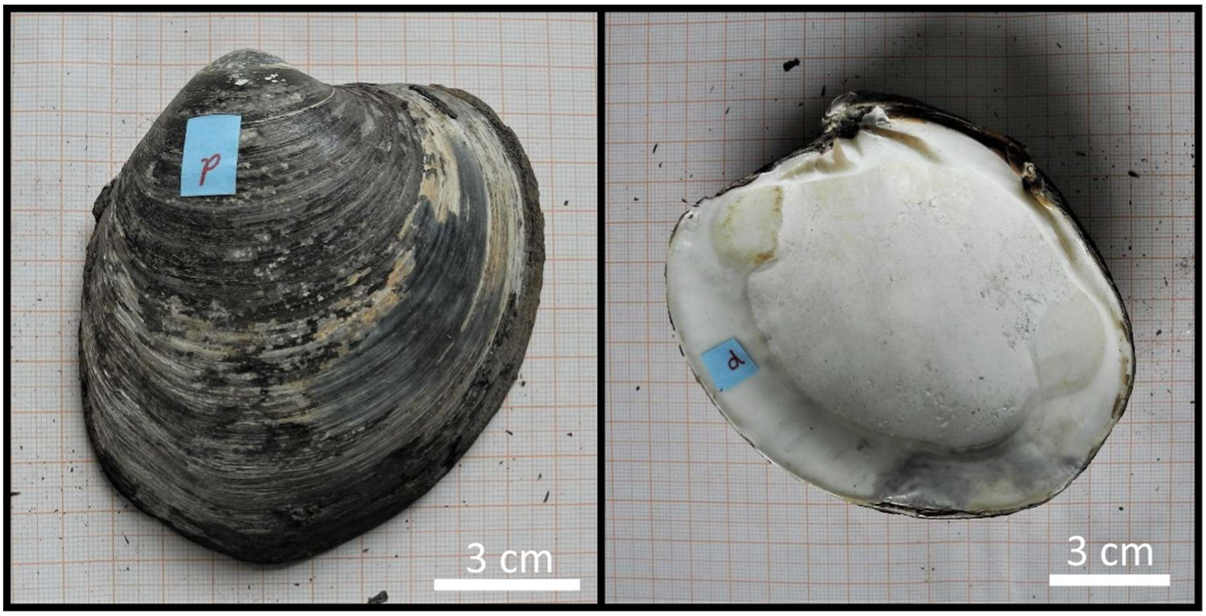

Figure 2.2: Overview of pristine *Arctica islandica* (own material).

2.1.1.3 *Haliotis ovina*

The only gastropod investigated in this research, *Haliotis ovina* (Gmelin 1791) (figure 2.3), belongs to the family Haliotidae (Gmelin 1791, recorded in World Register of Marine Species WoRMS). It lives as an "epifaunal grazer" in environments such as reefs, buildups, or bioherms (Ladd 1966, Short and Potter 1987, Wilson et al. 1993, recorded in the Paleobiology Database Fossilworks, accessed 18.03.2019).

Haliotis ovina shows two ultrastructural units. Towards the outside of the shell lies a layer of aragonite prisms that are enclosed by a network of biopolymer fibrils. Towards the inside of the shell a layer of columnar nacre tablets can be found.

This specimen was collected at the reef flat of Heron Island in Queensland, Australia. All pristine and altered material was cut from one shell that had the approximate size of 3,5 x 5 cm. To get portions that are as similar as possible, the pieces were cut close together from the middle portion of the shell.

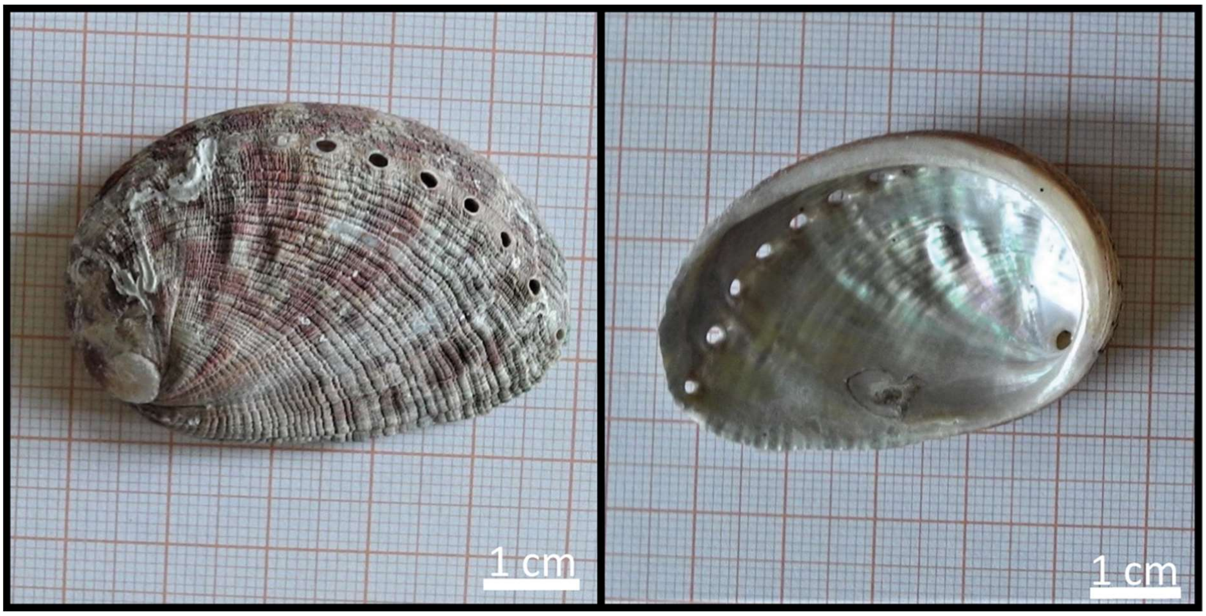

Figure 2.3: Overview of pristine *Haliotis ovina* (own material).

2.1.1.4 *Mytilus edulis*

The bivalve *Mytilus edulis* (Linnaeus 1758) (figure 2.4) belongs to the family of the Mytilidae. It lives as a "stationary epifaunal suspension feeder" in shallow subtidal marine environments such as coastal reefs, buildups, or bioherms (Coan et al. 2012, Hertlein und Grant 1972, Kafanov 2003, Richards 1962, Wood 1848, recorded in the Paleobiology Database Fossilworks, accessed 18.03.2019).

The mineralogy of this species shows two different layers. The outer layer is build up of calcite fibres, while the inner layer consists of aragonitic nacre tablets, which are compiled in a brick-and-mortar arrangement. In this type of nacre, the tablets are slightly thicker than in columnar nacre, which can for example be found in *Haliotis ovina* (Casella et al. 2018a, Travis 1968).

The bulk of *Mytilus edulis* specimen was collected from the subtidal zone of the Menai Strait, that separates the island Anglesey from mainland Wales, UK. The pieces of the different alteration experiments were cut from the same portions of different, but very similarly sized adult valves. One valve was utilized for one alteration experiment. The portion that was cut out was always the same middle portion, where there was minimal curvature of the shell (in contrast to the area at the umbo), and where not only one ultrastructure was present as it is the case in the proximity of the commissure.

Figure 2.4: Overview of pristine *Mytilus edulis* (own material).

2.1.1.5 *Porites* sp.

The genus *Porites* (Link 1807) (figure 2.5) emerged 55.8 Ma ago and is extant to this day. It is the only coral that has been investigated in this work. The samples taken for the alteration series and utilized as pristine comparison material are of unknown species. The fossil reference material belongs to the species *Porites pusilla.* This fossil species lived from 23.03 to 13.65 Ma ago. The genus *Porites* belongs to the family of the Poritidae, which comprises roughly 200 different species. *Porites* lives as a "stationary intermediate-level epifaunal photosymbiotic-suspension feeder" in solely marine environments, such as shallow subtidal reefs or buildups (López-Pérez 2005, Sepkoski 2002, recorded in the Paleobiology Database Fossilworks, accessed 18.06.2020). For more information of the macro-scale growth pattern of this genus and more see the publication of Richmond (1997).

Porites sp. is a scleractinian coral (stony coral), comprising solely aragonitic material in the form of an acicular ultrastructure. On a microscopic scale one sees radially arranged bundles of aragonite needles with scattered small and round cavities (centres of calcification) (Perrin and Smith 2007).

The utilized *Porites* sp. material originated from one specimen, depicted below (figure 2.5). This piece is a roughly 70 years old coral, collected at Moorea, which lies approximately 17 kilometres northwest of Tahiti in French Polynesia.

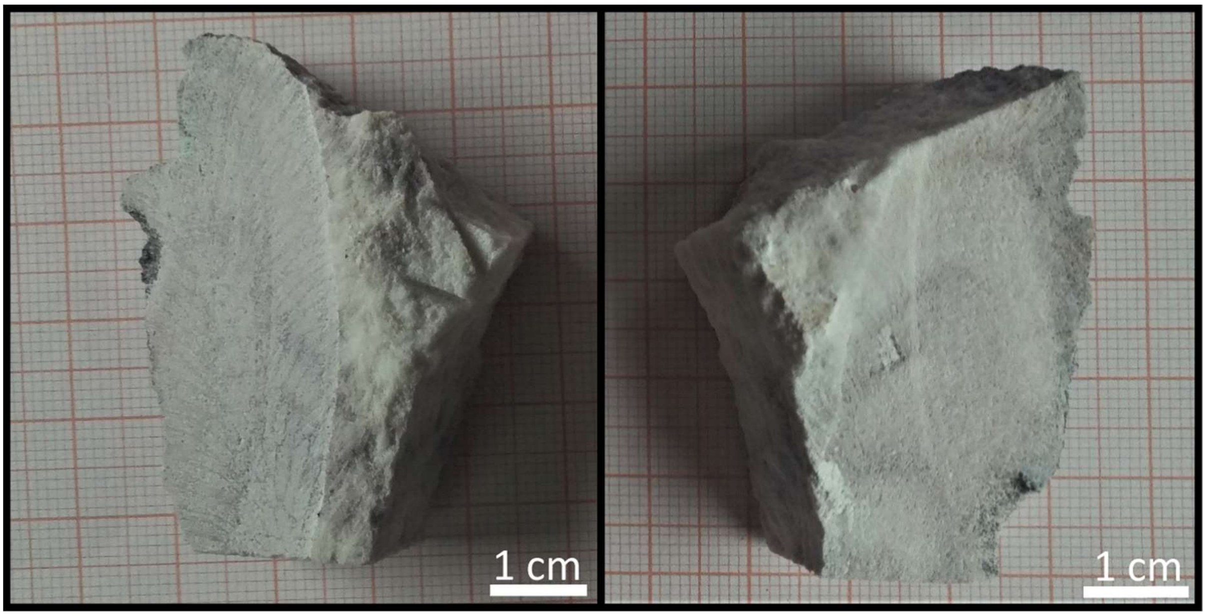

Figure 2.5: Overview of pristine *Porites* sp. (own material).

2.1.1.6 Inorganic monocrystals

The pristine and altered specimens from the inorganic materials (figure 2.6) originated from one respective aragonite and calcite monocrystal. The crystals had a size of 1 x 2 cm each and were split up along the respective slip-plane for the various alteration experiments. The materials originate from the collection of the museum *Reich der Kristalle*, which is situated in the same building where this work was carried out, belonging to the Ludwig-Maximilians University.

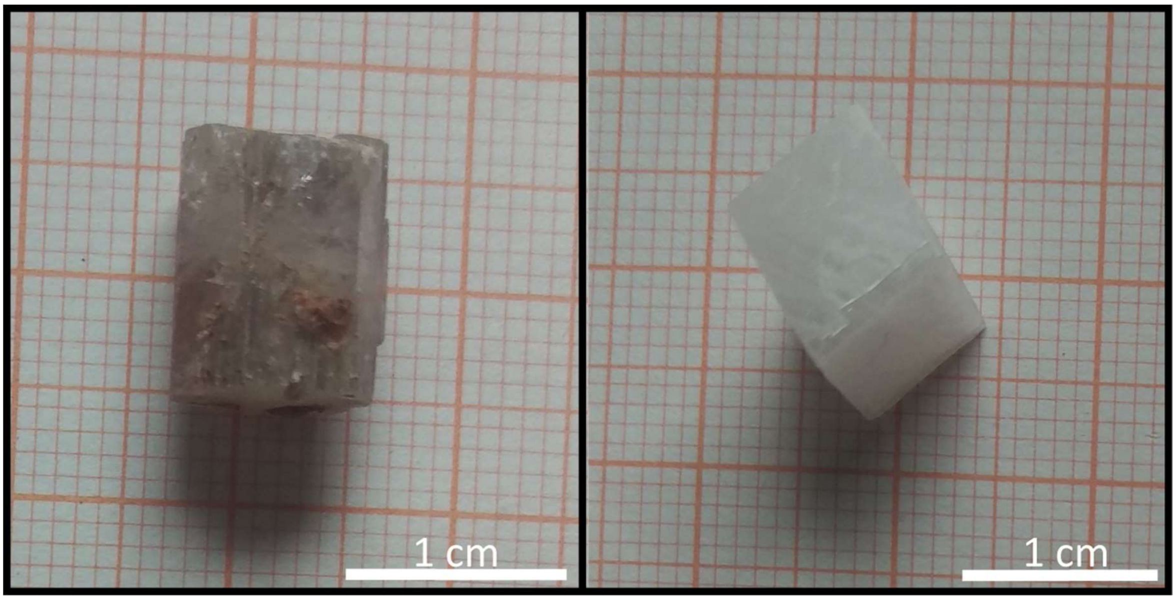

Figure 2.6: Overview of pristine samples of the inorganic comparison material. Left side shows aragonite monocrystal, right side shows calcite monocrystal.

2.1.2 Fossil project

The specimens of the fossil project are all to be characterized as belonging to the phylum of brachiopoda. All specimens were living exclusively in marine environments and had exclusively calcitic shell material comprised of a primary, fibrous, and / or columnar layer. It is also to note that all taxa of the fossil project are extinct. All materials examined in this project were carefully selected from the palaeontological collection of the University of Milano with the kind help of Prof. Dr. Lucia Angiolini. For an overview of the fossil material and the applied methods see table 2.2 above).

2.1.2.1 *Afghanospirifer* sp.

The genus *Afghanospirifer* (figure 2.7) of the family Spiriferidae was firstly characterized by Plodowski in 1968. It emerged 318.1 Ma ago and became extinct 314.6 Ma ago. *Afghanospirifer* lived as a “stationary epifaunal suspension feeder” (Sepkoski 2002, Williams et al. 2006, recorded in the Paleobiology Database Fossilworks, accessed 29.06.2020).

The samples that were investigated for this work showed a thick columnar layer and a thinner fibrous layer. The external characters were illustrated and described in great detail by Angioini et al. (1999): The genus *Afghanospirifer* has a “biconvex shell with a subrectangular outline, hinge with slightly less than maximum width, cardinal extremities rounded, anterior commissure uniplicate. ventral valve with shallow ‘V’ shaped median sulcus, ventral interarea triangular with vertical traces of denticulations, dorsal valve with low fastigium, ornamentation of large bifurcating costae on entire valve surface, costae number about 13-14 each flank, sulcus ornamented by one central rib and two lateral ones, dorsal fastigium ornamented by 3-4 ribs, microornamentation of growth lamellae, when observable. dimensions width 34-47 length 23-29”.

The locality of origin for these samples lies in the Twin Valleys Section (bed L35) at Karambar Pass of the Karakoram Basin in northern Pakistan. These specimens are Bashkirian (Carboniferous) of age.

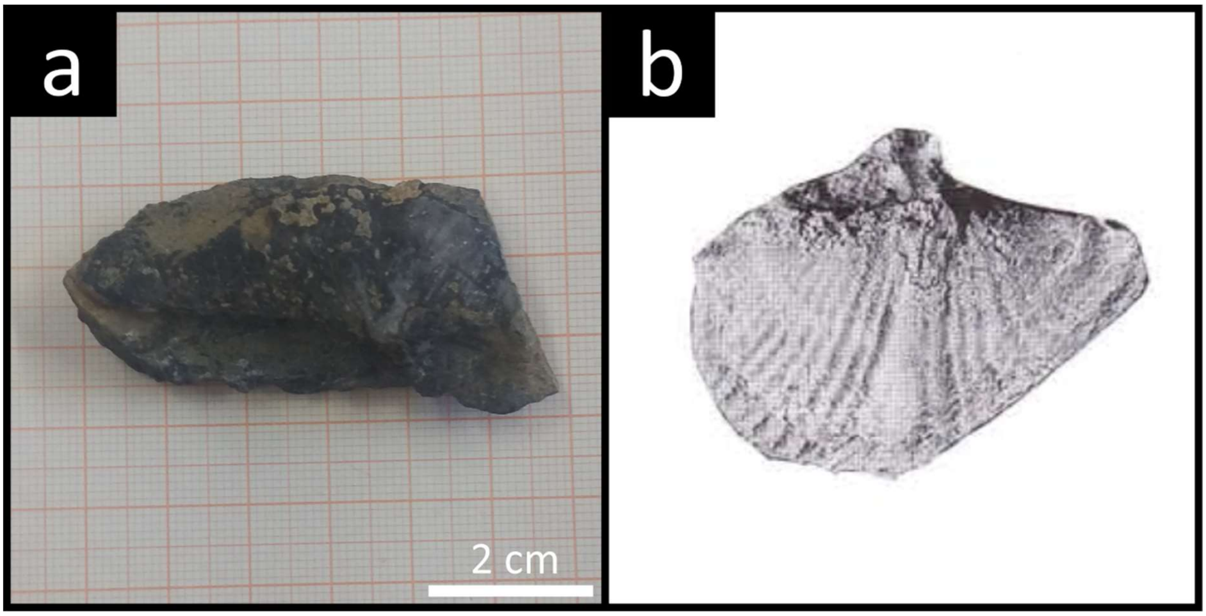

Figure 2.7: Overview of fossil *Afghanospirifer* sp.. a) shows own material, b) shows graphic of a complete valve from Angiolini et al. (1999).

2.1.2.2 *Alispirifer* cf. *middlemissi*

The species *Alispirifer* cf. *middlemissi* belongs to the family of the Strophopleuridae (Sepkoski 2002, Williams et al. 2006, recorded in the Mineralienatlas, accessed 30.04.2020). It was firstly characterized by Diener in 1915, but reattributed to the genus *Alispirifer* by Angiolini et al. (1999). The genus *Alispirifer* lived in the timeframe of 345.3 to 306.95 Ma ago as a "stationary epifaunal suspension feeder" in lagoonal and deep subtidal shelf regions (Sepkoski 2002, Waterhouse 2004, Williams et al. 2006, recorded in the Paleobiology Database Fossilworks, accessed 29.06.2020).

This species has a "biconvex shell with transverse outline" with the "maximum width at the hinge". The ventral valve has a "'V' shaped shallow sulcus ornamented by three ribs". The dorsal valve has a "low fastigium, rounded on top, widening anteriorly, bearing 2 finer ribs on its flanks". It has a "ornamentation of simple rounded costae, numbering at least 7 on each flank and dense growth lamellae". The microornamentation is "finely capillate" (Angiolini et al. 1999).

The bulk sample of this species came from two localities of the Karakoram Basin in northern Pakistan. Locality one is the Lupsuk Formation at the Lashkargaz Gulley (bed L42 to 12; locality at 4450 m above sea level). Locality two lies in the Twin Valleys Section of the Karambar Pass (beds L26 and L30). These localities were dated Moscovian to Kasimovian (Carboniferous).

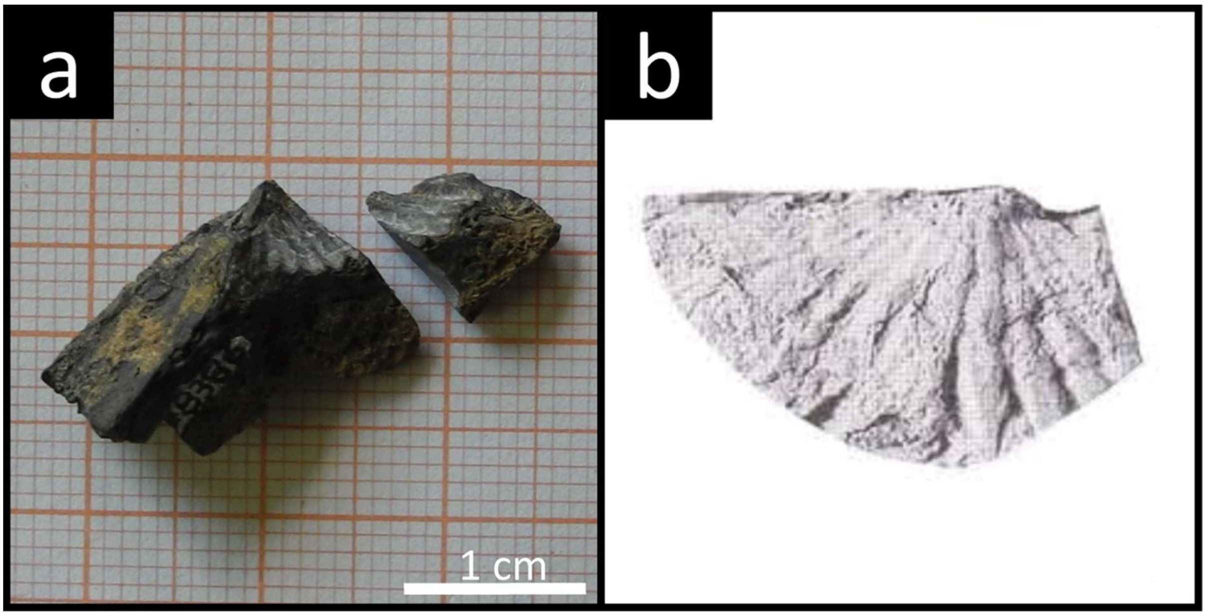

Figure 2.7: Overview of fossil Alispirifer cf. middlemissi. a) shows own material, b) shows graphic from Angiolini et al. (1999).

2.1.2.3 *Gigantoproductus* sp.

The genus *Gigantoproductus*, firstly described by Sepkoski (2002), is part of the family Monticuliferidae. *Gigantoproductus* lived from 339.4 to 318.1 Ma ago as a "stationary low-level epifaunal suspension feeder" (Sepkoski 2002, recorded in the Paleobiology Database Fossilworks, accessed 29.06.2020; recorded in the Mineralienatlas, accessed 01.05.2020).

As the taxonomic name strongly suggests, this species distinguishes itself by its unusually large size. The preserved ultrastructural units found in the material of this work are the columnar layer, which takes up a major part of the preserved shell thickness, and a thinner primary layer.

The locality of origin for the six specimen received for this work, is the Once-a-week quarry, situated in the Pennine Basin, Peak District of Derbyshire, UK. It was picked from the Eyam Limestone Formation which is aged Early Carboniferous.

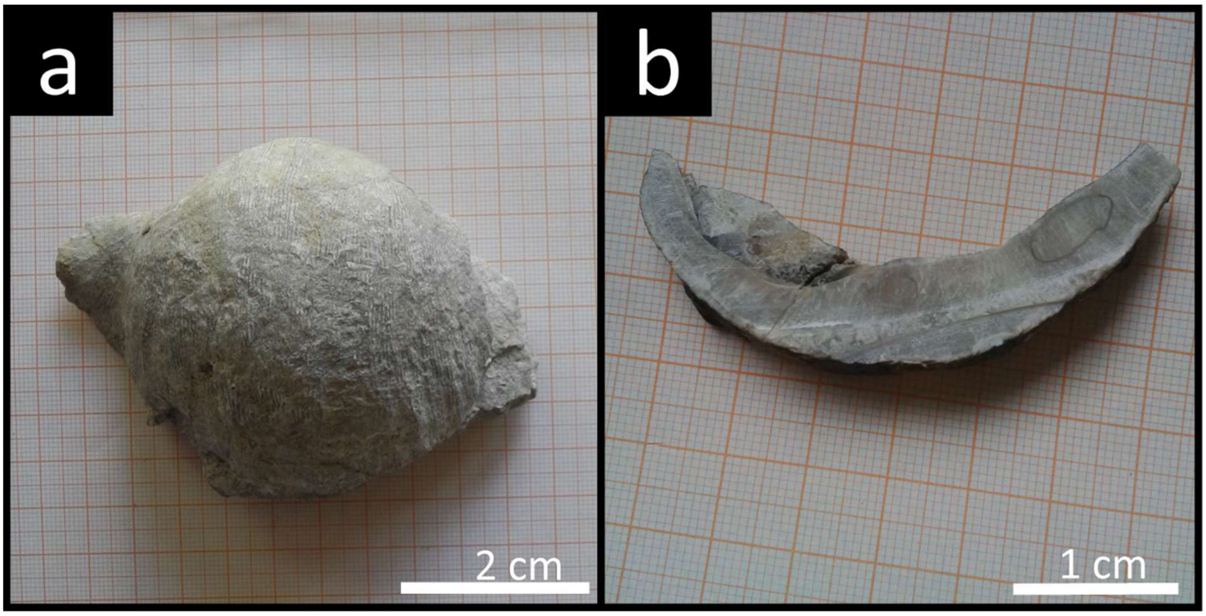

Figure 2.9: Overview of fossil *Gigantoproductus*. a) shows left complete valve of *Gigantoproductus elongatus* (not investigated, own material), b) shows cut sample of *Gigantoproductus* sp. that has been investigated in this work.

2.1.2.4 *Gypospirifer* sp.

The genus *Gypospirifer* belongs to the family of the Trigonotretidae and was firstly described by Cooper and Grant in 1976. It lived from 314.6 to 254.0 Ma ago as a “stationary epifaunal suspension feeder” in subtidal reefs, buildups or bioherms (Sepkoski 2002, Waterhouse 2004, recorded in the Paleobiology Database Fossilworks, accessed 16.04.2020).

The specimen examined herein preserved only one ultrastructure, a columnar layer. For a very detailed description of specimen from the same locality see page 18 of Angiolini et al. (1999).

The specimen was collected at the Twin Valleys Section of the Karambar Pass in the Karakoram Basin in northern Pakistan, and is aged Bashkirian (Carboniferous).

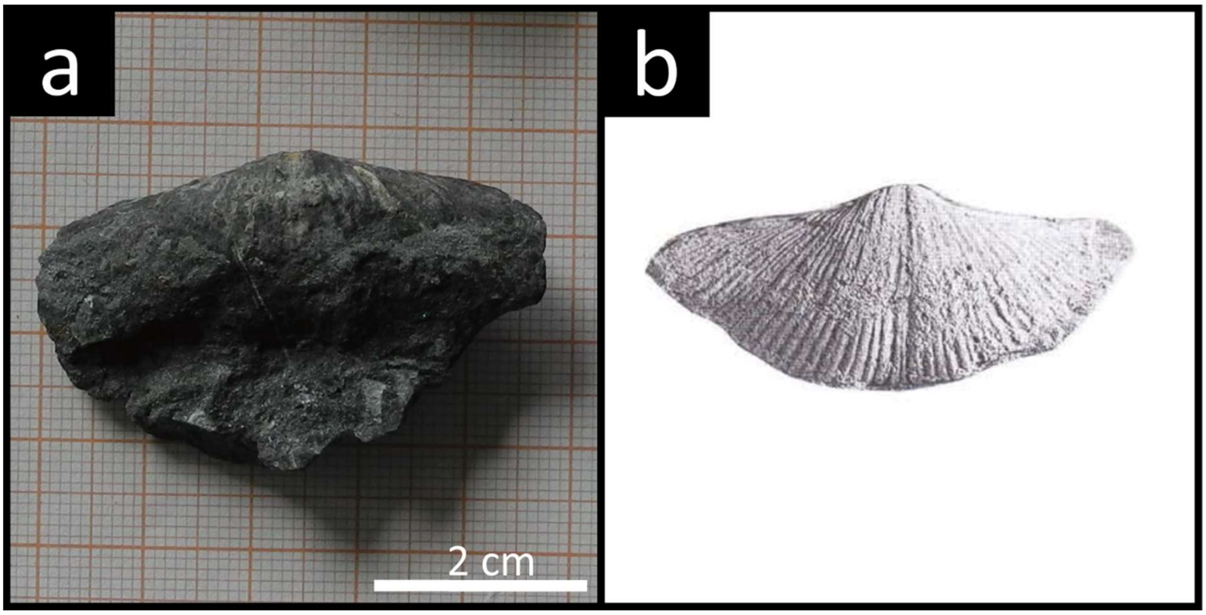

Figure 2.10: Overview of fossil *Gypospirifer* sp.. a) shows own material, b) shows material from Angiolini et al. (1999).

2.1.2.5 *Hunzina electa*

Hunzina electa is a species that was firstly described by Angiolini in 1995. It belongs to the family Spiriferellidae. The age range lies between 295.0 and 290.1 Ma ago. It lived as a "stationary epifaunal suspension feeder" in the open shallow subtidal region (Angiolini 1995, Waterhouse 2004, recorded in the Paleobiology Database Fossilworks, accessed 29.06.2020).

The specimen from this work show a thicker columnar layer and a thinner fibrous layer. In the original description of the species Angiolini (1995) gives the characteristics as follows: "biconvex shell, with elongate oval outline. cardinal extremities rounded, anterior commissure uniplicate with high fold. ventral valve strongly convex with thickened shell in the posterior region. umbo pointed. dorsal valve less convex with oval to sub-rounded outline. ornamentation of ventral valve of 5-6 rounded costae on each flank, ornamentation of dorsal valve of costae irregularly bifurcating, forming bundles of 3 costae each".

The specimen used in this work comes from the same locality as the type specimen, which is the Lashkargaz Formation of the Baroghil Pass, belonging to the Karakoram Basin in the Karakoram range in northern Pakistan. The material is dated back to the Sakmarian (Early Permian).

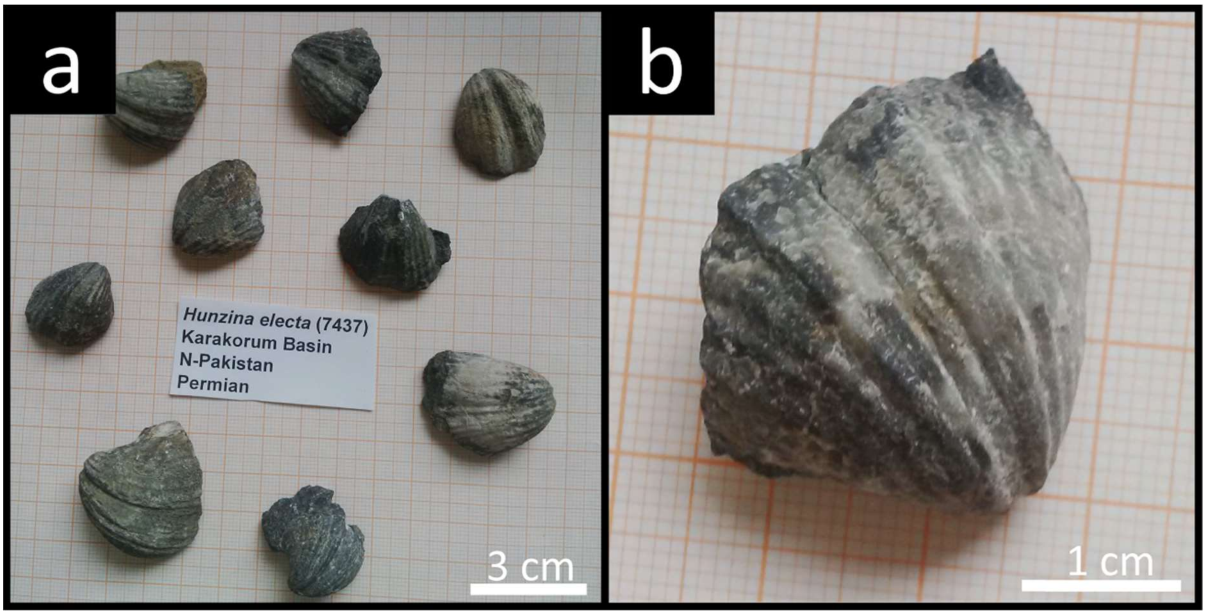

Figure 2.11: Overview of fossil *Hunzina electa*. a) shows bulk of own material, b) shows analyzed specimen V6a.

2.1.2.6 *Terebratula scillae*

The species *Terebratula scillae* (Segeunza 1871) is ranked under the family of the Terebratulidae (Gray 1840). The species was firstly introduced by Segeunza in 1871, but it was newly classified as belonging to the genus *Terebratula* by E. Taddei Ruggiero and R. Taddei in 2006. Although extinct, it lived not long ago from 1.806 to 0.781 Ma ago in basinal and offshore terrain (Gaetani and Sacca 1985, recorded in the Paleobiology Database Fossilworks, accessed 16.04.2020).

In this work´s specimen solely a fibrous ultrastructure with punctae could be found. In the research of Dr. Gaia Crippa (University of Milano) a primary layer was found additionally to the fibrous ultrastructure.

The material was collected from the Castell'Arquato Formation close to the Stirone River, lying in the Castell'Arquato Basin in the Paleo-Adriatic region in northern Italy. The designated age is the Early Pleistocene (Quaternary).

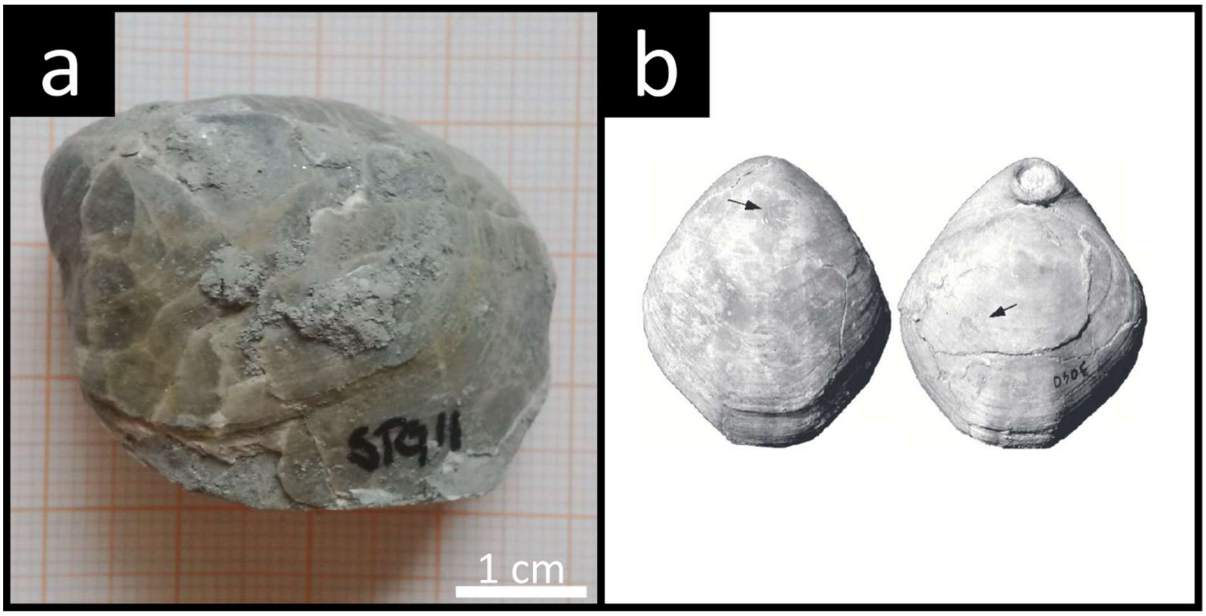

Figure 2.12: Overview of fossil *Terebratula scillae*. a) shows own material, b) shows a graphic from Ruggiero and Annunziata (2002) (the arrows are irrelevant for this work).

2.1.2.7 *Tetractinella trigonella*

This species, *Tetractinella trigonella*, firstly introduced by Schlotheim (1820), belongs to the family Diplospirellidae. The species lived from 242.0 to 235.0 Ma ago. They lived as "stationary low-level epifaunal suspension feeder" in reefs of the shallow subtidal terrain (Bittner 1890, Iordan 1993, Mantovani 2002, Palfy 2003, Torti and Angiolini 1997, recorded in the Paleobiology Database Fossilworks, accessed 29.06.2020).

Angiolini (1993) could not observe a primary layer, but found a thin secondary layer consisting of "orthodoxly stacked fibres, subparallel to the surface of the valve, which show [a] flattened keel and saddle shape in transverse section". Likewise, in the material of this work only a fibrous ultrastructure was found. For a very detailed description see Mantovani (2002).

The stratum the material originates from is the Calcare di Angolo Formation. It was collected at Valle dell'Acqua Fredda, in the Lombardian Basin, located in Lombardy, Southern Alps, northern Italy. The samples are dated back to the Anisian stage (Middle Triassic).

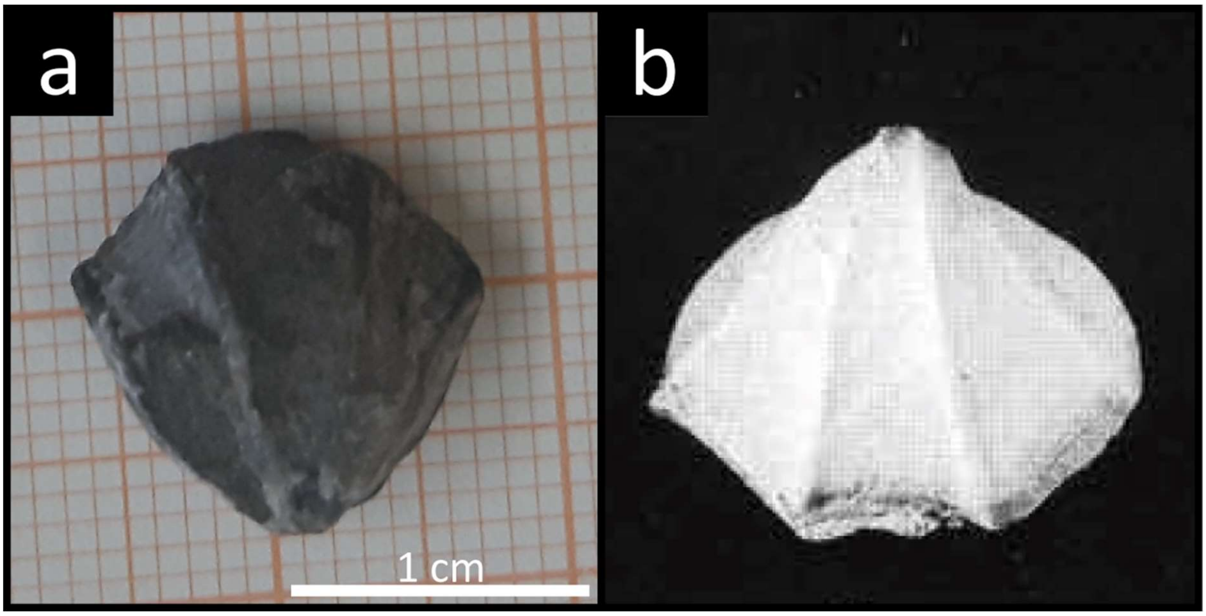

Figure 2.13: Overview of fossil *Tetractinella trigonella*. a) shows own material, b) shows graphic from Mantovani (2002).

2.1.2.8 *Trigonotreta larghii*

The species *Trigonotreta larghii* (Angiolini et al. 2005) belongs to the family Trigonotretidae. The animals of this genus lived as "stationary epifaunal suspension feeder" in shallow subtidal reefs, buildups, or bioherms. The age range for this species was 298.9 to 295.0 Ma ago (Angiolini et al. 2005, recorded in the Paleobiology Database Fossilworks, accessed 25.06.2020).

Old materials of this species were initially assigned to the species *Trigonotreta stokesii* (Koenig 1825) by Angiolini, but have been reassigned by Angiolini when analysing an additional bulk sample. *Trigonotreta larghii* has a biconvex shell with a "semicircular to subpentagonal outline" and an uniplicate commissure (Angiolini et al. 2005). For a detailed description and the reassignment see Angiolini et al. (2005). The material for this work showed three ultrastructures: a primary, a fibrous, and a columnar layer.

The samples were collected from the Gircha Formation at the Chapursan Valley of the Karakoram Basin in northern Pakistan. The age of these specimen was dated to the Late Asselian to Early Sakmarian (Early Permian).

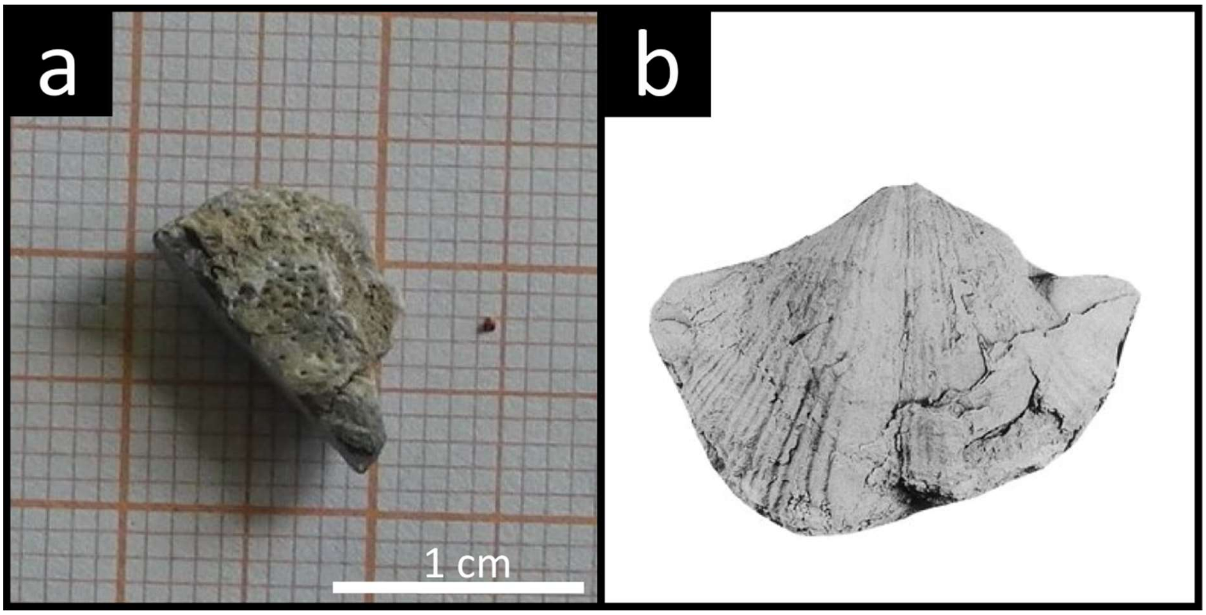

Figure 2.14: Overview of fossil *Trigonotreta larghii*. a) shows own material, b) shows graphic from Angiolini et al. (2005).

2.1.2.9 *Trigonotreta lyonsensis*

The species *Trigonotreta lyonsensis*, firstly described by Archbold and Thomas (1986), belongs to the extinct family of the Trigonotretidae. *Trigonotreta larghii* lived in shallow subtidal reefs, buildups, or bioherms as a "stationary epifaunal suspension feeder". It lived from 295.0 Ma until 290.1 Ma ago (Angiolini et al. 2005, Archbold and Thomas 1986, recorded in the Paleobiology Database Fossilworks, accessed 25.06.2020).

Angiolini et al. (2005) give an extremely detailed description of the species. The distinctive features are a "transverse trigonal outline [...], high and sharp dorsal fastigium, distinctive fascicles of relatively coarse ribs and a thick shell substance". The only ultrastructural units found in the material of this work was a fibrous layer.

The two localities of origin for the specimen received for this research are the Gircha Formation in the Chapursan Valley and the same formation in the Karambar Pass, both lying in the Karakoram Basin in northern Pakistan. The age of the samples is Late Asselian to Early Sakmarian (Early Permian).

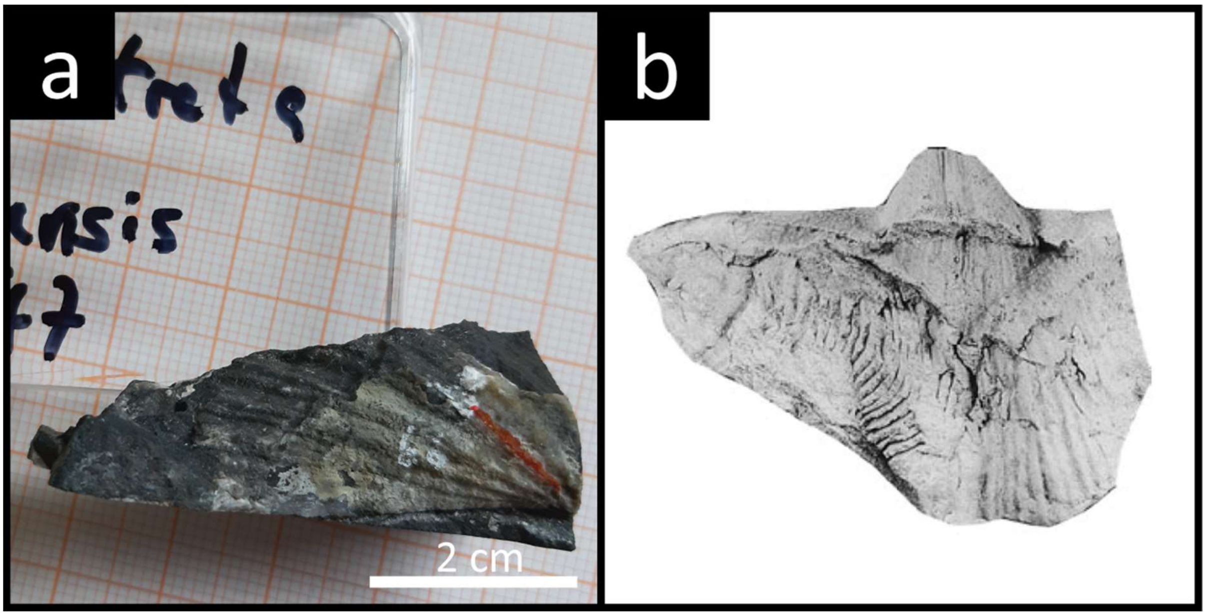

Figure 2.15: Overview of fossil *Trigonotreta lyonsensis*. a) shows own material, b) shows graphic from Angiolini et al. (2005).

2.2 Methods

2.2.1 Alteration experiments

When new specimens were obtained they were photo-documented and assigned an individual sample number and sample box. The first step, before starting the alteration experiments or the preparation, was to work out which spot and perspective would be best to investigate to acquire the information sought-for. For each individual experiment, three different pieces were cut out of each specimen with a circular saw: one for the electron microscope (including SEM, EBSD, and EDS), one for AFM, and one for XRD investigation. New photos were taken of the cut-up pieces before further preparation and alteration.

Two different alteration fluids were employed for this study. One was a burial fluid with the chemical composition 100 mM NaCl + 10 mM $MgCl_2 \cdot 6H_2O$. The burial fluid came from a batch made on the 27th of May 2016 and was already used by Laura Casella for her own alteration experiments in the course of her doctoral research (Casella 2018). The second alteration fluid in use was a marine fluid, coming from the GEOMAR Helmholtz Centre for Ocean Research in Kiel, Germany. There the fluid was used in a water tank for the breeding of brachiopods. The base fluid was distilled water to which the advised amount of PRO-REEF sea salt by Tropic Marine was admixed. An extensive chemical analysis of the sea salt can be found in the publication “elemental composition of commercial seasalts” by Atkinson and Bingman (1996).

The day before the start of each alteration experiment the oven was preheated. On the starting day the temperature was monitored and adjusted if necessary. When the desired temperature of 175 °C was reached and stable, the material was set up for alteration:

All three pieces cut from one specimen were put into a teflon crucible with the internal dimensions of 3.8 cm in height and 2.4 cm in diameter. 10 ml of alteration fluid was filled into the crucible with an Eppendorf pipette, taking care that the sample pieces didn´t overlap so that all would have the same and maximal fluid exposure. The thread coupling of the metal autoclave was greased with LIQUI MOLY copper paste for connections placed under high thermal loads. The filled crucible was carefully put into the autoclave, which then was sealed and put into the preheated oven. The time was noted in the laboratory journal to determine the time of the end of alteration. When the intended duration of the alteration ended, the autoclaves were taken out of the oven to cool down in a fume cupboard for one to two hours, before being disassembled. The samples were taken out of the crucible with tweezers and set to dry in their individual sample boxes in the fume cupboard.

2.2.2 Preparation

For all five analytical methods there were only two different main preparation methods necessary. One is for the X-ray diffraction measurements (XRD) and one is for investigations in the electron microscope (for SEM, EBSD, and EDS) as well as the atomic force microscope (AFM).

For XRD the samples were crushed and ground into finest powder in three differently sized agate mortars, before being filled into the sample holders aided by a small spatula. If enough material was available, a sample holder with a round depression was used, that was filled with the material and pressed down with a glass plate to obtain a smooth surface. If only few material was available, a sample holder with a rectangular quartz slap, ensuring a zero background, was utilized by mixing the powder with ethanol and dripping the mixture onto the quartz slap, resulting in a gapless covering and a smooth surface.

For AFM, EBSD, EDS, and SEM analyses the samples had to fit into a small round mould (2.7 cm diameter) to be filled up with resin. The surface of the sample to be investigated was fixed onto the bottom lid of the mould with a double-sided tape, and the sides of the mould were covered with laboratory-grade vaseline for easy removal after the hardening of the epoxy mixture. After assembling the mould, the samples were covered with a mixture of one fluid ounce of EpoFix resin and 4 ml EpoFix hardener (both from Struers). Air bubbles were taken out in a desiccator, where afterwards the product was left to cure for 24 hours. After this time the embedded specimens were taken out and washed clean in a set cleaning regimen, that was applied after each small step of the preparation described in the next paragraphs: First, they were rinsed off with tap water to remove coarse dirt, then spritzed with diluted dish soap to reduce the surface tension and loosen smaller dirt particles, then again with tap water to rinse off these dirt particles. This was followed up by a thorough rinse with ultrapure water of type 1 (mQ water) to avoid chemical reactions on the samples´ surface, until lastly the samples were blown dry with a common hair dryer.

After the process of embedding, the MetaServ 250 grinder-polisher by BUEHLER equipped with SiC abrasive paper (CarbiMet, BUEHLER) with grit size P320, was utilized to grind off the uneven surface, the double-sided tape, and all sharp edges. This step only facilitated the following steps, which represent the preparation of the actual sample: The sample surface was carefully ground with P600 and P1200 abrasive paper, twice for each grit size respectively rotated 90 degrees in between. Between each change of direction or abrasive paper the sample was treated with the cleaning regimen described in the last paragraph and was being surveyed under a light microscope to identify and erase possible errors.

The epoxy block with the specimen was sawn and ground down on the back side, opposite to the sample surface, to achieve a thickness of under 3 mm to fit the specifications of the electron microscope (Hitachi SU5000). Next, the sample was hand polished (with the same machine as used for grinding) with MetaDi Supreme polycrystalline diamond suspension (3 µm, undyed, BUEHLER) on a VerduTex polishing cloth (BUEHLER) for five to over thirty minutes, dependent on the surface quality. With adhesive resin the samples were glued onto a metal weight (by melting of the resin through contact with the hot metal weight heated to 150 °C on a heating plate) and put into a vibratory polisher (VibroMet 2, BUEHLER) with MasterPrep polishing suspension (0.05 µm, BUEHLER) on the MicroFloc polishing cloth (BUEHLER) for three hours in a circular motion and set at $^1/_3$ speed. After this last polishing step, the metal weights could often be separated from the sample disc by simply snapping it off or being slightly heated with the hair drier. If not, the metal weights with the sample attached to it were put onto the heating plate at 150 °C until the adhesive resin became fluid enough to slide the sample off. The set cleaning regimen was again applied very thoroughly to assuredly remove the very small particles of the polishing suspension. Then the adhesive resin remaining on the backside of the sample was cleaned off with acetone and the sample was put through the cleaning regimen once again.

For EBSD, SEM, or EDS investigations epoxy surrounding the sample was minimized by being ground down with the P320 abrasive paper to enable the perfect placement on the stub for an optimal measurement. The cleaning regimen was applied one last time. The finished specimens were mounted on small stubs with conductive silver paste, which was also spread over the bordering resin around the sample and onto a small portion of the sample to ensure good conductivity under beam exposure. After drying, the samples were covered with a 4 to 6 nm thick carbon coating and hereafter ready for SEM, EBSD, and EDS investigations. If the coating was not thick enough to stabilize the sample in the electron microscope for the requisite time of the measurement, it was coated again up to a maximum of three times in total.

For AFM analysis the embedded samples were also ground down, polished and reduced to a 3 mm thick disc like described earlier, but not reduced on the sides to enable easier handling of the sample. After the vibratory polisher they were etched by flushing the surface with laboratory grade ethanol for five seconds. Lastly the sample was put into a glass vessel, covered with purified water, put into an ultrasonic bath for ten minutes, and hereafter blown dry.

2.2.3 XRD analysis

X-ray powder diffraction (XRPD) was the chosen method for phase differentiation between aragonite and calcite. Models describing the observed X-ray diffractograms can be refined to optimize the identification of the composition. There are different types of this method. For these studies the Bragg-Brentano focussing method was used in the diffractometer system XRD 3003 TT by GE Inspection Technologies.

A preliminary analysis of the measured data was done with the program Match! in order to get a first idea. To attain the results presented in this work, Rietveld refinement was applied using the program FullProf Suite and the structural model by Jarosch and Heger (1986) for aragonite (no. 32100) and by Markgraf and Reeder (1985) for calcite (no. 40114), both were found in the ICSD (Inorganic Crystal Structure Database by the science information centre Karlsruhe). It is to note that in the process of Rietveld refinement with this program the scaling factors are calculated separately for each phase and rounded to two decimal places. This leads to volume percentage values that do not automatically add up to 100 vol %. Furthermore, the estimated standard deviation is calculated separately for each phase. This way, if the calculated volume percentage of one phase is zero or close to zero, the standard deviation is so low that it is rounded to 0.00 vol % by the program, which can not represent the true value.

2.2.4 AFM analysis

The atomic force microscope used was the NanoWizard II by JPK. Raw data measurements of lateral deflection, vertical deflection and height were performed with the JPK SPM Desktop software. A tip cantilever with a round base (in contrast to a square base) was used in contact mode in a dry setting. Because of the difference in material the settings were always adjusted to get high quality data. From the raw data, pictorial representations (maps) were produced with the programs JPK Data Processing and JPK Gwyddion.

2.2.5 SEM, EBSD, and EDS analyses

SEM, EBSD, and EDS measurements were all done with a Hitachi SU5000, equipped with the Oxford Instrument AZtecHKL software.

Scanning electron microscopy (SEM) is the method to produce high resolution images from a focused electron beam. For this imaging process the electron beam was set to 20 kV.

Electron backscatter diffraction (EBSD) maps are pictorial representations of measured data sets and are comprised of many point measurements arranged in a grid pattern. Each measured point gives a multitude of information. In this work mainly information on mineralogy and crystallographic orientation were collected. The measured information was used to compile orientation maps, phase maps, band contrast maps, misorientation profiles, pole figures showing the orientation distribution of a mineral phase, the MUD value, and grain statistics. In the figures within this work, EBSD orientation maps are colour coded as inverse pole figures (IPF) after the x-, y-, or z-axis of the displayed map. The colour legends are given in figure 4.1.2. For all EBSD maps the applied IPF axis is mentioned in the respective figure caption. EBSD measurements were performed with a beam intensity of 20 kV, at an angle of 70 ° and varying step sizes, which were determined by the necessary size and quality of the measured map.

Energy dispersive x-ray spectroscopy (EDS or EDX) can be measured during an EBSD measurement or done separately. It gives chemical information on the concentration and dispersion of the elements that were selected. The data can be depicted in a spectrum, or, as EBSD, in a map.

3 Geology and stratigraphy

The fossil brachiopod samples originate from four different geological basins. These basins were chosen for the reason that they exhibit different types and varying levels of diagenetic overprint, and also because they were very well investigated in this detail by various scientists. Herein, the four different basins are ranged by the thermal gradients (diagenetic temperatures) they underwent, which range from below 50 °C to up to 350 °C.

The numerical specifications on the respective diagenetic temperature frames originate from a discussion of several qualified scientists involved in this project – Prof. Dr. Lucia Angiolini, Prof. Dr. Wolfgang Schmahl, Dr. Erika Griesshaber, and me, Viola Mages – and is based on various geological proxies from each basin.

3.1 Castell'Arquato Basin

Samples from this basin were collected from the Castell'Arquato Formation within the eponymous geological basin. The locality lies at the Stirone river in the paleo-Adriatic region in northern Italy (figure 3.1).

Immature organic matter of mostly marine origin with additionally organic material from land plants, as well as unpublished data from Prof. Lucia Angiolini and Prof. Maurizio Gaetani (University of Milano) investigating physical and geochemical proxies, indicate that the succession is near pristine and should not have undergone temperatures exceeding 50 °C.

The Castell'Arquato Formation is a very fossiliferous marine succession, Gelasian to Calabrian (2.58 – 0.774 Ma, Early Pleistocene) in age. This succession crops out repeatedly along the Arda and Stirone rivers. It is comprised of sandstones, siltstones, and mudstones, which were deposited in a tectonically active area within the Paleo-Adriatic Sea during periods of progress of fan deltas (Crippa et al. 2016, Ghielmi et al. 2010, Ghielmi et al. 2013, Monegatti et al. 2001).

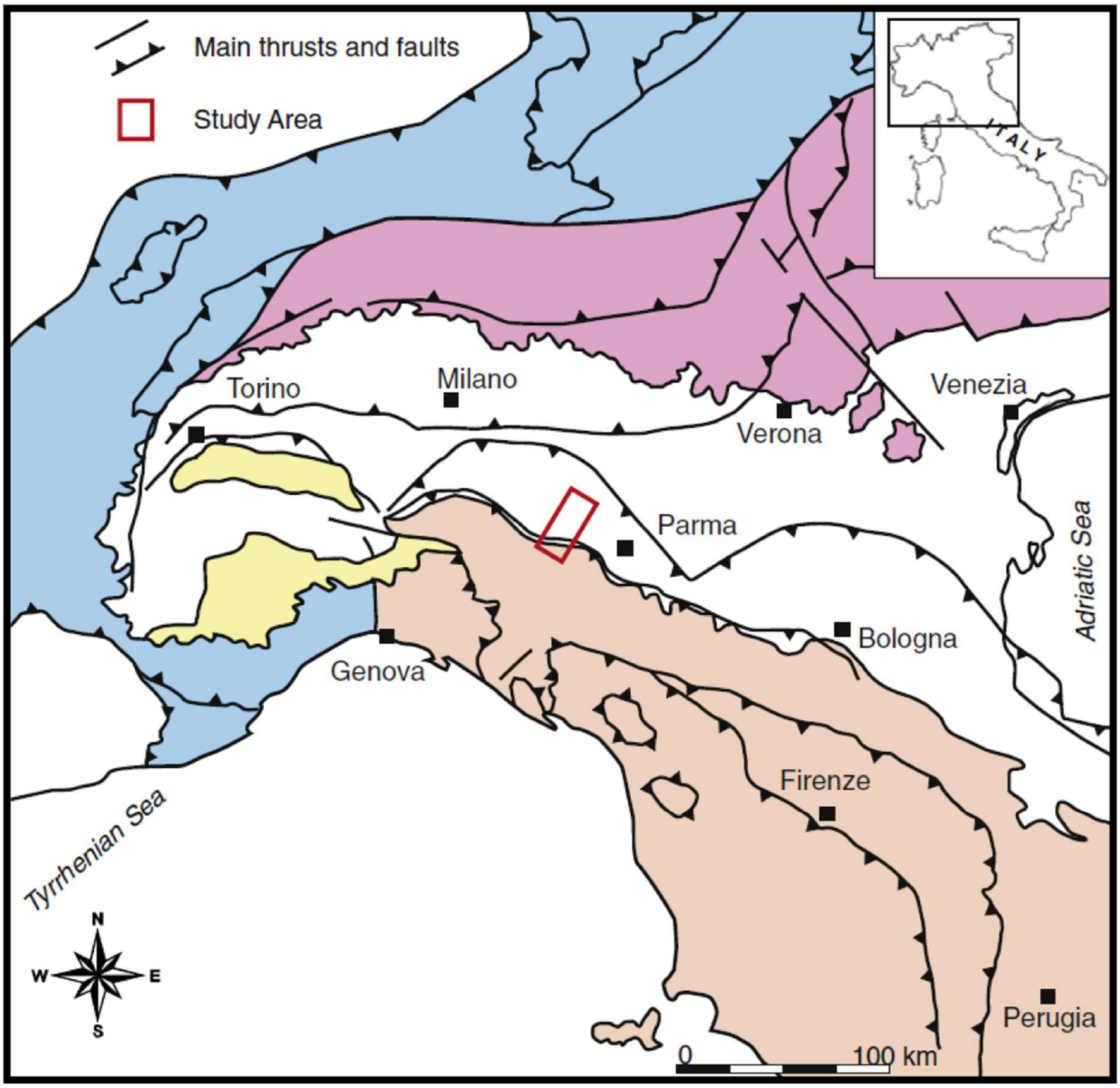

Figure 3.1: Graphic of the locality of the Castell'Arquato Basin from Crippa et al. (2016) (slightly modified).

3.2 Pennine Basin

The material from the Pennine Basin originates from the Eyam Limestone Formation at Once-a-week quarry. This quarry is situated between the villages of Sheldon and Monyash in Peak District National Park, Derbyshire, central northern England (figure 3.2).

Based on extensive studies (e.g. Breislin 2018, Ewbank et al. 1995, Hollis and Walkden 1996, Hollis 1998, Hollis and Walkden 2002) and thermal modelling for a shale gas project of the British Geological Survey (Andrews 2013), the thermal heat flow has been determined to lie between 100 and 120 °C.

The Eyam Limestone Formation is Mississippian (Early Carboniferous) of age and highly fossiliferous. This formation represents the youngest of four shallow water sequences at the Derbyshire High ramp carbonate succession; the oldest being the Woo Dale Limestone, being followed by the Bee Low Limestone, the Monsal Dale Limestone, and finally the Eyam Limestone Formation. It constitutes a mud mound facies, comprising light grey limestone with a high amount of brachiopods, corals, echinoderms, and molluscs. The brachiopod genus *Gigantoproductus*, which solely represents this work´s material that was collected at this location, is a very common and, through its size, a very distinctive fossil at the Once-a-week quarry, but also at other natural outcrops, and active as well as disused quarries around the area of Ible, Matlock, and Monyash (Aitkenhead and Chrisholm 1982, Aitkenhead et al. 1985, Angiolini et al. 2011, Gutteridge 1983, Gutteridge 1987, Gutteridge 1991, Gutteridge 1995, Gutteridge 2003, Nolan et al. 2017).

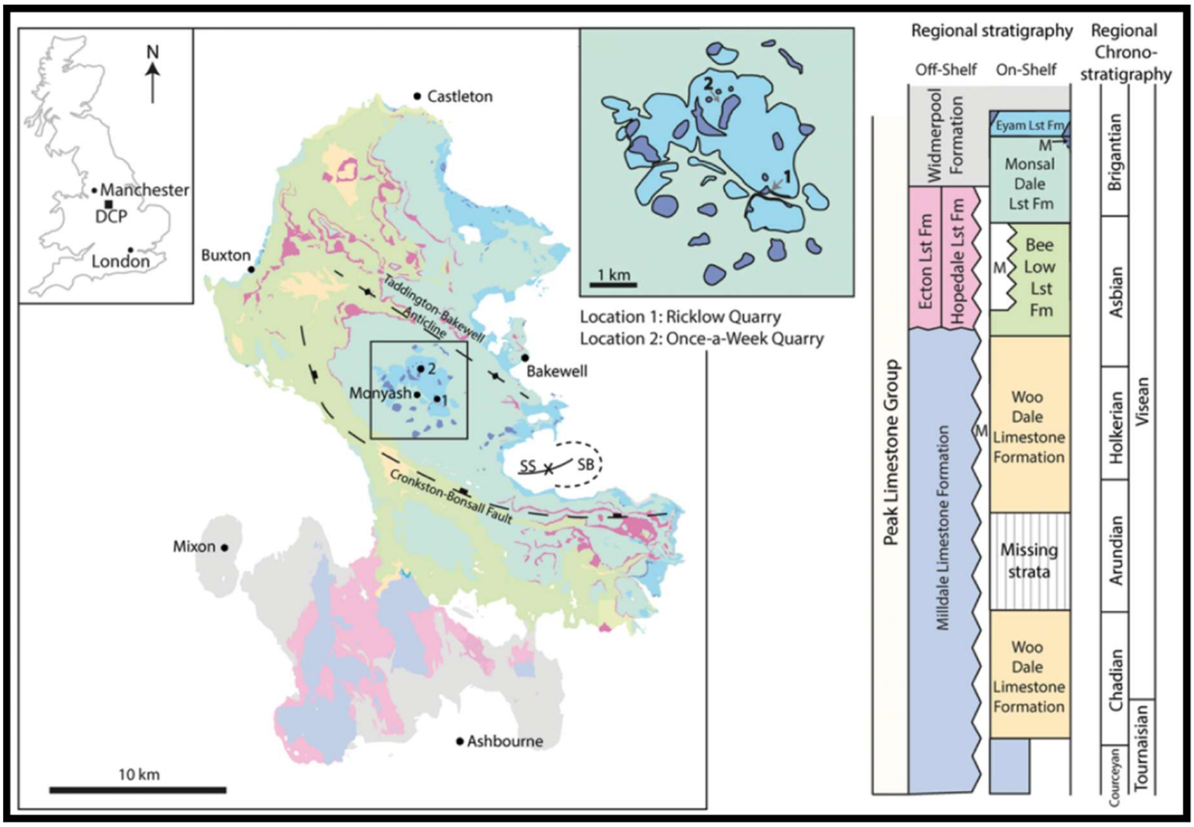

Figure 3.2: Graphic of the locality of the Pennine Basin from Nolan et al. (2017) (slightly modified).

3.3 Lombardian Basin

The Lombardian Basin lies in the Southern Alps and Austroalpine Nappe in northern Italy. The samples were collected from the Calcare di Angolo Formation in Valle dell'Acquafredda, Lombardy, northern Italy (figure 3.3).

The thermal heat flow of the Lombardian Basin ranges from 150 to 200 °C, based on vitrinite reflectance, CAI (colour alteration index) of conodonts and illite crystallinity data (Gaetani et al. 1992).

The stratum where the samples were collected from dates back to the Anisian stage, Middle Triassic. This calcareous layer presents a highly fossiliferous content of ammonioids, bivalves, brachiopods, corals, echinoderms, foraminifera, and gastropods (Gaetani et al. 2010).

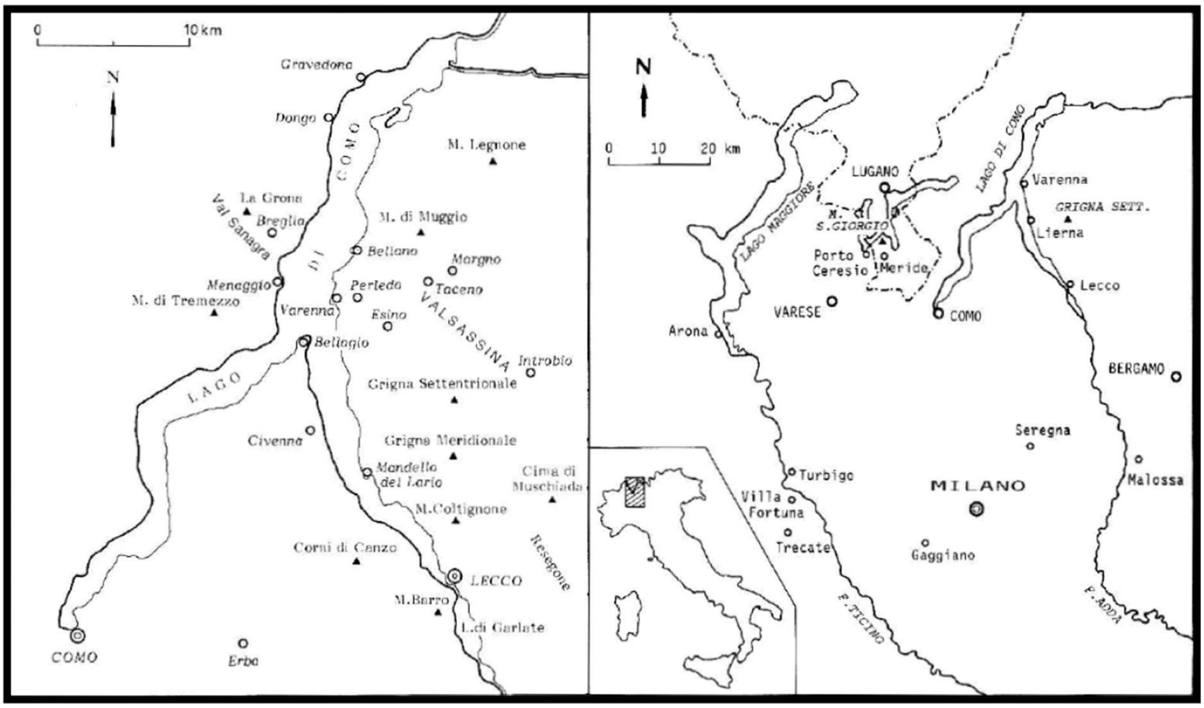

Figure 3.3: Graphic of the locality of the Lombardian Basin from Gaetani et al. (1992).

3.4 Karakoram Basin

The Karakoram Basin lies in the very north-east of Pakistan (figure 3.4). It is by far the most investigated locality of all four, but it is also by far the most complex locality as well. The samples collected from this area come from five different localities and different tectonic units which underwent different amounts of strain.

The heat flow of this large basin represents the highest temperatures of all basins studied herein and lies between 300 and 350 °C, based on the deformational history, mineral parageneses (sericite, quartz recrystallization), slaty cleavage, CAI of conodonts (4 dark grey) and organic maturity through vitrinite (Fossen 2010, Gaetani et al. 1995, Gaetani 1997, Gaetani et al. 2013, Searle and Tirrul 1991, Zanchi and Gaetani 2011).

The history of origin of the Karakoram Terrane ranges from the Ordovician to Cretaceous stage, recording a continental block of Gondwanan affinity, which, in the course of the rifting and opening of the Neo-Tethys during the Carboniferous to mid-Permian, drifted away from Gondwana during the Late Permian and Triassic and collided with Eurasia in the Early Jurassic (Angiolini et al. 2013, Gaetani 1997, Zanchi and Gaetani 2011). The samples collected from the Karakoram are aged Carboniferous to Early Permian. They originate from an abundantly fossiliferous marine succession with brachiopods, corals, echinoderms, foraminifera, and molluscs (see Angiolini 1995, Angiolini 1996, Angiolini 2001, Gaetani et al. 1995, Gaetani 1997).

3.4.1 Baroghil Pass, Lashkargaz Fm.

Locality one (bed CK172) lies in the Baroghil Pass and the Upper Yarkhun Valley. The samples were collected from the Lashkargaz Formation and are Sakmarian (Early Permian) of age. The lithology of this bed is marlstones.

3.4.2 Chapursan Valley, Gircha Fm.

Locality two (bed KK26) is located in the Chapursan Valley within the Upper Hunza Valley. The stratum of origin is the Gircha Formation, which is Late Asselian to Early Sakmarian (Early Permian) of age. The samples from this locality belong to the species *Trigonotreta larghii*, and this locality is also the type locality of this species (Angiolini et al. 2005). The lithology of this bed is fine-grained sandstones (arkoses).

3.4.3 Karambar Pass, Gircha Fm.

Locality three is situated in the Karambar Pass, Ribat Section. Samples were collected from the Gircha Formation (beds CK1121 and CK1122). The age is dated to be Late Asselian to Early Sakmarian (early Permian) (Angiolini et al. 2005). This locality´s lithology is calcareous siltstones.

3.4.4 Karambar Pass, Lupsuk Fm.

Locality four (beds L35 and L46) lies in the Twin Valleys Section of the Karambar Pass. The material comes from the Lupsuk Formation, with the age of Serpukhovian to the latest Carboniferous stages. The present lithology is black marly limestones (Angiolini et al. 1999).

3.4.5 Lashkargaz Gulley, Lupsuk Fm.

Locality five (bed L42) lies in the Lashkargaz Gulley. The stratum of origin is the Lupsuk Formation that has been assigned to the Moscovian to Kasimovian stages (Late Carboniferous). This locality`s lithology is characterized by marly limestones.

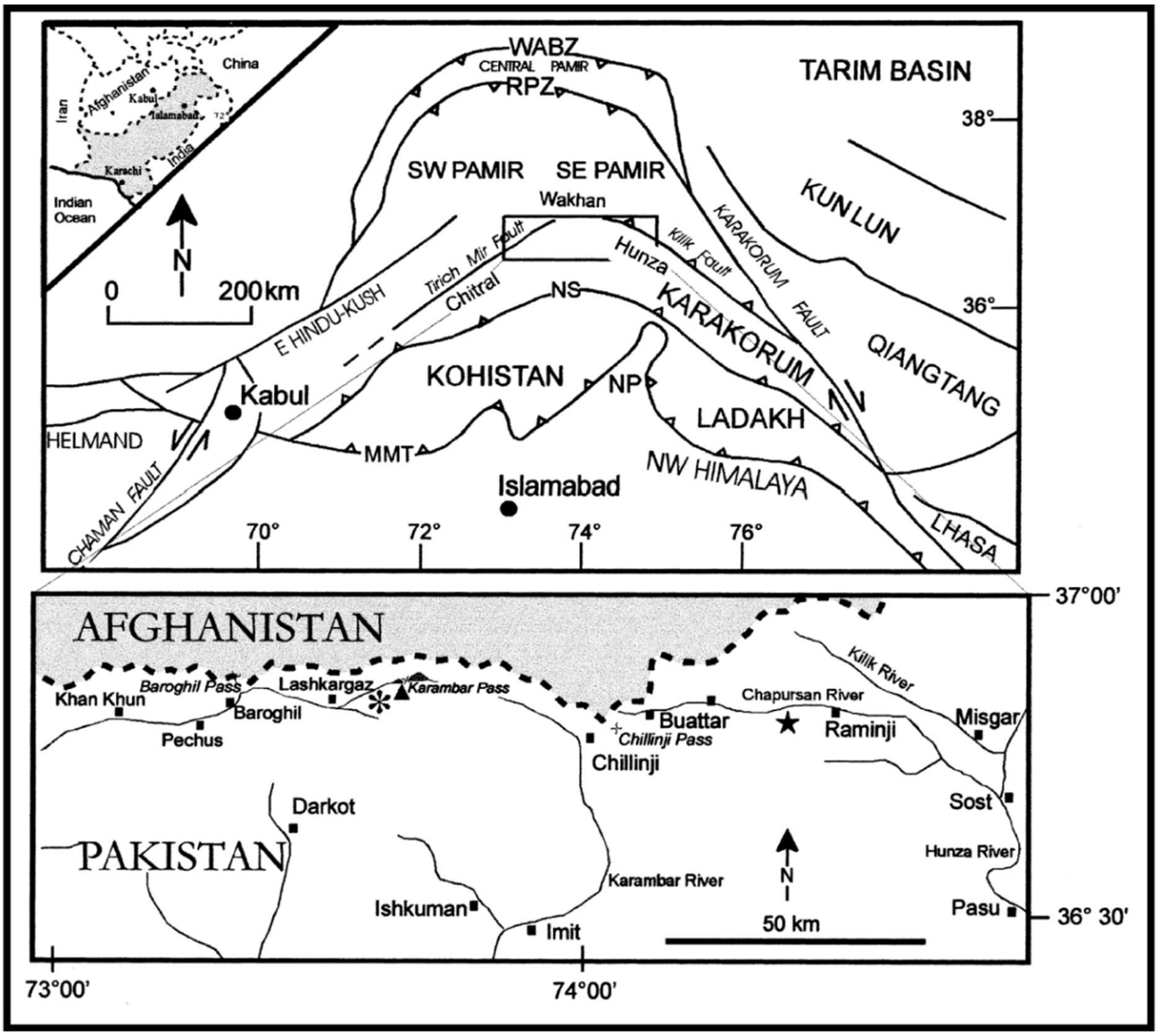

Figure 3.4: Graphic of the locality of the Karakoram Basin from Angiolini et al. (2005).

4 Results

4.1 Alteration series project

4.1.1 *Arctica islandica*

XRD: The pristine material contains about 98 vol % aragonite, which remains equivalent up to 7 days of alteration. Thereafter the aragonite content declines steadily: after 14 days of alteration an aragonite content of 89 vol %, and after 28 days 68 vol % aragonite was measured. Thereof it can be concluded that calcite formation occurs after 14 days of alteration.

Table 4.1: Aragonite and calcite content values for the bivalve *Arctica islandica* in vol %, as determined by X-ray diffraction and subsequent Rietveld refinement.

Arctica islandica	aragonite [vol %]	calcite [vol %]
pristine	98.40 ± 2.62	1.60 ± 1.43
4 days	98.52 ± 0.94	1.48 ± 0.13
7 days	98.43 ± 0.98	1.57 ± 0.01
14 days	89.44 ± 0.94	10.56 ± 0.28
28 days	68.34 ± 0.27	31.66 ± 0.42

AFM and SEM: The 4 days long alteration already shows signs of overprint: After the loss of the high organic content, bands of enhanced porosity as well as some fissures run along the growth lines and sub-parallel to the shell`s surface (figure 4.1.1.a). After 14 days SEM images show more but finer fissures (now positioned in various directions) (figure 4.1.1.b), and very dense regions of secondary calcite that are located mainly in the middle of the shell (figure 4.1.1.c). However, the pre-existing aragonitic phase is still present. AFM results also show these areas of respectively primary and recrystallized nanostructural characteristics: the ultrastructure characteristic for this species, and the compact angular nanostructure of inorganically grown calcite (figure 4.1.1.d). After 28 days of alteration AFM measurements show a marked increase in grain size. SEM images of 28 days altered material show thin bands of high porosity along the growth lines and mostly open fissures (figure 4.1.1.e and f). The fossil material is very compact, but presents a heightened porosity along the regions of former growth lines on the outer edge.

EBSD: After 4 days of alteration no conclusive impact on the microstructure could be observed; no signs of merging were found. The pristine microstructural characteristics are not disturbed.

Such as in the SEM images, the accompanying EBSD measurements show the formation of cracks and cavities (secondary porosity) through the decomposition of organic matter, while the overall porosity is not high. Only very few and small secondary calcite grains are present after the 4 days of alteration. After 14 days, however, a large share of the primary microstructure is replaced by secondary calcite. This newly formed material has a very high co-orientation (high MUD value) and possesses tattered outlines. Especially along fissures, where the percolation of fluid was aided through the plenty of voids, the pristine material became recrystallized, being substituted by a wide band of secondary calcite with one solid orientation (figure 4.1.1.g). The fossil material, however, shows no calcitization (defined in chapter 5.1.3) at all, as well as no fissures. The primary mineral units seem to still be present and the growth lines are still recognizable. The crystal orientations of the aragonitic mineral units are accumulated in multiple preferred orientations, but present a relatively wide distribution. The MUD value for an area of about 310 x 220 µm is 86.

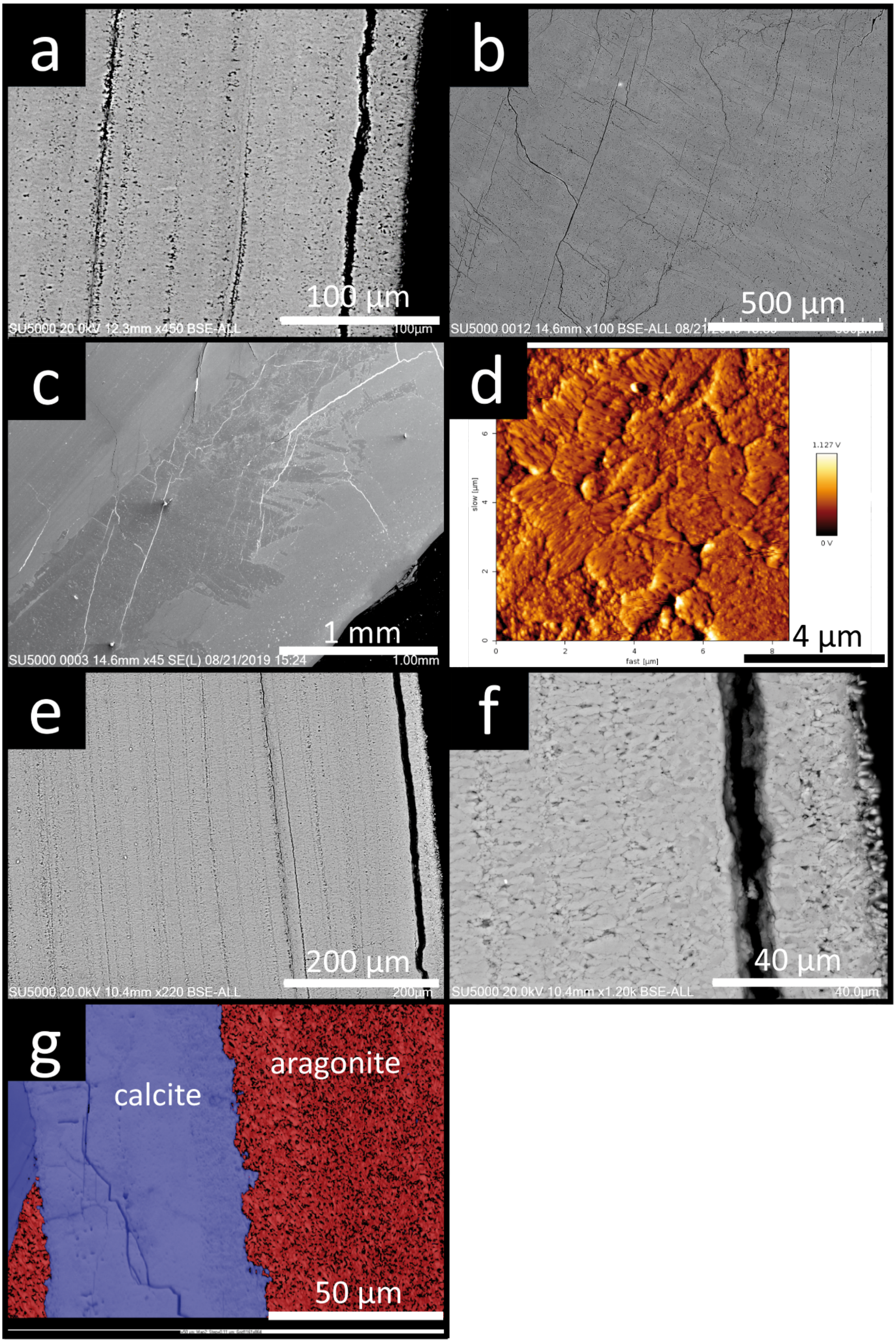

Figure 4.1.1: Microscopic analyses of *Arctica islandica*: a) SEM image of enhanced porosity and fissuring after 4 d of alteration, b) SEM image of fissures after 14 d of alteration, c) SEM image of the formation of secondary calcite in the middle of the shell after 14 d of alteration, d) AFM map of secondary calcite grains formed after 14 d of alteration, e and f) SEM images of thin bands of high porosity along growth lines after 28 d of alteration, g) EBSD phase map of high-crystalline calcite forming along a fracture after 14 d of alteration.

4.1.2 *Mytilus edulis*

XRD: The pristine shell has an aragonite content of 46 vol % and a calcite content of about 54 vol %. After only 4 days of alteration the aragonite content is already reduced to 32 vol %. After 7 days there is an only slight decrease in the aragonite content by about 1 vol %, while between 7 and 14 days a drastic drop down to 18 vol % aragonite occurred. The material, which was altered for 28 days, breaks away from this trend of decrease, having an aragonite content of about 70 vol %, which strongly points to an error.

As it was shown above, the aragonite content steadily decreases with ongoing alteration time. However, a defective result occurred in the longest alteration duration, which is 28 days, presenting significantly more aragonite content than even the pristine shell. The reason for this error might be the strong deviation in the thickness of the nacreous layer or simply an error in the implementation of the experiment.

Table 4.2: Aragonite and calcite content values for the bivalve *Mytilus edulis* in vol %, as determined by X-ray diffraction and subsequent Rietveld refinement.

Mytilus edulis	aragonite [vol %]	calcite [vol %]
pristine	45.74 ± 1.22	54.26 ± 1.17
4 days	32.49 ± 1.19	67.51 ± 0.76
7 days	31.04 ± 1.25	68.96 ± 1.67
14 days	17.95 ± 0.45	82.05 ± 0.88
28 days	69.60 ± 0.87	30.40 ± 0.48

AFM and SEM: After 4 days of alteration, due to the organic content having disintegrated, there is relatively strong breakage sub-parallel to the shell´s surface (figure 4.1.2.a). Especially at the previously organic-rich interface, where the nacreous and fibrous layers connected, a gaping crack regularly occurs, so that these two microstructures became separated in every altered sample (figure 4.1.2.b). At the outer rims of the shell, where the material was directly subjected to the fluid, a definite increase in porosity can be detected. SEM images show only very slight merging of the fibres after 4 days. AFM measurements might indicate some beginning amalgamation through the adaptation of the orientations of neighbouring fibres (figure 4.1.2.c). Amalgamation is more obvious in the nacreous ultrastructure. A major part of the nacre tablets merged on the short end, forming long strands (figure 4.1.2.d). After 7 days of alteration also the fibrous layer shows definite signs of alteration: the fibres lost the typical mushroom-shape and became more irregular and rounded through the process of amalgamation (figure 4.1.2.e). Also, fractures can be seen more frequently throughout the fibrous layer. Within the nacre signs of amalgamation became enhanced, but merging still takes place mainly at the short edges while merging along the long sides is sparse. Within both ultrastructural units there are areas with high porosity and areas with high density, tracing back to the growth pattern of the shell. After 14 days the fibrous ultrastructure is still easily identifiable, but it shows increased merging of fibres into larger clusters (figure 4.1.2.f). Likewise, in the nacreous layer the nacre tablets are still discernible but merging increased. With 28 days of alteration the fractures became even more frequent, especially the smaller-scale fissures (figure 4.1.2.g). Although the corruption of both structural units progressed further, even now single nacre tablets and single fibres can be identified.

EBSD: In contrast to what can be seen in the SEM images, where the nacre tablets seem to merge at the short edge forming long strands, the EBSD measurements of 4 days altered *Mytilus edulis* show that the nacre tablets adopt one common orientation with the mineral unit at the long edge (figure 4.1.2.h). 4 days altered fibres also show first signs of amalgamation (figure 4.1.2.i). No secondary calcite formation can be seen after 4 days of alteration. After 7 days the size of the merged fibre compounds significantly increased and, as witnessed in the SEM images and AFM measurements, the outlines of the single fibres lose their typical mushroom-shape and become more rounded (figure 4.1.2.j). Also within the nacreous layer the merging intensifies and the amalgamated units grow in size (figure 4.1.2.k). After 14 and 28 days of alteration the same trends continue: larger growing conglomerates of merged mineral units (more strongly so in the fibrous layer) and continued blurring of the pristine shape of the mineral units, while no calcite formation appears (figure 4.1.2.l).

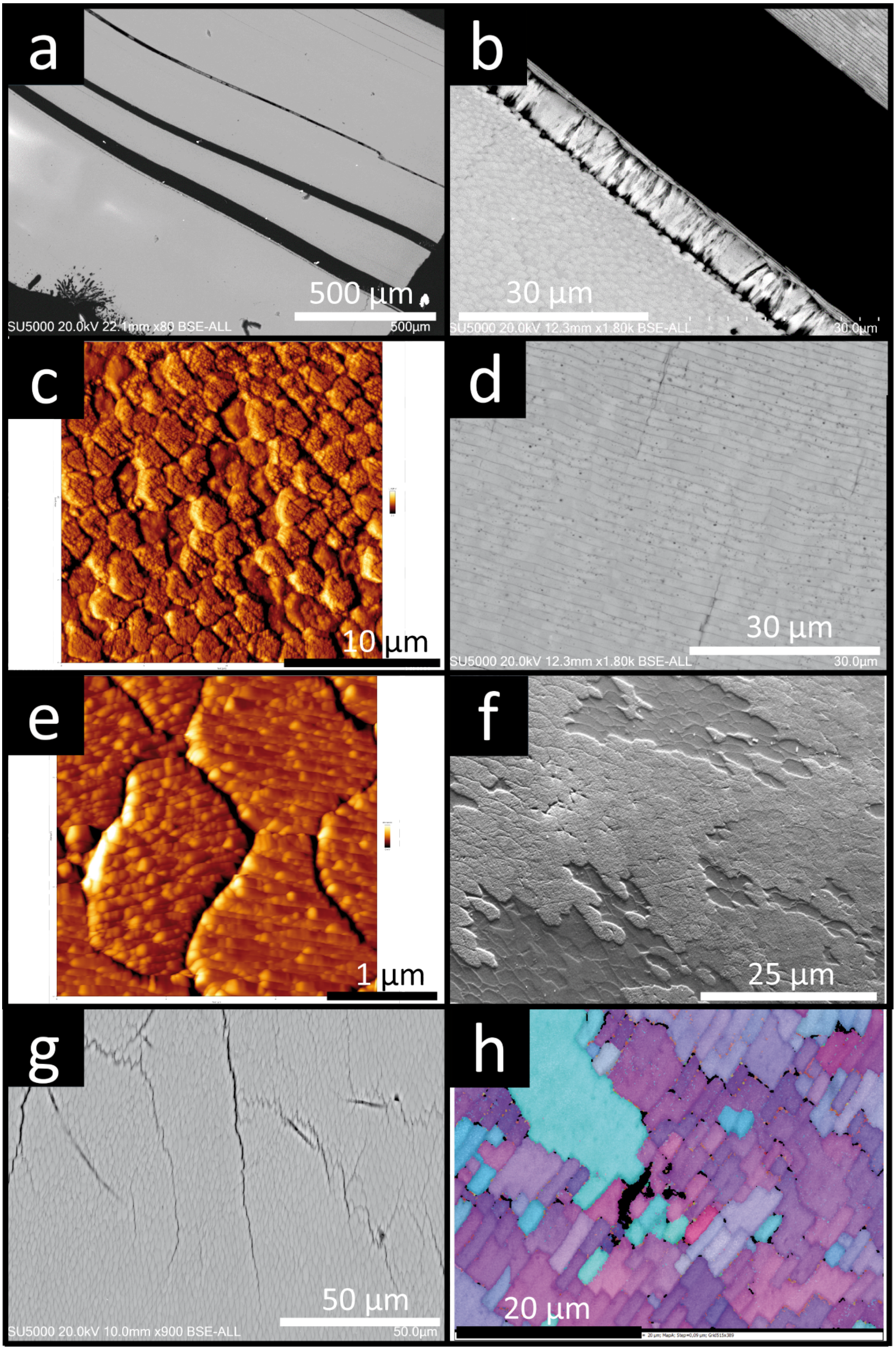
a
500 µm
SU5000 20.0kV 22.1mm x80 BSE-ALL
500µm
b
30 µm
SU5000 20.0kV 12.3mm x1.80k BSE-ALL
30.0µm
c
10 µm
d
30 µm
SU5000 20.0kV 12.3mm x1.80k BSE-ALL
30.0µm
e
1 µm
f
25 µm
g
50 µm
SU5000 20.0kV 10.0mm x900 BSE-ALL
50.0µm
h
20 µm

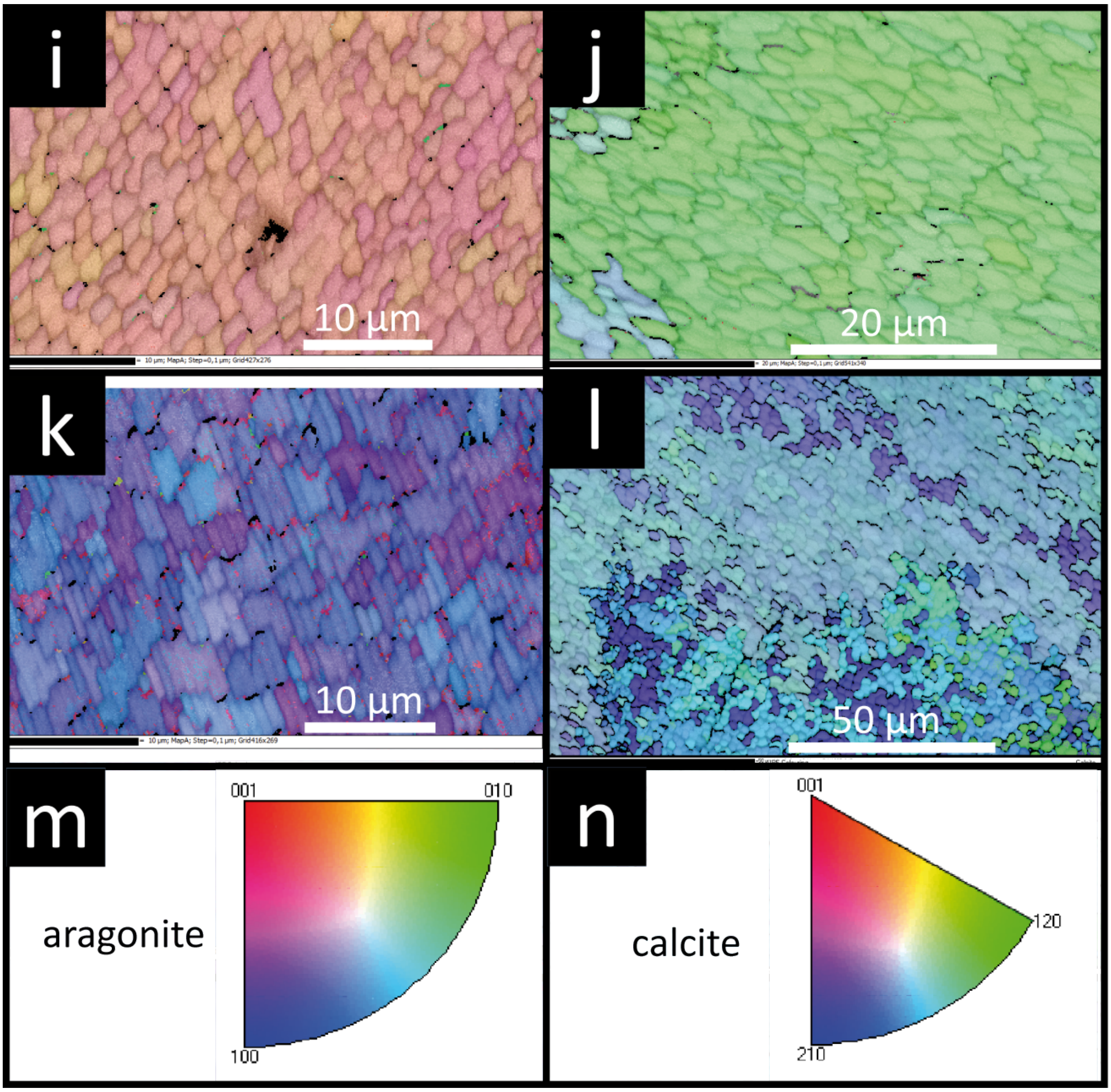

Figure 4.1.2: Microscopic analyses of *Mytilus edulis*: a) SEM image of breakage subparallel to the shell´s surface after 4 d of alteration, b) SEM image of frequent separation line along the interface of the two ultrastructural units after 4 d of alteration, c) AFM map of a beginning amalgamation within the fibrous layer after 4 d of alteration, d) SEM image of the amalgamation of the nacre tablets into long strands after 4 d of alteration, e) AFM map of two merging fibres after 7 d of alteration, f) SEM image of advanced amalgamation within the fibrous layer through the formation of larger clusters after 14 d of alteration, g) SEM image of the formation of frequent fissures after 28 d of alteration, h) EBSD orientation map (IPF colour code x-axis) of beginning amalgamation within the nacreous ultrastructure after 4 d of alteration, i) EBSD orientation map (IPF colour code z-axis) of beginning amalgamation within the fibrous layer after 4 d of alteration, j) EBSD orientation map (IPF colour code z-axis) of significant increase of amalgamation within the fibrous layer and loss of the typical mushroom-shape of the fibres after 7 d of alteration, k) EBSD orientation map (IPF colour code x-axis) of increase of amalgamation within the nacreous layer through the formation of larger cluster of merged mineral units after 7 d of alteration, l) EBSD orientation map (IPF colour code y-axis) of intensification of amalgamation after 14 d of alteration, m) inverse pole figure (IPF) legend for aragonitic material in EBSD orientation maps of this work, to which axis of the map the IPF legend is referring is stated in the figure description of the respective EBSD orientation map, n) inverse pole figure (IPF) legend for calcitic material in EBSD orientation maps of this work, to which axis of the map the IPF legend is referring is stated in the figure description of the respective EBSD orientation map.

4.1.3 *Porites* sp.

XRD: In the aragonitic material of the coral sample the alteration experiments had an extremely low impact. In the course of 28 days of hydrothermal alteration the calcite content varied by less than 1 vol %. The aragonite volume percentage still lies at over 98 for the 28 days alteration. However, in the fossil, which is the species *Porites pusilla*, no aragonite was found and the complete material became calciticized.

Table 4.3: Aragonite and calcite content values for the stony coral *Porites* sp. in vol %, as determined by X-ray diffraction and subsequent Rietveld refinement.

Porites sp.	aragonite [vol %]	calcite [vol %]
4 days	99.29 ± 0.90	0.71 ± 0.09
7 days	99.23 ± 0.98	0.77 ± 0.10
14 days	99.37 ± 1.22	0.63 ± 0.10
28 days	98.62 ± 1.28	1.38 ± 0.17
(*Porites pusilla*) fossil	0.00 ± 0.00*[1]	100.00 ± 0.78

AFM and SEM: SEM images show that the ultrastructure of this specimen, although seemingly highly porous, is very resistive to dissolution and recrystallization. After 4 days until up to 14 days of alteration there is no visible disturbance of the ultrastructure (figure 4.1.3.a to c), but some slight dissolution on the surface areas as well as in well distributed spots within the material can be found (figure 4.1.3.d and e). With ongoing time some accumulation areas with a more pronounced dissolution developed (figure 4.1.3.f and g). The 28 days altered sample presented frequent secondary calcite grains in the dissolved spots within the material and also along fine fissures (figure 4.1.3.h and i).

EBSD: After 4 days the outline of the single aragonite needles is slightly tattered and disturbed, but the general microstructure of the primary aragonitic needles is still obvious (figure 4.1.3j). No calcite formation can be found after 4 days of alteration. There is slight merging of neighbouring needles of the same cluster and of similar orientation. After 14 days not much change can be seen compared to 4 days of alteration, merely the merging of the neighbouring needles has slightly progressed. The outlines of the needles are not tattered any more but became more rounded (figure 4.1.3.k). No calcite formation was found after 14 days of alteration. After 28 days the merged needle bundles became more assimilated in orientation.

The needle clusters, however, are still very differently oriented relative to each other. The fossil material of *Porites pusilla* shows a very different ultrastructure and mineralogy. It is completely recrystallized with randomly oriented roundish secondary calcite grains. No needles or bundles are visible, and no aragonite is left. However, the primary ultrastructure is preserved in that way, that the structures of primary aragonite needle clusters is now substituted by small grained secondary calcite, while the pre-existing cavity space has been filled by much larger grained secondary calcite or was left void (figure 4.1.3.l).

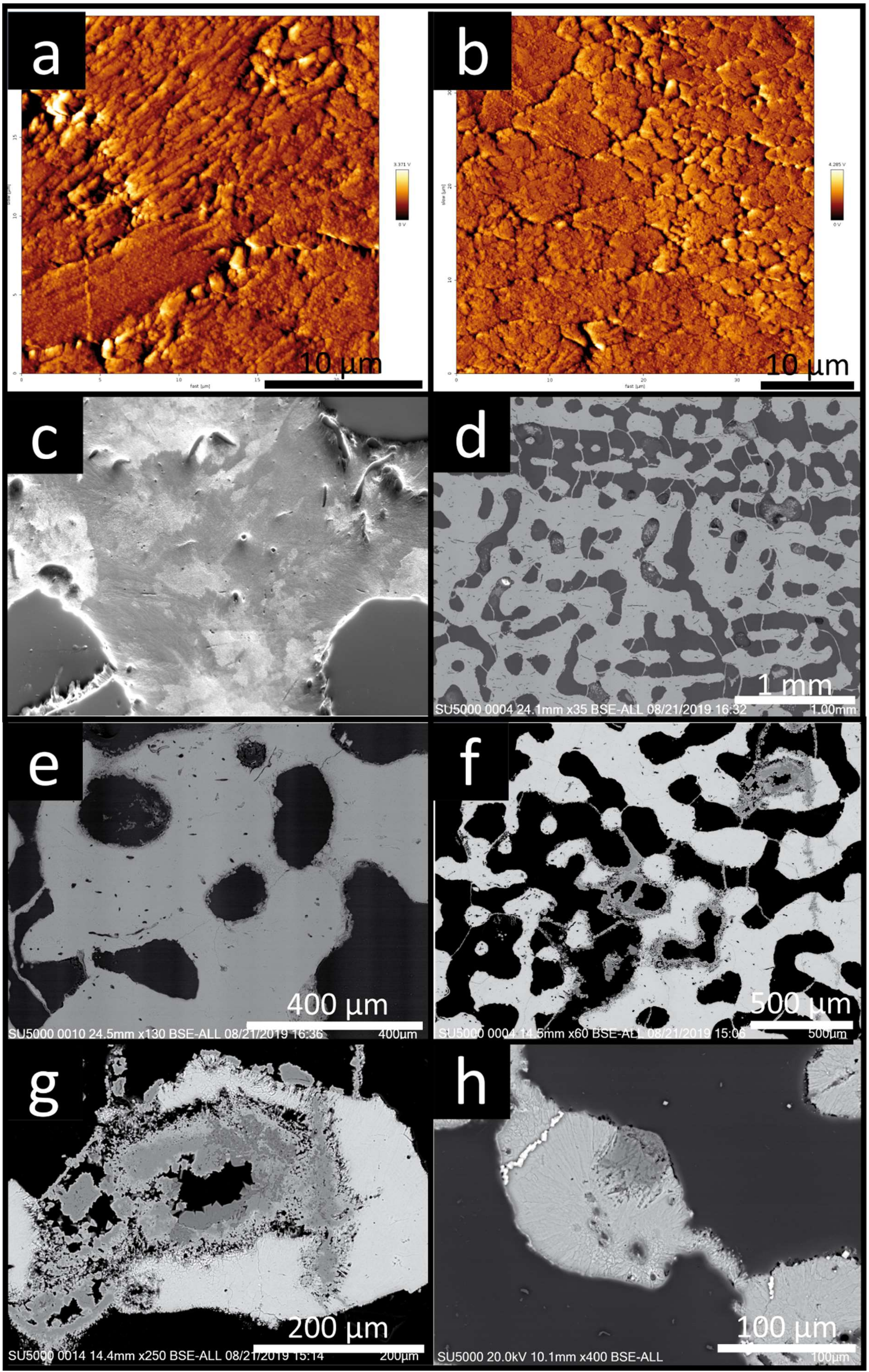
a
3.371 V
0 V
slow [µm]
fast [µm]
10 µm
b
4.285 V
0 V
slow [µm]
fast [µm]
10 µm
c
d
1 mm
SU5000 0004 24.1mm x35 BSE-ALL 08/21/2019 16:32 1.00mm
e
400 µm
SU5000 0010 24.5mm x130 BSE-ALL 08/21/2019 16:36 400µm
f
500 µm
SU5000 0004 14.5mm x60 BSE-ALL 08/21/2019 15:06 500µm
g
200 µm
SU5000 0014 14.4mm x250 BSE-ALL 08/21/2019 15:14 200µm
h
100 µm
SU5000 20.0kV 10.1mm x400 BSE-ALL 100µm

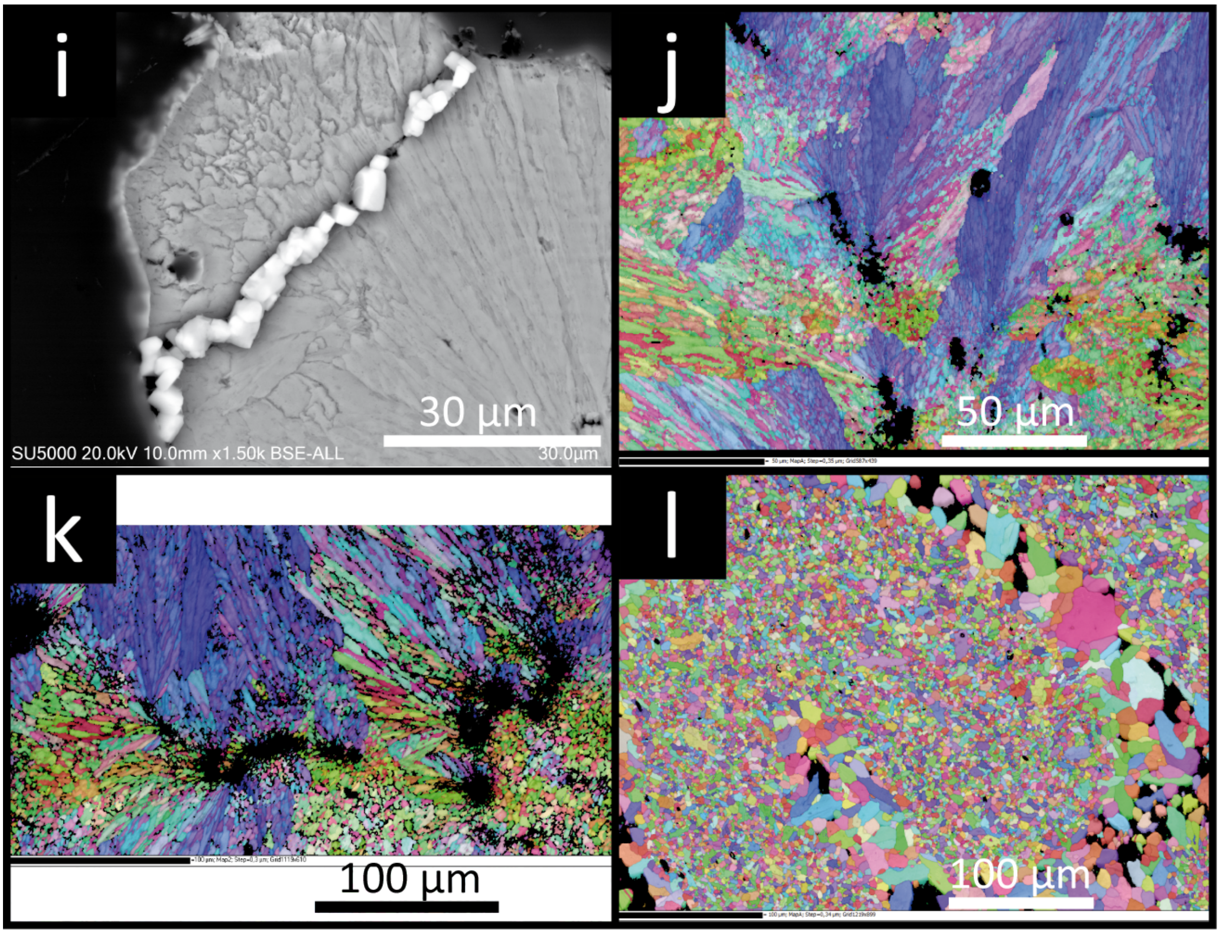

Figure 4.1.3: Microscopic analyses of *Porites* sp.: a+b) AFM maps of the low impact on the ultrastructure after 14 d of alteration, c) SEM image of the low impact on the ultrastructure after 4 d of alteration, d) SEM image of beginning dissolution on the outer edges as well as in cavities within the material after 4 d of alteration, e) SEM image of continued dissolution after 7 d of alteration, f+g) SEM images of intensification of the dissolution in certain areas after 14 d of alteration, h+i) SEM images of beginning formation of secondary calcite in areas of dissolution and fissures after 28 d of alteration, j) EBSD orientation map (IPF colour code y-axis) of only slight distortion of the primary ultrastructure after 4 d of alteration, k) EBSD orientation map (IPF colour code y-axis) of an only slightly increased impact after 14 d of alteration, l) EBSD orientation map (IPF colour code z-axis) of the fossil sample of Porites pusilla shows completely calciticized material with complete loss of the primary ultrastructure.

4.1.4 *Haliotis ovina*

XRD: There is a steady increase of calcite within the first 7 days of alteration. However, the calcite content increases by only about 6 vol % within this time frame, while the aragonite content decreases from about 96 vol % in pristine state to just over 90 vol % in the 7 days alteration. From 7 to 14 days of alteration the calcite content rises dramatically by 70 vol % to a total of over 80 vol %. In the 28 days alteration the aragonite content is again inconsequentially high (like in some other 28 days alterations of the other species), with about 97 vol %. The fossil material, from the sister taxon *Haliotis tuberculata*, contains about 80 vol % aragonite and 20 vol % calcite.

The incoherent result of the 28 days alteration, as equally found in the sample of *Mytilus edulis*, which was altered simultaneously, could be reasoned with the same cause. This reason could be the likely case that in the implementation of the alteration with the duration of 28 days, some error occurred and the affected samples became falsified. Another possibility would be that the alteration samples were cut out from different positions of the same shell, not from the same section of equivalent shells (like in *Aequipecten opercularis* and *Mytilus edulis*). This way a natural fluctuation in the structure and mineralogy in different sections of the shell could lead to a deviation in mineral composition.

Table 4.4: Aragonite and calcite content values for the marine gastropod *Haliotis ovina* in vol %, as determined by X-ray diffraction and subsequent Rietveld refinement.

Haliotis ovina	aragonite [vol %]	calcite [vol %]
pristine	95.77 ± 2.28	4.23 ± 0.54
4 days	92.21 ± 1.07	7.79 ± 0.30
7 days	90.19 ± 1.24	9.81 ± 0.72
14 days	19.18 ± 0.66	80.82 ± 1.15
28 days	96.89 ± 1.39	3.11 ± 0.41
(*Haliotis tuberculata*) fossil	79.99 ± 0.54	20.01 ± 0.69

AFM and SEM: The 4 days altered sample already shows strong alteration characteristics. There are quite large areas of dissolution and a secondary calcite phase within the prismatic layer (figure 4.1.4.a and b). The nacre tablets merged into columns (along the long edge), but are much more resistive towards recrystallization, for at this point no secondary phase is present (figure 4.1.4.c). After 7 days of alteration there is still no calcite formation within the nacreous layer. The SEM images as well as the AFM measurements of this specimen nicely show that the recrystallization process starts at the originally organic-rich interface between the two ultrastructural units and proceeds into the prismatic layer (figure 4.1.4.d to f). However, through the growth of the secondary calcite grains at the interface, they push into the nacreous layer leading to strong deformation and amplified amalgamation in these areas (figure 4.1.4.g). After 14 days the calcitization advanced into the nacreous layer (figure 4.1.4.h). In conformity with the XRD measurements, the SEM images of the 28 days alterations show very few calcitization; only few individual calcite grains were found. The porosity is high, especially within the nacreous layer, but also in some areas within the prismatic layer (figure 4.1.4.i). The outer edge of the prismatic layer (outside of the shell) shows signs of extensive dissolution (figure 4.1.4.j).

EBSD: The EBSD measurements of the 4 days altered samples show some smaller individual grains of secondary calcite (roughly 20 x 40 µm and 60 x 80 µm) amidst the prismatic layer (figure 4.1.4.k), but much larger grains (above 100 µm in diameter) accumulated at the interface of the two ultrastructures (figure 4.1.4.l). The secondary calcite grains are mostly monocrystalline, only the larger grains can exhibit a slight inner misorientation. Their rims of the secondary calcite grains that grow within the confined space of the prismatic ultrastructure are tattered where they slowly incorporate the much smaller prismatic mineral units. The EBSD measurements underpin the observation of the SEM images that the secondary calcite grains at the interface push into the nacreous layer, resulting in noticeably stronger amalgamation in these areas (figure 4.1.4.l). The material altered for 7 days shows the ongoing growth of secondary calcite, as before predominantly at the interface of the two different ultrastructures (figure 4.1.4.m). The prisms appear more rounded, the prismatic layer slightly less porous. After 14 days the calcitization proceeded into the nacreous layer. Now, the whole shell material consists predominantly of secondary calcite. Only little nacreous material is left. In the areas where nacre has not yet been substituted and the calcite has relatively recently grown, the secondary calcite consists of many smaller and differently sized grains with tattered grain borders (figure 4.1.4.n). But in the former prismatic layer, where the calcite grains started to replace the primary ultrastructure much longer ago, the calcite grains show the typical angular and straight edges of inorganically grown crystals and present a high crystallinity (figure

4.1.4.o). The nacreous material still has the similar and slightly dispersed orientation of the pristine material. However, with proceeding amalgamation, some bundling of the orientations due to the merging of the nacre tablets along the long edges into columns, can be observed. After 28 days of alteration there are still remaining patches of nacreous ultrastructure, but the strength of impact of the alteration is obvious in the well-advanced amalgamation, stronger scattering of the orientations, and more frequent nucleation of secondary calcite grains within the cavities between the merged tablets (figure 4.1.4.p). The material of the fossil species *Haliotis tuberculata* still presents a lot of aragonitic material, both of the prismatic and the nacreous layer (figure 4.1.4.q). As in the alteration experiments, calcitization began at the interface of the two ultrastructures. The crystals of secondary calcite show random orientations and a variation of sizes. Compared to the altered samples, the secondary calcite grains within the fossil material are larger with more random orientations and a higher crystallinity.

EDS: The fossil material shows an elevation of the Mg content within the secondary calcite grains (figure 4.1.4.r). Larger grains seem to have higher contents. The edges of the fractures, where the calcitization started, show elevated Mg ratios.

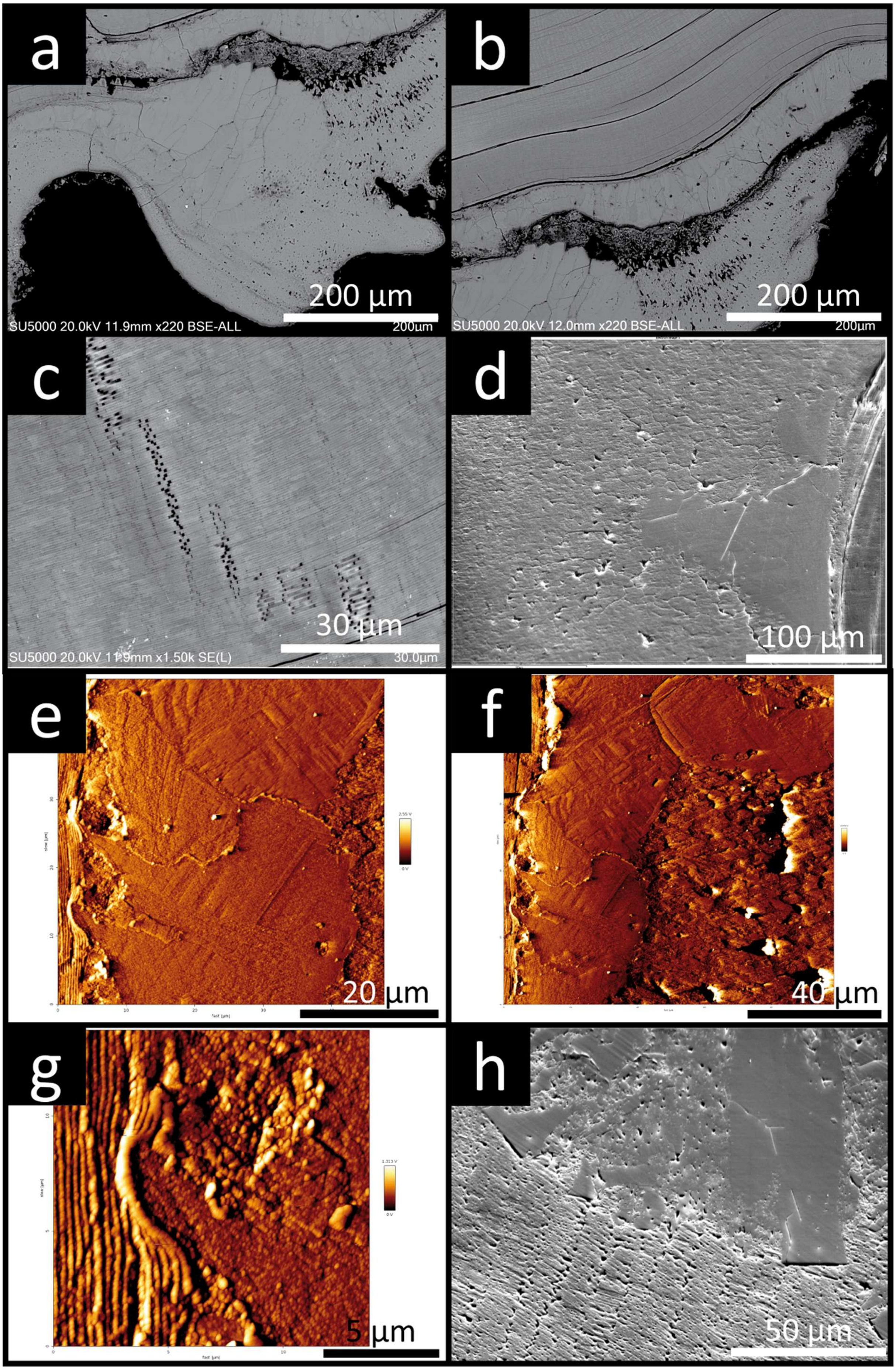
a
200 µm
SU5000 20.0kV 11.9mm x220 BSE-ALL
200µm
b
200 µm
SU5000 20.0kV 12.0mm x220 BSE-ALL
200µm
c
30 µm
SU5000 20.0kV 11.9mm x1.50k SE(L)
30.0µm
d
100 µm
e
2.55 V
0 V
slow [µm]
fast [µm]
20 µm
f
40 µm
g
1.313 V
0 V
slow [µm]
fast [µm]
5 µm
h
50 µm

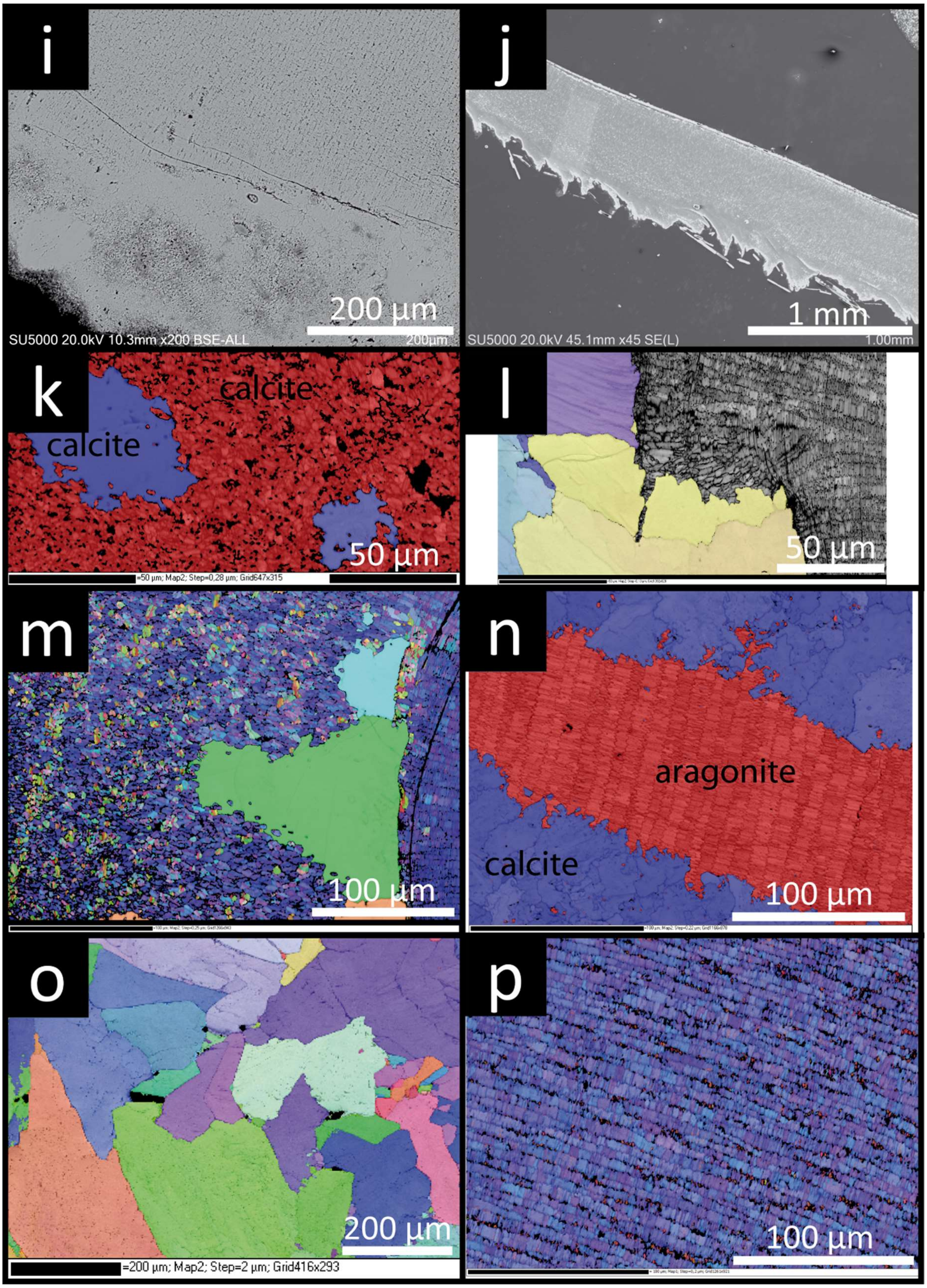
i
200 µm
SU5000 20.0kV 10.3mm x200 BSE-ALL
200µm
j
1 mm
SU5000 20.0kV 45.1mm x45 SE(L)
1.00mm
k
calcite
calcite
50 µm
=50 µm; Map2; Step=0,28 µm; Grid647x315
l
50 µm
m
100 µm
n
aragonite
calcite
100 µm
o
200 µm
=200 µm; Map2; Step=2 µm; Grid416x293
p
100 µm

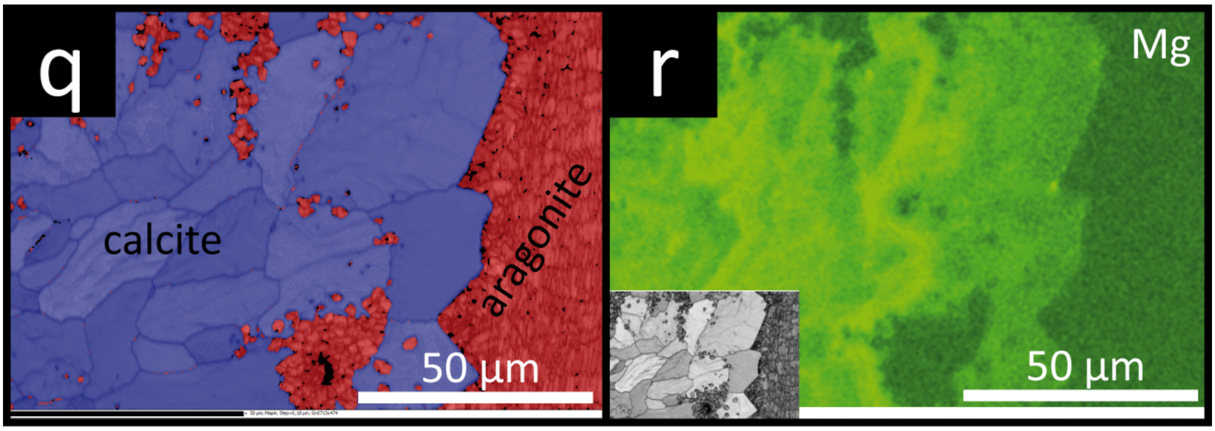

Figure 4.1.4: Microscopic analyses of *Haliotis ovina*: a+b) SEM images of intensive dissolution and early formation of secondary calcite after 4 d of alteration, c) SEM image of amalgamation within the nacreous layer after 4 d of alteration, d) SEM image of typical beginning calcitization within the prismatic layer at the interface to the nacreous layer after 7 d of alteration, e+f) AFM maps showing beginning calcitization at the interface within the prismatic layer after 7 d of alteration, g) AFM map of distortion through the growth of secondary calcite grains after 7 d of alteration, h) SEM image of progression of the calcitization into the nacreous ultrastructure after 14 d of alteration, i) SEM image of areas of high porosity after 28 d of alteration, j) SEM image of extensive dissolution on the surface of the outer side of the shell after 28 d of alteration, k) EBSD phase map of isolated calcite grains within the prismatic ultrastructure after 4 d of alteration, l) EBSD orientation map (IPF colour code x-axis) of larger calcite grains at the interface after 4 d of alteration, m) EBSD orientation map (IPF colour code x-axis) of ongoing calcitization at the interface after 7 d of alteration, n) EBSD phase map of younger and smaller grains of secondary calcite within the nacreous layer after 14 d of alteration, o) EBSD orientation map (IPF colour code x-axis) of older and larger grains of secondary calcite within the prismatic layer after 14 d of alteration, p) EBSD orientation map (IPF colour code x-axis) of amalgamation within the nacreous ultrastructure with small secondary calcite grains (red) nucleating in the cavital space after 28 d of alteration, q) EBSD phase map of fossil *Haliotis tuberculata* with prismatic as well as nacreous ultrastructure preserved, r) EDS map showing elevated Mg signatures within the secondary calcite grains in fossil *Haliotis tuberculata*.

4.1.5 *Aequipecten opercularis*

XRD: Except for the 14 days alteration, the calcite content of the pristine, altered, and fossil material stays in the range 94 to 98 vol %. The 14 days alteration shows about 6 vol % more aragonite compared to the 7 days altered specimen, probably due to natural variation in the mineral composition of the starting material.

Table 4.5: Aragonite and calcite content values for the bivalve *Aequipecten opercularis* in vol %, as determined by X-ray diffraction and subsequent Rietveld refinement.

Aequipecten opercularis	aragonite [vol %]	calcite [vol %]
pristine	2.63 ± 0.28	97.37 ± 0.28
4 days	3.28 ± 0.32	96.72 ± 0.93
7 days	4.55 ± 0.46	95.45 ± 2.13
14 days	11.72 ± 1.23	88.28 ± 1.61
28 days	1.77 ± 0.48	98.23 ± 1.42
fossil	5.71 ± 0.08	94.29 ± 1.83

AFM and SEM: SEM images of the pristine material show the multi-faceted texture (figure 4.1.5.a) and an overall low porosity. After 4 days there is a multitude of fractures and a heightened porosity (figure 4.1.5.b and c). Except of slight dissolution marks, SEM and AFM data of the 4 days and 7 days altered specimen show no notable change to the pristine microstructure and nanostructure. Even after 14 days the shell still shows the characteristics of the primary ultrastructures (figure 4.1.5.d), pointing to a missing or weak amalgamation. Generally, dissolution is prominent at the undulations on the shell´s outside, so that the domes of the mounds disappeared and only pointed peaks from the base of the pre-existing mound remains. Fine fractures along the course of the various ultrastructures, dissolution on the outer rim, and micro-porosity are also the prominent traits of the 28 days altered shell material (figure 4.1.5.e). Within the fossil material the traits of the primary ultrastructure, including the thin layer of aragonite on the inside of the shell, is still discernible and there is no sign of secondary grown calcite (figure 4.1.5.f and g). The material also shows the pointed peaks on the outer side of the shell, caused through dissolution in the area of the mounds (figure 4.1.5.h). The only notable difference to the alterations is the more compact nature of the fossil shell.

EBSD: In conformity with the SEM and AFM results, the EBSD maps of the 7 days altered specimen show no clear signs of overprint, but a good preservation of the ultrastructural characteristics (figure 4.1.5.i). Throughout all alterations the ultrastructure retains its characteristics, without signs of significant distortion of the primary ultrastructural features, signs of amalgamation, or the nucleation of secondary calcite (figure 4.1.5.j). What is observable is dissolution on the outer shell and a slight adaptation of orientations within the primary ultrastructure. Even in the fossil material the ultrastructural features are roughly preserved, while only some of the details vanished: The detailed band of aragonitic microstructure directly at the interface to the calcite layer is still discernible, even if hardly. The following zig-zag structure in the aragonite layer is practically gone. Both areas are now build-up of small roundish aragonite minerals. So, although the details of the respective ultrastructural units got lost, the mineralogy did not change and no calcitization occurred. The interface of aragonite to calcite is still very even and clear (figure 4.1.5.k and l).

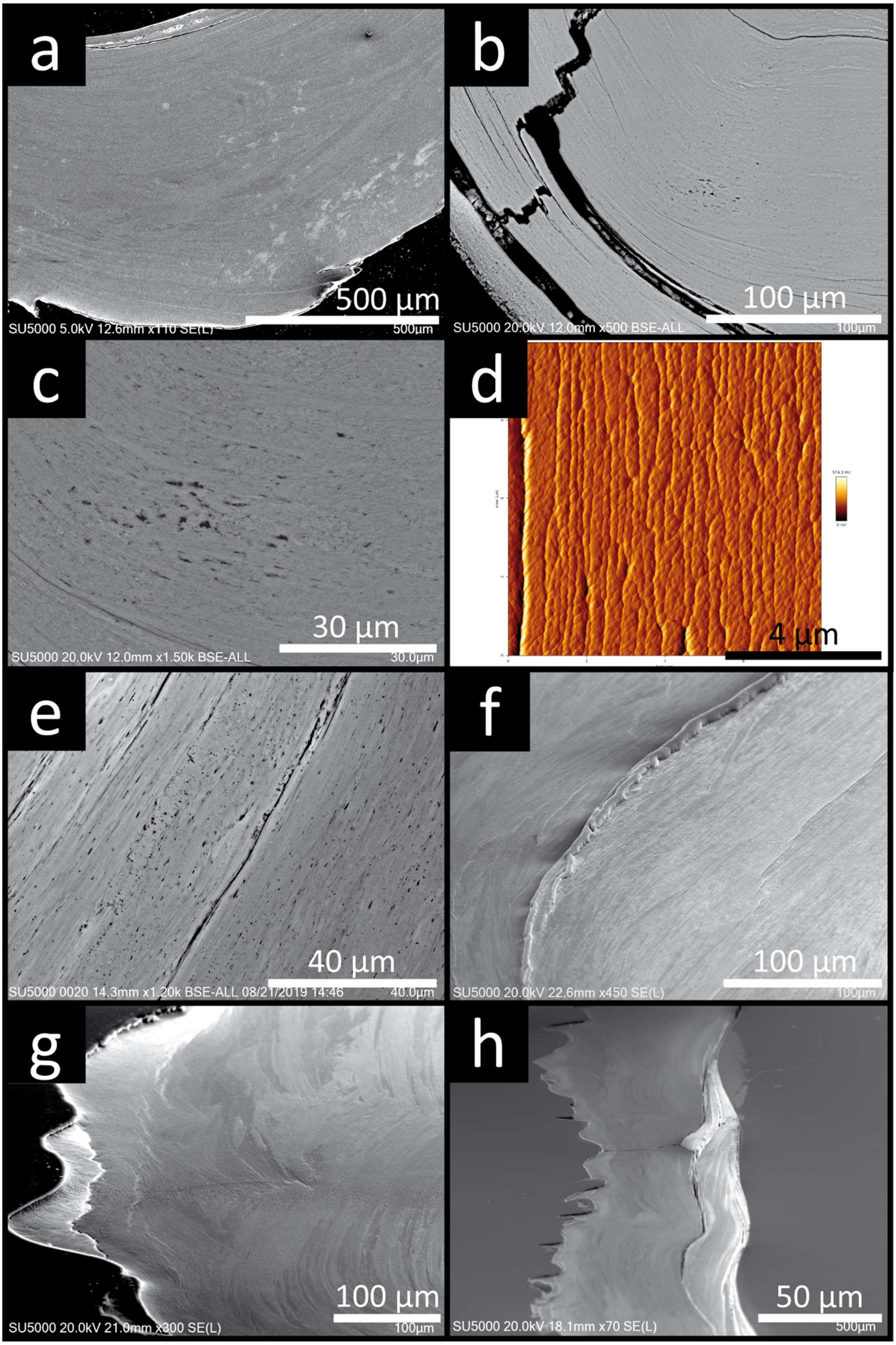
a
500 µm
SU5000 5.0kV 12.6mm x110 SE(L)
500µm
b
100 µm
SU5000 20.0kV 12.0mm x500 BSE-ALL
100µm
c
30 µm
SU5000 20.0kV 12.0mm x1.50k BSE-ALL
30.0µm
d
4 µm
e
40 µm
SU5000 0020 14.3mm x1.20k BSE-ALL 08/21/2019 14:46
40.0µm
f
100 µm
SU5000 20.0kV 22.6mm x450 SE(L)
100µm
g
100 µm
SU5000 20.0kV 21.0mm x300 SE(L)
100µm
h
50 µm
SU5000 20.0kV 18.1mm x70 SE(L)
500µm

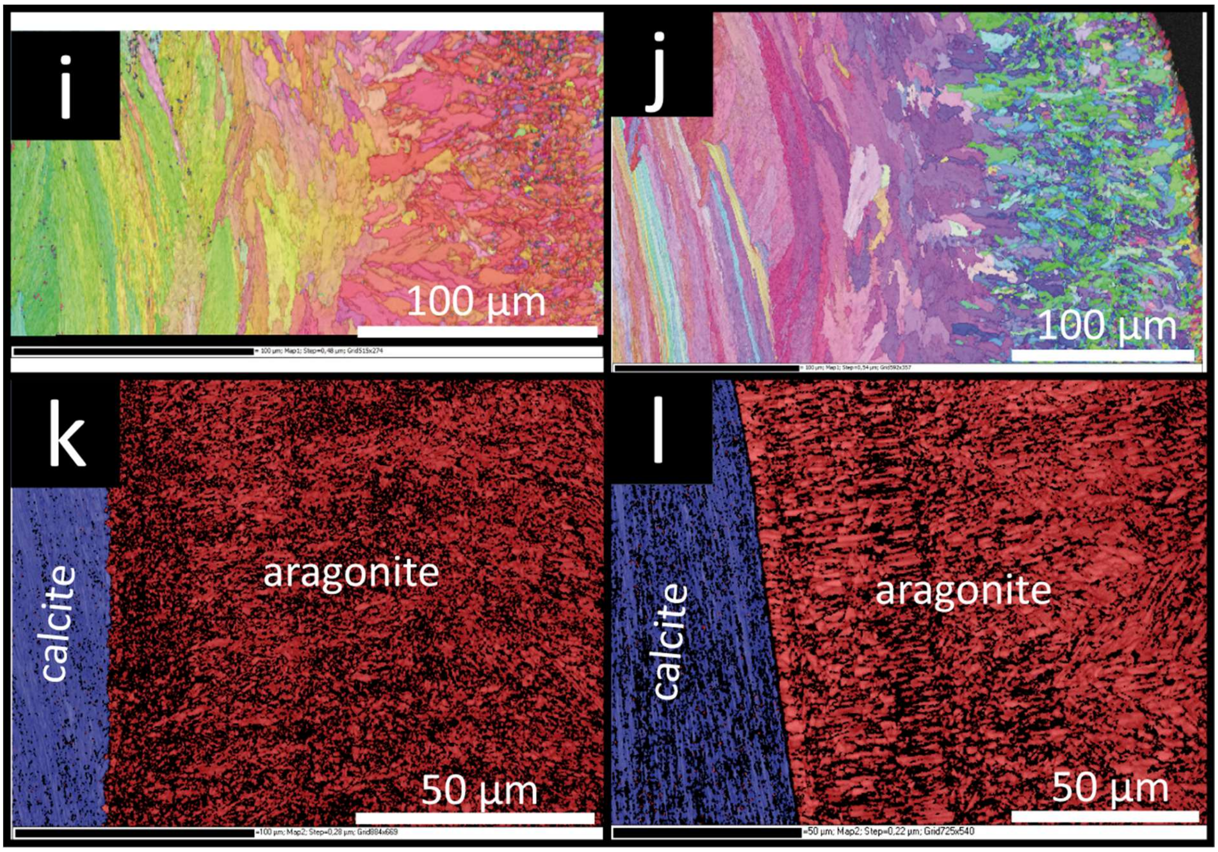

Figure 4.1.5: Microscopic analyses of *Aequipecten opercularis*: a) SEM image of texture of the pristine shell, b+c) SEM images of formation of fractures and secondary porosity after 4 d of alteration, d) AFM map of the preservation of the ultrastructural characteristics after 14 d of alteration, e) SEM image of high porosity and frequent fractures within the preserved ultrastructural features after 28 d of alteration, f+g) SEM images of the preservation of the primary ultrastructure and lack of calcitization in the fossil material, h) SEM image of the same dissolution pattern on the outer side of the shell in the fossil material as also found in the alteration experiments, i) EBSD orientation map (IPF colour code y-axis) of the low impact on the texture after 7 d of alteration, j) EBSD orientation map (IPF colour code z-axis) of an area with no obvious change after 28 d of alteration, k) EBSD phase map of the well preserved interface of the aragonitic and calcitic layers in the fossil specimen, l) EBSD phase map of the interface of the aragonitic and calcitic layers in the pristine material.

4.1.6 Inorganic monocrystals

To see possible differences in the reaction of organically and inorganically grown material during hydrothermal alteration and to help decipher the role of the alteration fluid, naturally grown aragonite and calcite monocrystals were added to the alteration series project. Two alterations were carried out for each mineral. One time with marine fluid, and one time with burial fluid. The temperature was set at 175 °C and the duration was 28 days.

Table 4.6: Aragonite and calcite content values for the inorganic materials, aragonite monocrystals and calcite monocrystals, in vol %, as determined by X-ray diffraction and subsequent Rietveld refinement. All samples were altered for 28 days at a temperature of 175 °C.

inorganic material, alteration fluid	aragonite [vol %]	calcite [vol %]
aragonite, burial fluid	95.61 ± 0.83	4.39 ± 0.87
aragonite, marine fluid	99.49 ± 1.65	0.51 ± 0.24
calcite, burial fluid	1.30 ± 0.58	98.70 ± 1.53
calcite, marine fluid	3.25 ± 1.26	96.75 ± 1.99

4.1.6.1 Inorganic aragonite, burial fluid

XRD: After 28 days of alteration of the aragonite hydrothermally altered in burial fluid, it presents a calcite content of over 4 vol % and an aragonite content of 96 vol %.

SEM: On the outer rim there are regions of dissolution (about 600 µm deep) while the newly emerged rim maintains the angles typical for the crystal lattice of aragonite (figure 4.1.6.a). Fine fissures are frequent in some areas, emanating from the areas of dissolution (figure 4.1.6.b). In the areas of dissolution, secondary calcite crystallites formed with sizes of mostly 25 x 20 µm, but up to 50 µm (figure 4.1.6.c).

EBSD: The EBSD orientation map shows that at the areas of dissolution the crystal develops deviations in the crystal orientation, breaking up the single crystal. Small grains of secondary calcite can be seen in these areas of dissolution (indicated in figure 4.1.6.d).

EDS: The Mg, Si, and Sr signature in the dissolving, fine grained aragonite is notably higher than in the main aragonite crystal (figure 4.1.6.e). Ca is pronounced in the main aragonite crystal and slightly showing in the secondary calcite, while the dissolving aragonite shows no signature. All mentioned signatures are distributed evenly in the respective phases.

4.1.6.2 Inorganic aragonite, marine fluid

XRD: XRD measurements for aragonite altered with marine fluid for 28 days show only 0.5 vol % of calcite and accordingly still 99.5 vol % aragonite.

SEM: The aragonite crystal altered with marine fluid shows quantitatively less dissolution than the aragonite altered with burial fluid. However, the dissolution did not form long straight edges (as it is the case in the aragonite altered with burial fluid) but created a very tattered outline (figure 4.1.6.f). Fissures are scarcely present, too (figure 4.1.6.g).

EBSD: Here, probably resulting from the tattered outline, the regions showing a rotation of the orientation at the areas of dissolution are more pronounced than in the aragonite altered in burial fluid (figure 4.1.6.h), but grains of secondary calcite are rarer than in the aragonite altered with burial fluid (Figure 4.1.6.i).

EDS: In the dissolving aragonite phase Mg, Si, Sr, and Al signatures are markedly higher (Figure 4.1.6.j), while Fe and O signatures are only slightly higher than in the main crystal. Ca and Yb present a strong signature in the main crystal and none in the dissolving material (figure 4.1.6.k). All these signatures are distributed evenly in the respective mineral phases.

4.1.6.3 Inorganic calcite, burial fluid

XRD: The calcite material hydrothermally altered in burial fluid for 28 days has about 99 vol % calcite.

SEM: The calcite altered with burial fluid presents a very good preservation. Dissolution is present along the rims of the crystal, however the notches resulting from the dissolution are very shallow and there is only little dissolving phase. Additional to dissolution on the surface, there are a multitude of small cavities within the material. Only a few fissures are present, that run along the cleavage planes (figure 4.1.6.l).

EBSD: The EBSD maps show thin parallel streaks with a small deviance in orientation.

EDS: Ca and Yb are distributed evenly in the material, but the outer edge where the dissolution occurs shows a thin and strong band of Mg and O (Figure 4.1.6.m).

4.1.6.4 Inorganic calcite, marine fluid

XRD: The XRD results for the calcite crystal altered in marine fluid for 28 days shows 97 vol % of calcite.

SEM: Dissolution appears predominantly on the outer rims, which subsequently are notably pitted (figure 4.1.6.n). The dissolving phase occurs as a thin band along the previous outline of the primary calcite crystal, leaving a gap to the resulted new surface area (figure 4.1.6.o). Frequent small cavities are present throughout the crystal. Fissures are quite rare, but broader than in the calcite crystal altered with burial fluid.

EBSD: Like in the calcite crystal altered with burial fluid, EBSD orientation maps reveal thin parallel streaks within the main crystal that present a different second orientation (figure 4.1.6.p).

EDS: The Ca and Yb signatures show evenly throughout the material, but there is a thin band of Cl and Na on some part of the outer edge and along a fissure. The band of Mg and O shows thicker and very notably on the outer edge within the dissolving material (figure 4.1.6.q).

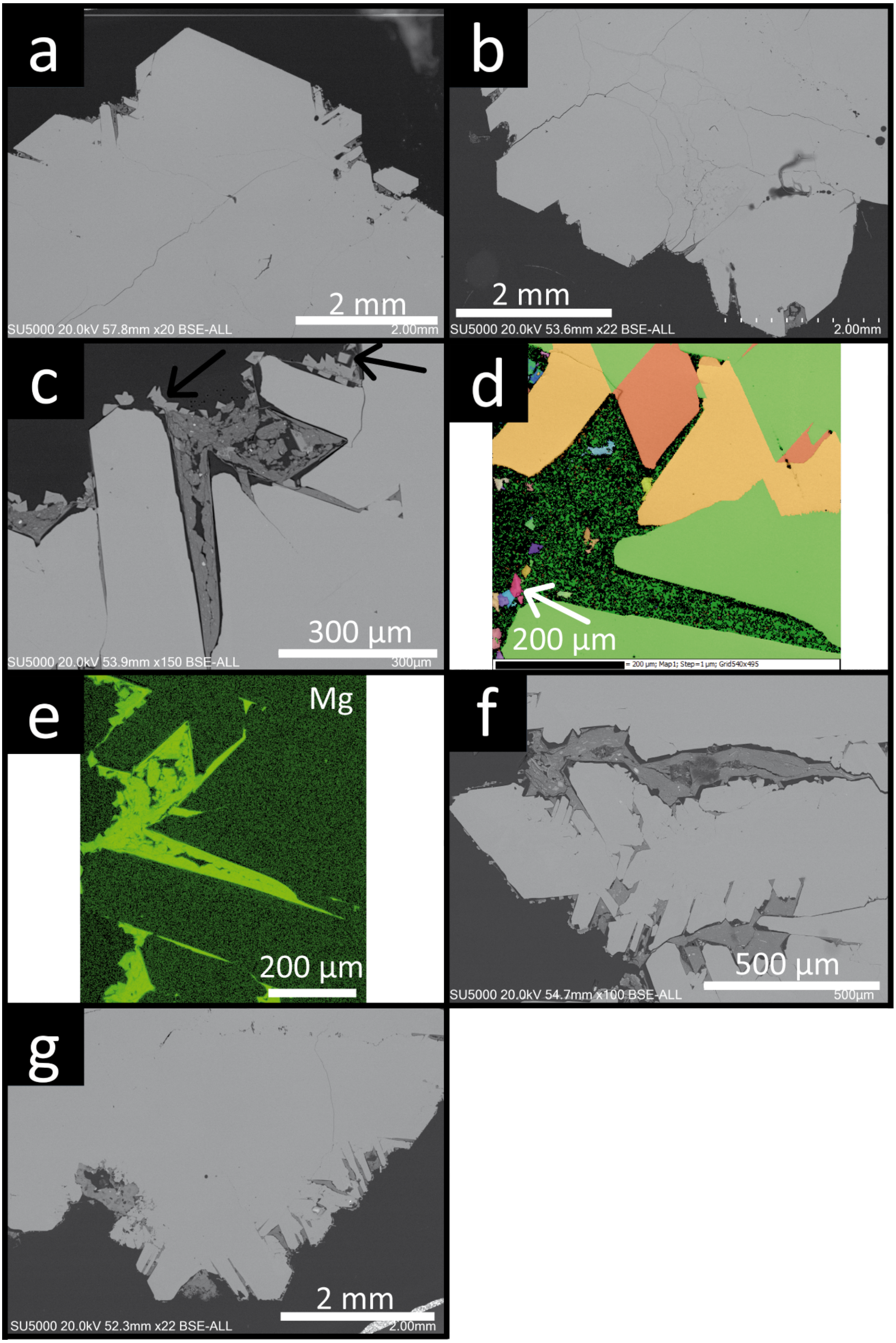
a
2 mm
SU5000 20.0kV 57.8mm x20 BSE-ALL
2.00mm
b
2 mm
SU5000 20.0kV 53.6mm x22 BSE-ALL
2.00mm
c
300 µm
SU5000 20.0kV 53.9mm x150 BSE-ALL
300µm
d
200 µm
= 200 µm; Map1; Step=1 µm; Grid540x495
e
Mg
200 µm
f
500 µm
SU5000 20.0kV 54.7mm x100 BSE-ALL
500µm
g
2 mm
SU5000 20.0kV 52.3mm x22 BSE-ALL
2.00mm

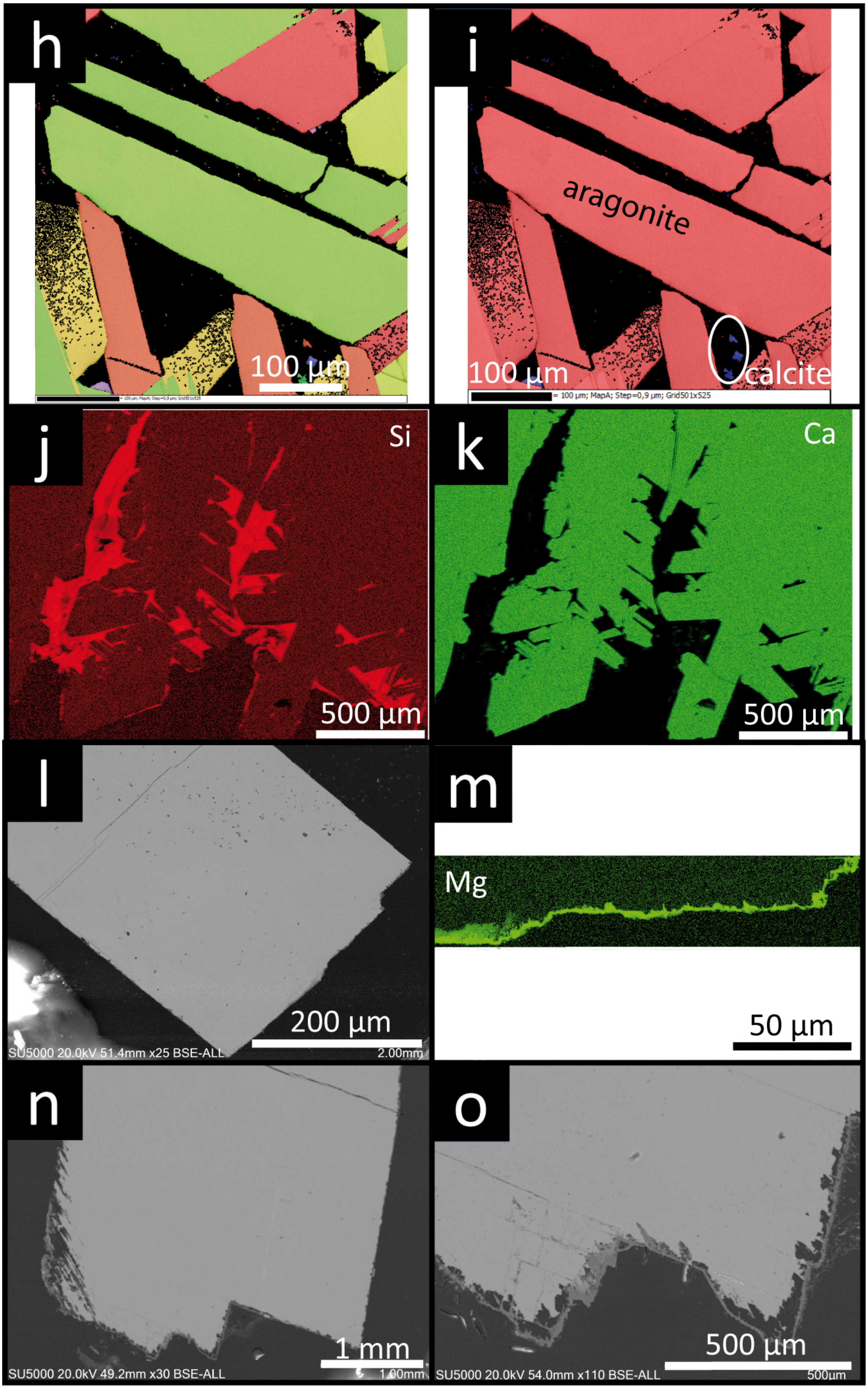
h
100 µm
= 100 µm; MapA; Step=0,9 µm; Grid501x525
i
aragonite
calcite
100 µm
= 100 µm; MapA; Step=0,9 µm; Grid501x525
j
Si
500 µm
k
Ca
500 µm
l
200 µm
SU5000 20.0kV 51.4mm x25 BSE-ALL
2.00mm
m
Mg
50 µm
n
1 mm
SU5000 20.0kV 49.2mm x30 BSE-ALL
1.00mm
o
500 µm
SU5000 20.0kV 54.0mm x110 BSE-ALL
500µm

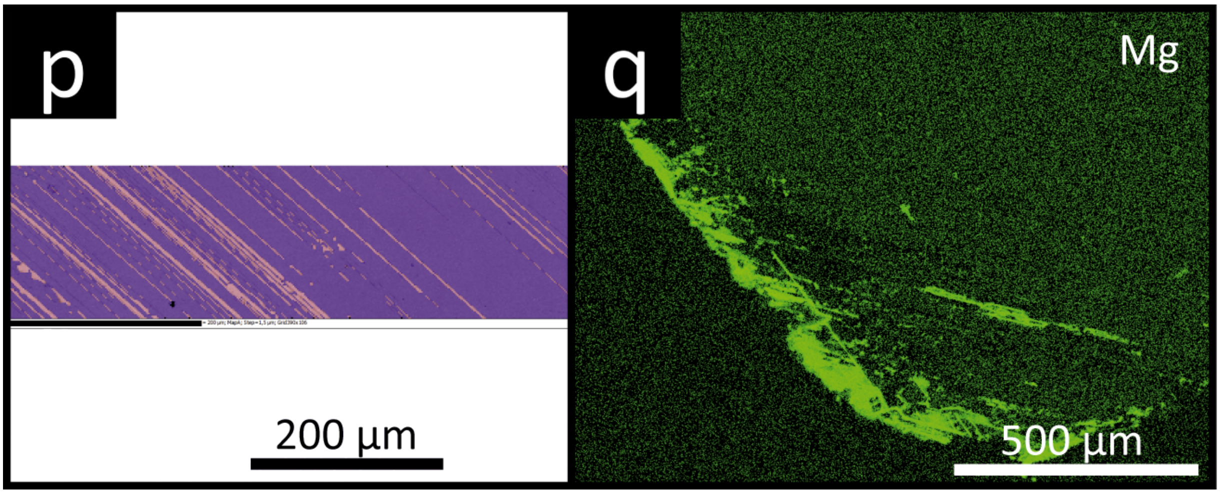

Figure 4.1.6: Microscopic analyses of the inorganic monocrystals: a) SEM image of 28 d altered aragonite (burial fluid) with regions of dissolution on the outer surface, b) SEM image of 28 d altered aragonite (burial fluid) with breakage emanating from the areas of dissolution, c) SEM image of 28 d altered aragonite (burial fluid) with small grains of secondary calcite on the outer edges in areas of dissolution, d) EBSD orientation map (IPF colour code x-axis) of 28 d altered aragonite (burial fluid) showing the development of deviant crystal orientations and the formation of secondary calcite, e) EDS map of 28 d altered aragonite (burial fluid) showing the high signal of Mg within the dissolving aragonitic material, f) SEM image of 28 d altered aragonite (marine fluid) showing the more aggressive dissolution patterns of the marine fluid resulting in a tattered outline, g) SEM image of 28 d altered aragonite (marine fluid) showing only few fissures, h) EBSD orientation map (IPF colour code x-axis) of 28 d altered aragonite (marine fluid) showing the more pronounced deviation in orientation in the areas of dissolution compared to the aragonite altered with burial fluid, i) EBSD phase map of 28 d altered aragonite (marine fluid) showing the alteration with marine fluid resulting in fewer grains of secondary calcite compared to the alteration with burial fluid, j) EDS map of 28 d altered aragonite (marine fluid) showing the heightened Si signature within the dissolving aragonitic phase, k) EDS map of 28 d altered aragonite (marine fluid) showing the Ca signature strong in the main crystal while non-existent in the dissolving phase, l) SEM image of 28 d altered calcite (burial fluid) showing only weak dissolution along the rims and few fissures that predominantly run along the cleavage planes, m) EDS map of 28 d altered calcite (burial fluid) showing a thin band of heightened Mg content on the outer edge where the dissolution occurs, n) SEM image of 28 d altered calcite (marine fluid) showing much more pronounced dissolution compared to the calcite altered with burial fluid, o) SEM image of 28 d altered calcite (marine fluid) showing a crust of dissolving calcitic material along the previous edges, p) EBSD orientation map (IPF colour code x-axis) of 28 d altered calcite (marine fluid) showing thin parallel strands of a deviant orientation within the main crystal, q) EDS map of 28 d altered calcite (marine fluid) showing the Mg signature significantly heightened in the dissolving phase.

4.2 Fossil project

For the fossil material no XRD analysis was applied, because the specimen in this category are brachiopods, the shell of which are comprised solely of calcitic ultrastructures and no aragonite. The description of the following specimen labelled “general overview” relates to the specifications that can be seen with the naked eye, but without any magnification tools. An overview on the analytical methods applied for the fossil project can be found in table 2.2 (page 16).

4.2.1 *Terebratula scillae* (V14b)

General overview: The overall state of preservation of this specimen is good, with the majority of both valves present. But the shell is thin and fragile with many cracks and plates chipping off. The inside of the shell is filled with loose sediment (figure 4.2.1.a).

SEM: The preserved ultrastructure of the shell is a fibrous layer with frequent punctae. Dissolution marks can be seen at the outer surfaces of the shell (figure 4.2.1.b).

EBSD: The only present ultrastructure consists of fibres with frequent punctae (figure 4.2.1.c). Strong merging is present throughout the shell (figure 4.2.1.d). Sub-parallel to the edge lies a band that presents a strong distortion of the material, so that the outlines of the merged mineral units are very undulating and tattered (see arrow in figure 4.2.1.c). This brachiopod species possesses punctae, which however are not filled with secondary calcite. An area of partially merged fibre strands of approximately 250 x 175 µm presents a high MUD value of 641 (area of the map in figure 4.2.1.d).

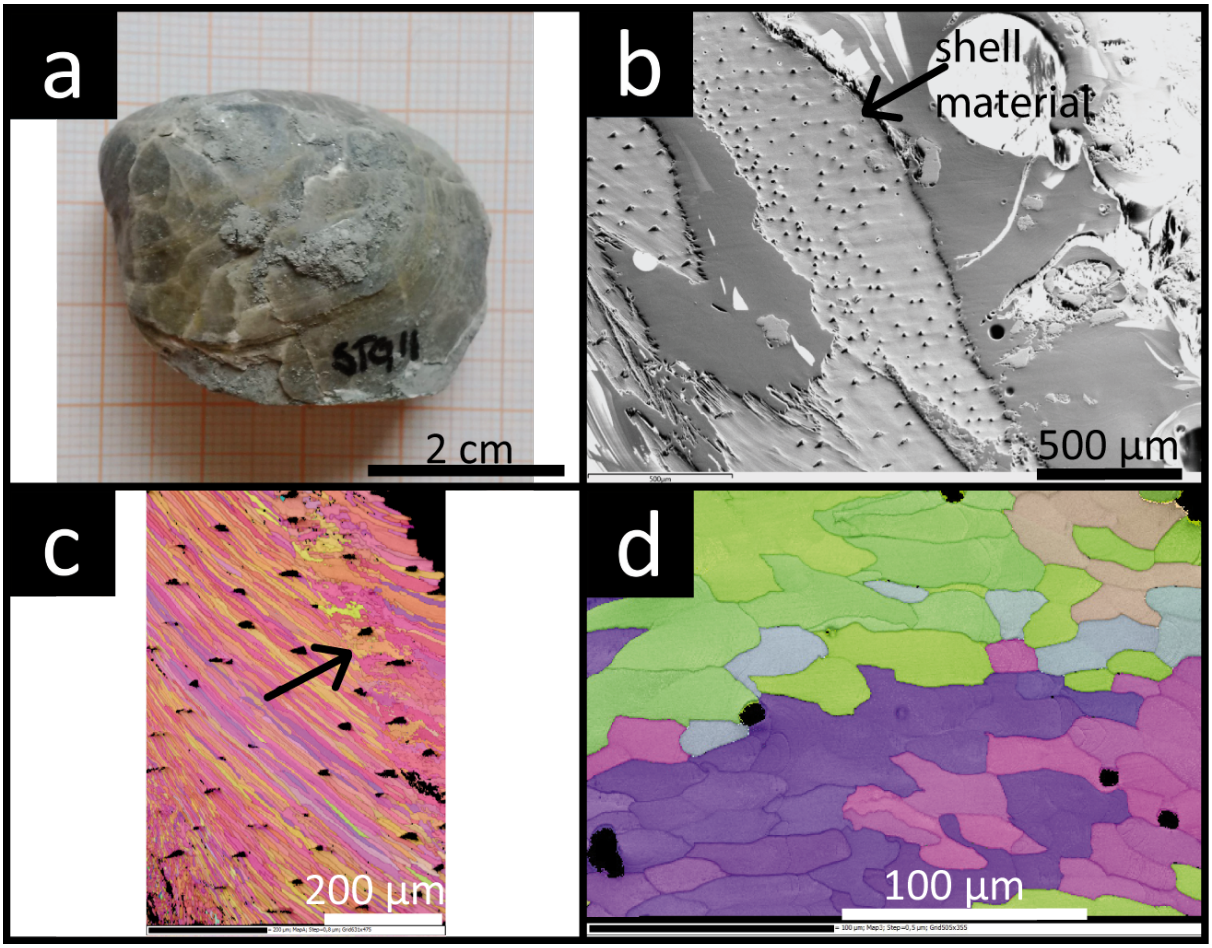

Figure 4.2.1: Photo and microscopic analyses of fossil *Terebratula scillae* (V14b): a) photo showing the majority of the shell material preserved, but chipping off, b) SEM image of the shell with frequent punctae and heavy dissolution, c) EBSD orientation map (IPF colour code x-axis) of the well preserved fibrous shell material with a band of strongly disturbed material, but no calcitization, d) EBSD orientation map (IPF colour code y-axis) of strong amalgamation of the fibres.

4.2.2 *Gigantoproductus* sp. (V2b)

General overview: The material of the specimen received consists of a ~2 cm thick and ~16 cm wide slice of one valve. No visible rock matrix is attached to the shell. The preservation of the cut section is good with no visible fractures or chipping of the shell (figure 4.2.2.a).

SEM: SEM images evince the large-scale mineral units of the columnar ultrastructure (figure 4.2.2.b). Regionally enhanced porosity can be found in the second, much more finely grained ultrastructure (figure 4.2.2.c).

EBSD: Two ultrastructures were detected through the EBSD maps. On the outer edge an approximately 200 µm thick primary layer can be found, consisting of small elongated mineral units, situated perpendicular to the shell´s surface (figure 4.2.2.d). Strong merging is present in the primary ultrastructure. Also within the primary layer but at the interface to the secondary layer, which consists of columnar mineral units, recrystallization in the form of bands of small granular secondary calcite can be found (figure 4.2.2.e). The most part of the preserved shell is made up of a layer of rather large columnar mineral units (figure 4.2.2.f). The columnar units also stand perpendicular to the shell´s surface and make up the majority of the shell´s thickness. The internal orientation of one columnar unit shows faceting and a gradient shift. While amalgamation and recrystallization can be found within the primary layer, the columnar layer presents a very low overprint. In the columnar layer no recrystallization can be found and distortion is not or only faintly present.

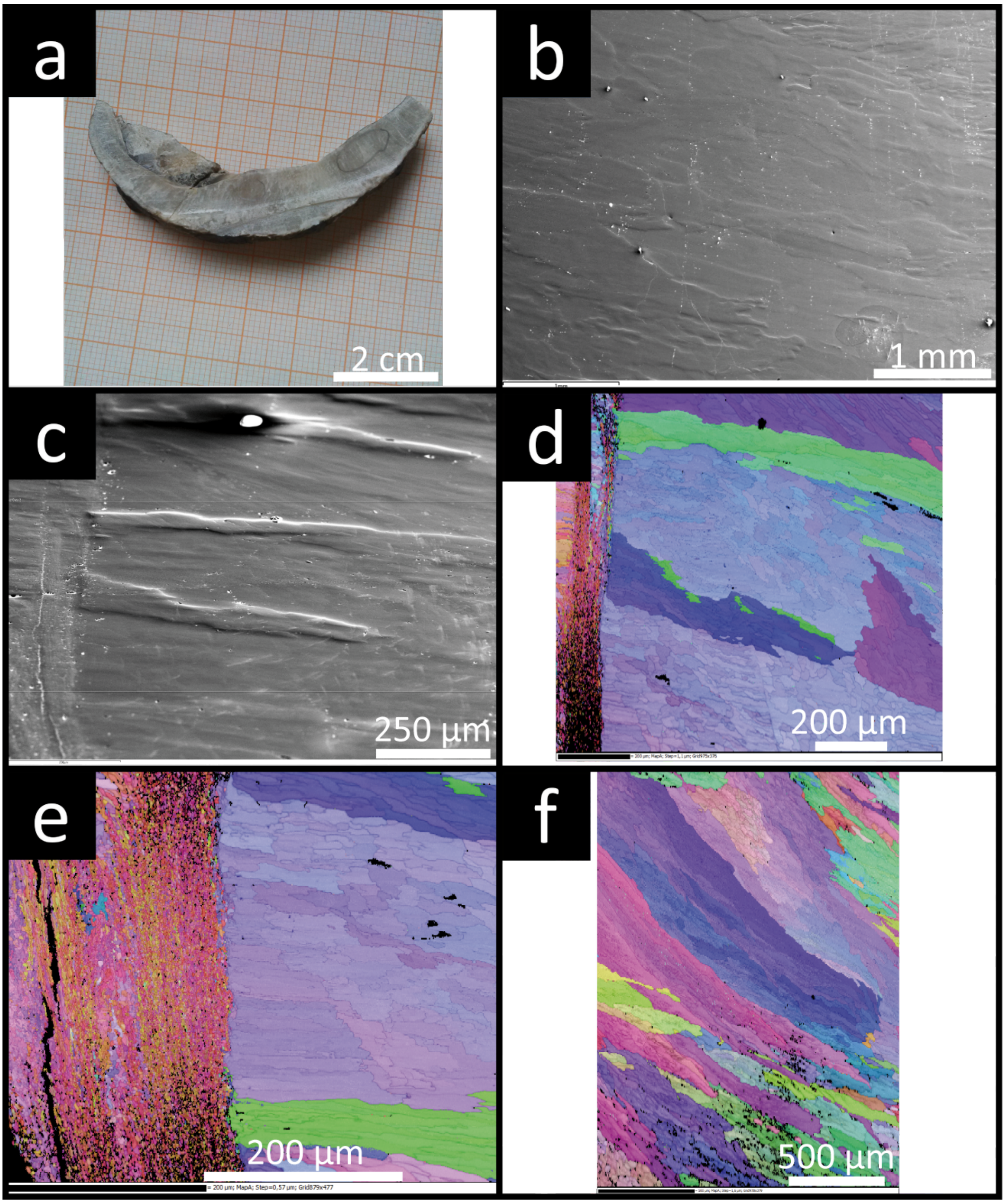

Figure 4.2.2: Photo and microscopic analyses of fossil *Gigantoproductus* sp. (V2b): a) photo showing the thickness of the shell, b) SEM image of columnar mineral units, c) SEM image of finely grained second ultrastructure attached to the columnar layer, d) EBSD orientation map (IPF colour code x-axis) showing the primary as well as columnar layer, e) EBSD orientation map (IPF colour code x-axis) of the band of recrystallized material within the primary layer at the interface to the columnar layer, f) EBSD orientation map (IPF colour code x-axis) of the large-scale mineral units of the columnar layer and their good preservation.

4.2.3 *Tetractinella trigonella* (V1a)

General overview: From this species a bulk of 9 specimens were obtained, which are all very well preserved and show both valves. However, the shell material is not completely preserved, there are some bits broken off and some rounded edges. On the outside of the shell there is not much rock matrix, but on the inside the shell is completely filled (figure 4.2.3.a).

SEM: SEM images of the prepared specimen exhibit a fibrous ultrastructure with the typical mushroom-shapes, although some slight merging is visible (figure 4.2.3.b).

EBSD: There is one type of ultrastructure preserved, which is a fibrous layer (figure 4.2.3.c). These mineral units show signs of alteration, such as occasional distortion of the typical mushroom-shape of the fibres as well as slight amalgamation, and breakage (figure 4.2.3.d). At the boundary of the shell to the internal rock matrix, the fibres merge into larger grains. There is no formation of secondary calcite within the shell material.

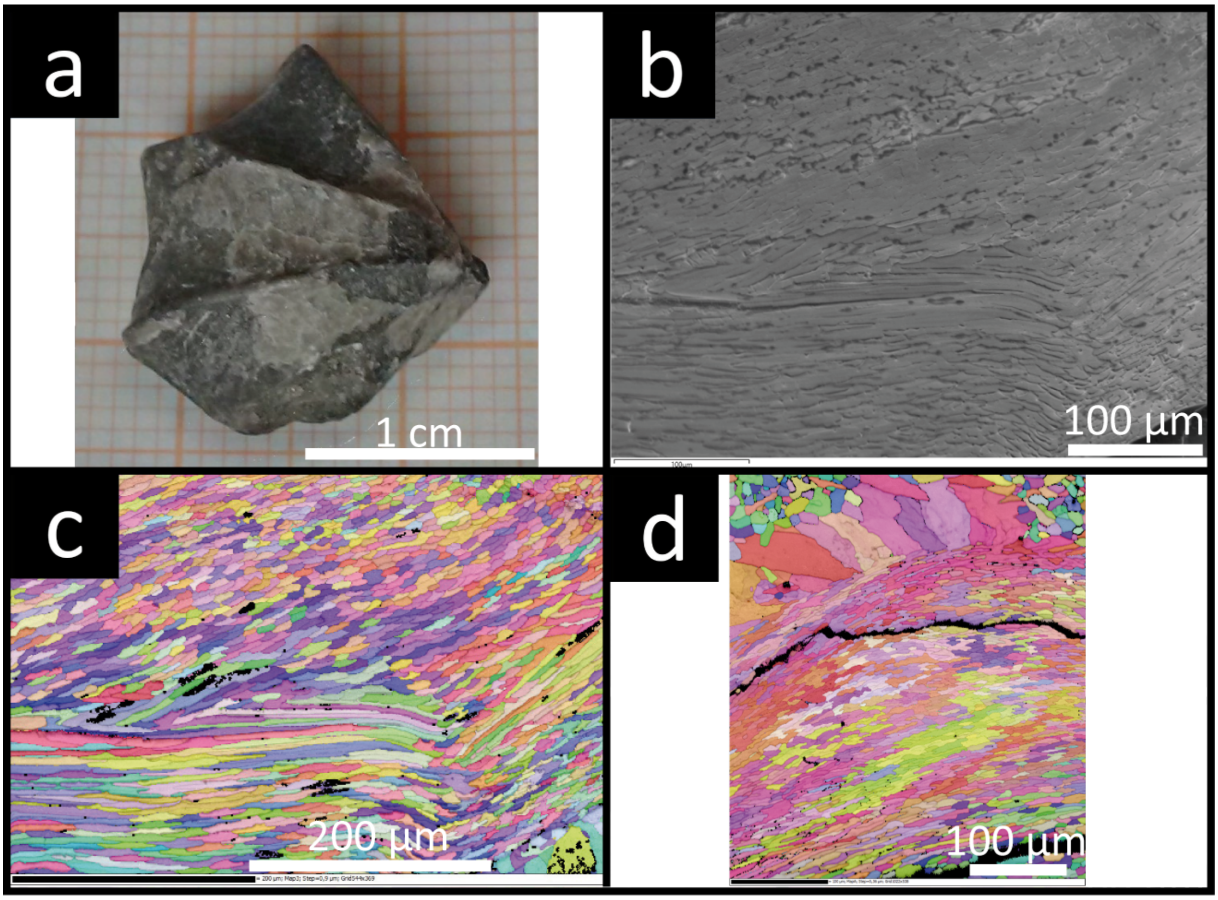

Figure 4.2.3: Photo and microscopic analyses of fossil *Tetractinella trigonella* (V1a): a) photo showing analyzed sample with both valves preserved, b) SEM image of well preserved fibres, c) EBSD orientation map (IPF colour code y-axis) of fibres showing only slight amalgamation, d) EBSD orientation map (IPF colour code x-axis) of another region within the fibrous layer showing breakage and stronger amalgamation.

4.2.4 *Hunzina electa* (V3a1)

General overview: From this species a bulk of 10 specimens were obtained, of which two were examined, with the dedicated sample numbers V3a1 and V6a (for the results on this specimen see the following chapter 4.2.5). All specimens of the bulk consist of the ventral valve and rock matrix, which is attached to the inside of the shell. The shape of the specimens is well preserved with the major part of the ventral valves preserved, but breakage points to a strong diagenetic impact (figure 4.2.4.a).

EBSD: One ultrastructure was found in this specimen: a columnar layer. The material presents a generally strong overprint, exhibiting wide fractures (figure 4.2.4.b), a strong distortion of the primary texture, and frequent and large grains of secondary calcite (figure 4.2.4.c).

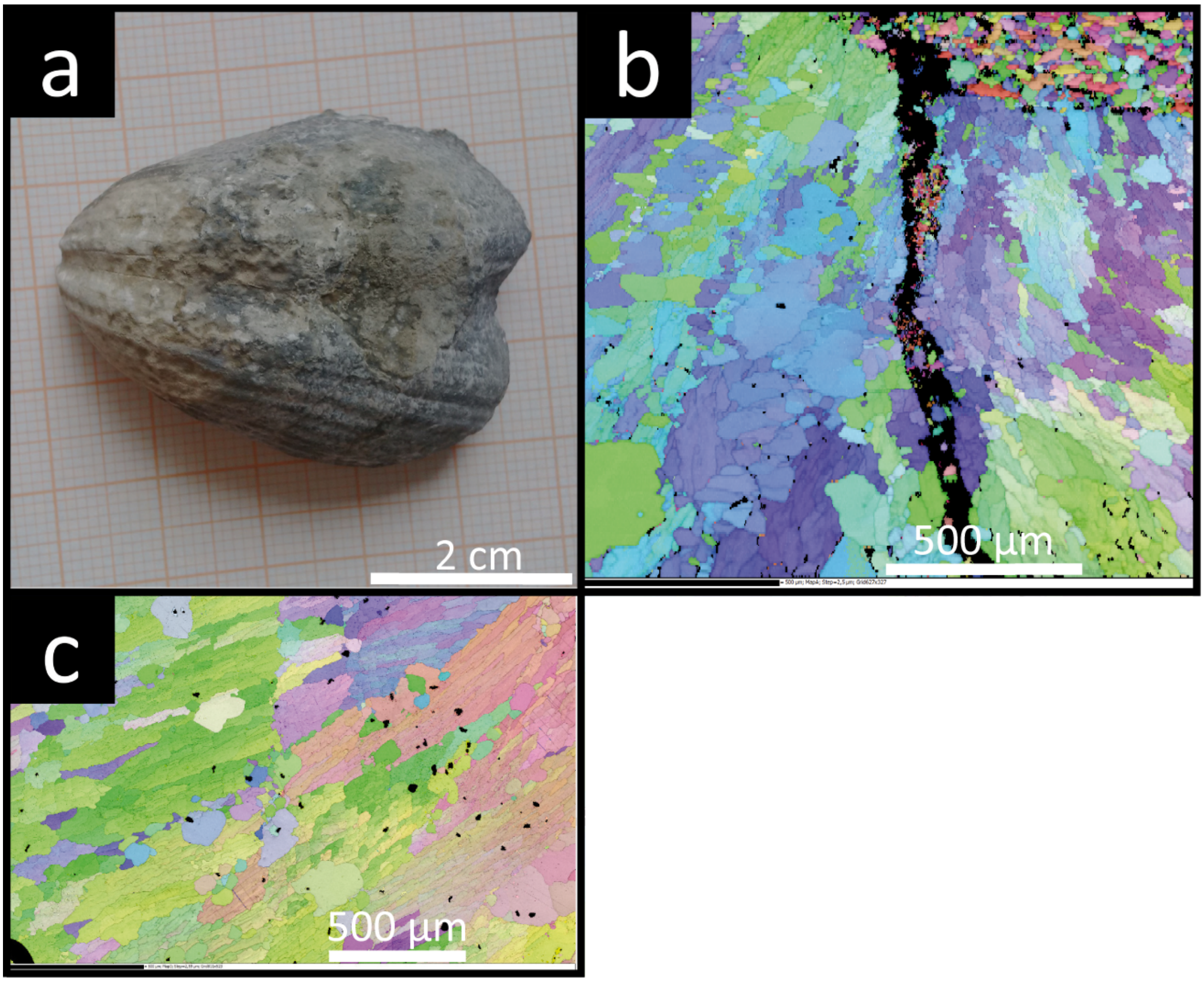

Figure 4.2.4: Photo and microscopic analyses of fossil *Hunzina electa* (V3a1): a) photo showing the ventral valve with most of the shell material preserved, b) EBSD orientation map (IPF colour code x-axis) of the columnar ultrastructure showing gaping fractures with recrystallized material in the cavities, c) EBSD orientation map (IPF colour code y-axis) showing frequent grains of secondary calcite throughout the shell.

4.2.5 *Hunzina electa* (V6a)

General overview: As described in the previous chapter 4.2.4, the samples of the bulk material of this species consist of the ventral valve and rock matrix which is attached to the inside of the shell. The shape of the specimens is well preserved with the major part of the ventral valves preserved (figure 4.2.5.a).

SEM: The SEM images show the columnar mineral units of the preserved shell and a small remnant of the presumable fibrous layer at the outer edge of the specimen (figure 4.2.5.b). Only very few fibres are preserved while the major part was dissolved or has been broken off. The remnants of the fibrous layer are strongly disturbed and fractured. Secondary calcite can already be found within the columnar layer, and after a maximal thickness of the preserved shell material of about 2 mm, the columnar mineral units become entirely substituted by the recrystallized secondary calcite on the inside of the shell (figure 4.2.5.c). Fissuring proceeds vertically from the outer surface inwards, penetrating through the shell material into the rock matrix.

EBSD: In this specimen the columnar layer as well as a small remnant of a second highly disturbed presumable fibrous layer were preserved (figure 4.2.5.d). Although the disturbance of the columnar ultrastructure appears to be not as strong as in the specimen V3a1, there is more secondary calcite present in this sample (indicated in figure 4.2.5.e). On one outer edge there is a very thin band (50 – 100 µm) of finely grained material, presumably the strongly altered fibrous layer.

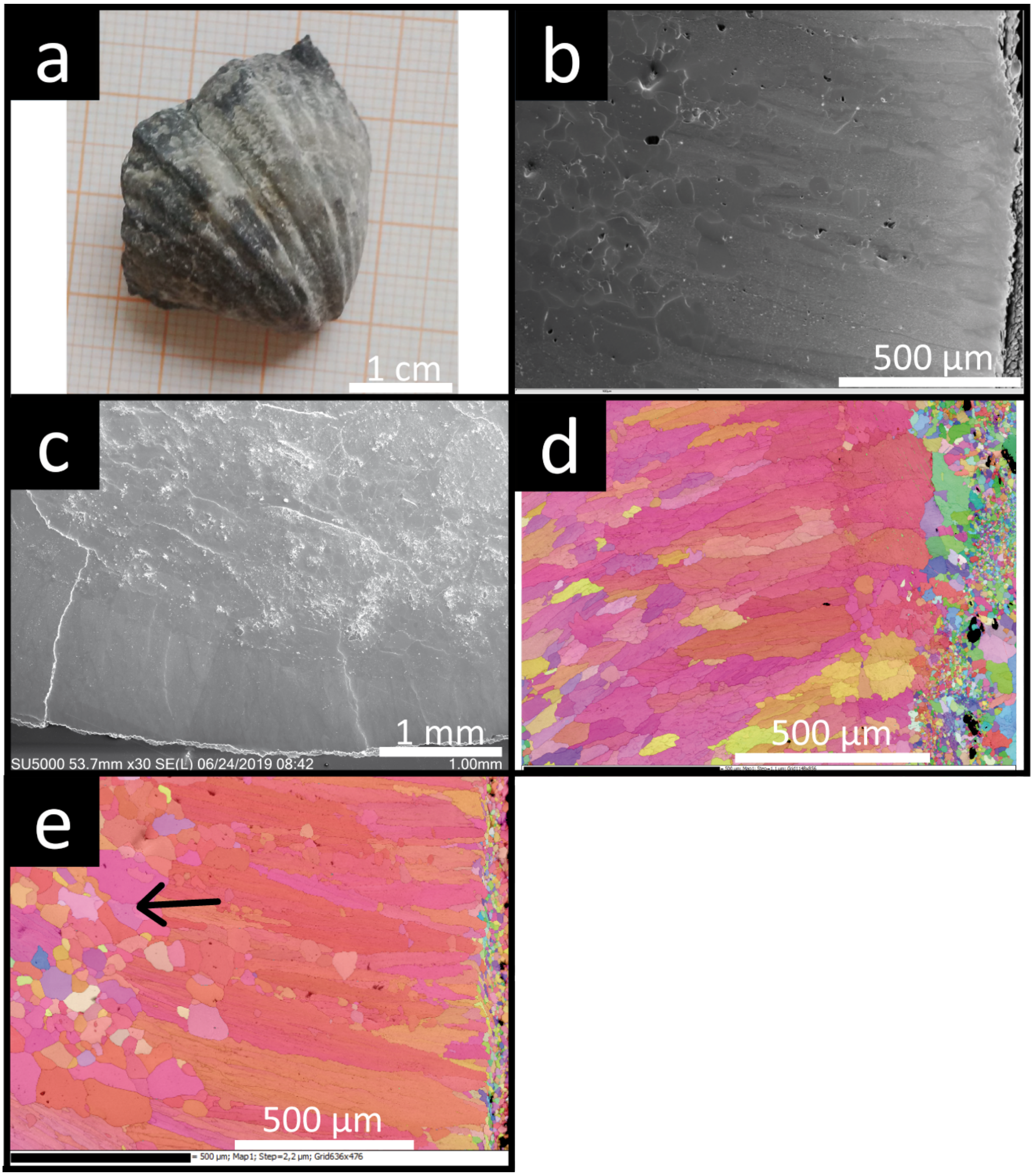

Figure 4.2.5: Photo and microscopic analyses of fossil *Hunzina electa* (V6a): a) photo showing the ventral valve with most of the shell preserved, b) SEM image of the columnar ultrastructure and a smaller grained second ultrastructure at the edge region, c) SEM image showing the thickness of the shell, the thin band of small-grained mineral units, and the thick columnar layer interlocked with the rock matrix, d) EBSD orientation map (IPF colour code x-axis) showing the columnar layer and the highly disturbed second ultrastructure, e) EBSD orientation map (IPF colour code x-axis) showing a large number of secondary calcite grains (arrow) within the columnar layer.

4.2.6 *Trigonotreta lyonsensis* (V41)

General overview: This sample was received as a relatively small fracture of a thick shell with a sawn off part. The available material belongs to a dorsal valve, but it was too small to make a further statement on the state of preservation (figure 4.2.6.a).

SEM: The small portion of the shell that represents this specimen shows large fractures and areas of dissolution (figure 4.1.6.b).

EBSD: The only preserved ultrastructure consists of fibres. Amalgamation is strong throughout the shell, but the fibrous character is still discernible in some parts. However, in the areas of contact to grains of secondary calcite the fibres are distorted and amalgamated beyond recognition (figure 4.1.6.c). Within the larger grains of secondary calcite (up to roughly 100 µm) pressure twins (e-twins) are present (indicated in figure 4.1.6.c). Despite the disturbance of the fibrous ultrastructure through the strong overprint, the crystallographic orientations within the shell are strongly bundled, so that a MUD value of 215 for an area of approximately 1300 x 900 µm including a grain of secondary calcite was measured (area of the measured map in figure 4.1.6.c).

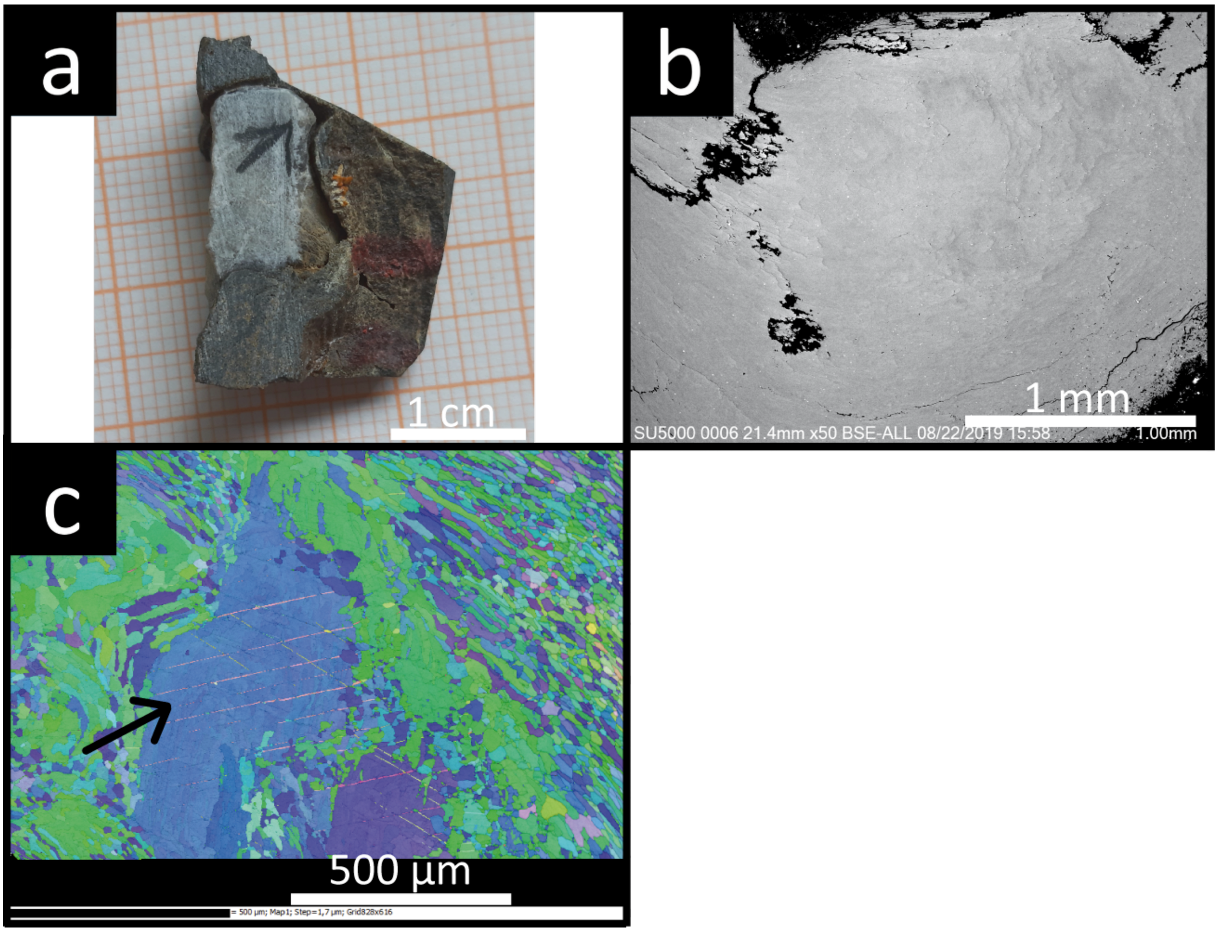

Figure 4.2.6: Photo and microscopic analyses of fossil *Trigonotreta lyonsensis* (V41): a) photo showing the small fraction preserved within the rock matrix with the arrow indicating the analyzed area, b) SEM image of the shell presenting strong dissolution and frequent fractures, c) EBSD orientation map (IPF colour code x-axis) showing the fibrous ultrastructure with strong disturbance in the area of grains of secondary calcite, which present pressure twinning (arrow).

4.2.7 *Trigonotreta larghii* (V49)

General overview: The shell of this specimen is only preserved in parts of one valve and was obtained cut in half through the umbo. A considerable part of the shell is broken off and the remaining shell surface is fractured and tattered. Rock matrix is attached to the inside of the shell (figure 4.2.7.a).

SEM: SEM images show three ultrastructural units: a primary layer, fibres, and columns. The primary layer is very thin and shows signs of dissolution and overprint (figure 4.2.7.b). A very fine porosity can be seen, amplified along fissures (figure 4.2.7.c). The fibrous and columnar layers, although easily discernible as such, also present signs of strong overprint. While within the fibrous layer some distortion of the pristine shapes as well as amalgamation can be found, the columnar layer shows very frequent twinning (figure 4.2.7.d)

EBSD: Although looked at it by the naked eye the preservation of the sample seems poor, the EBSD maps proof the preservation of three types of ultrastructures (figure 4.2.7.e). Directly on the rim of the shell lies a thin primary layer of approximately 30 – 50 µm. It consists of slightly elongate grains with divergent orientations, standing perpendicular to the shell´s surface. The primary ultrastructure shows strong amalgamation and disturbance (figure 4.2.7.f). Adjacent to the primary layer lies the fibrous layer. Although the type of ultrastructure is clearly discernible, fracturing and a heightened level of amalgamation is present while no formation of secondary calcite seems to have happened (figure 4.2.7.g). The third ultrastructure is the columnar layer with large oblong crystal units arranged perpendicular to the surface of the shell. This columnar layer boasts extensive pressure twinning (figure 4.2.7.h and i). A detailed examination of the relative crystallographic orientation of the twins (done for all specimens presenting twins) revealed that they are exclusively e-twins emerged from high pressure conditions (Lippmann 1973).

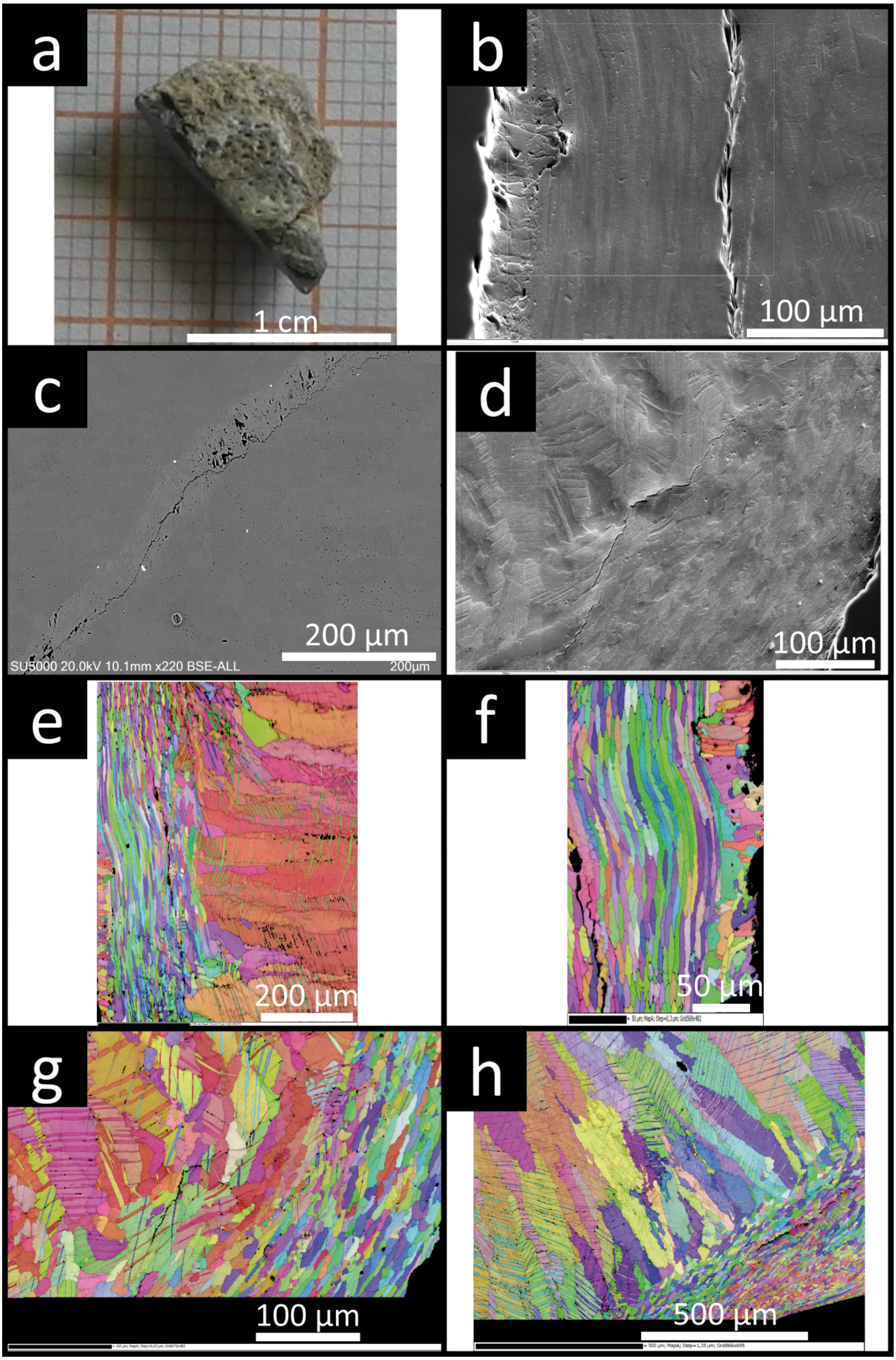
a
1 cm
b
100 µm
c
200 µm
SU5000 20.0kV 10.1mm x220 BSE-ALL
200µm
d
100 µm
e
200 µm
f
50 µm
g
100 µm
h
500 µm

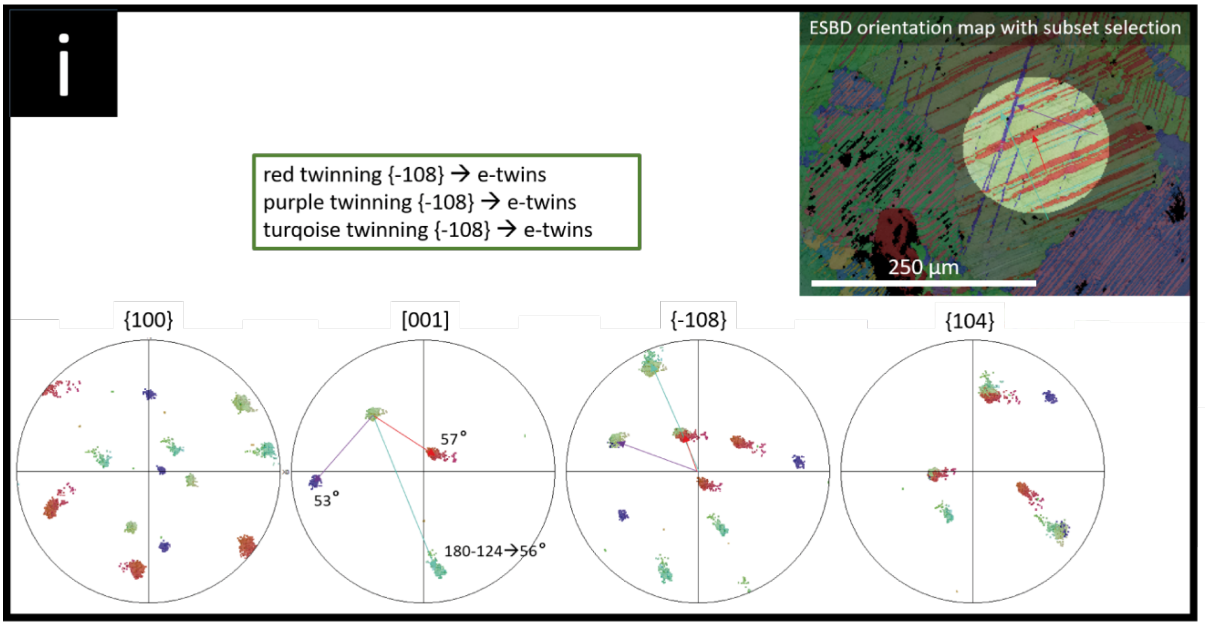

Figure 4.2.7: Photo and microscopic analyses of fossil *Trigonotreta larghii* (V49): a) photo showing the small portion of the valve with relatively poor preservation, b) SEM image of all three preserved ultrastructural units, c) SEM image of fine porosity, which is heightened along a fissure, d) SEM image of amalgamation within the fibrous layer and twinning within the columnar layer, e) EBSD orientation map (IPF colour code x-axis) of the three preserved ultrastructures: primary, fibrous, and columnar (left to right), f) EBSD orientation map (IPF colour code x-axis) showing amalgamation, disturbance, and dissolution of the primary ultrastructure, g) EBSD orientation map (IPF colour code z-axis) showing the strong diagenetic impact on the columnar and fibrous layers, h) larger EBSD orientation map (IPF colour code y-axis) showing the extent of pressure twins in the columnar layer, i) EBSD orientation map and pole figures for calculation of the angle of the twinning in respect to the main grain.

4.2.8 *Gypospirifer* sp. (V42)

General overview: This specimen consists of a relatively small fraction of a ventral valve around the umbo, while the commissural region is only preserved in some areas as a rough imprint. Characteristics like the elongate shape and the ridges are identifiable. Rock matrix is attached to the inside of the shell (figure 4.2.8.a).

SEM: SEM images show a columnar ultrastructure making up the whole preserved shell material, which presents a thickness of up to 3 mm. While the outer edge of the shell is even, at the inner side of the shell the columnar mineral units interlock with the rock matrix (figure 4.2.8.b). Fractures are very frequent and run mostly perpendicular to the shell´s surface (Figure 4.2.8.c).

EBSD: The EBSD maps show the columnar mineral units with strong pressure twinning (e-twins) and regions of dissolution (figure 4.2.8.d).

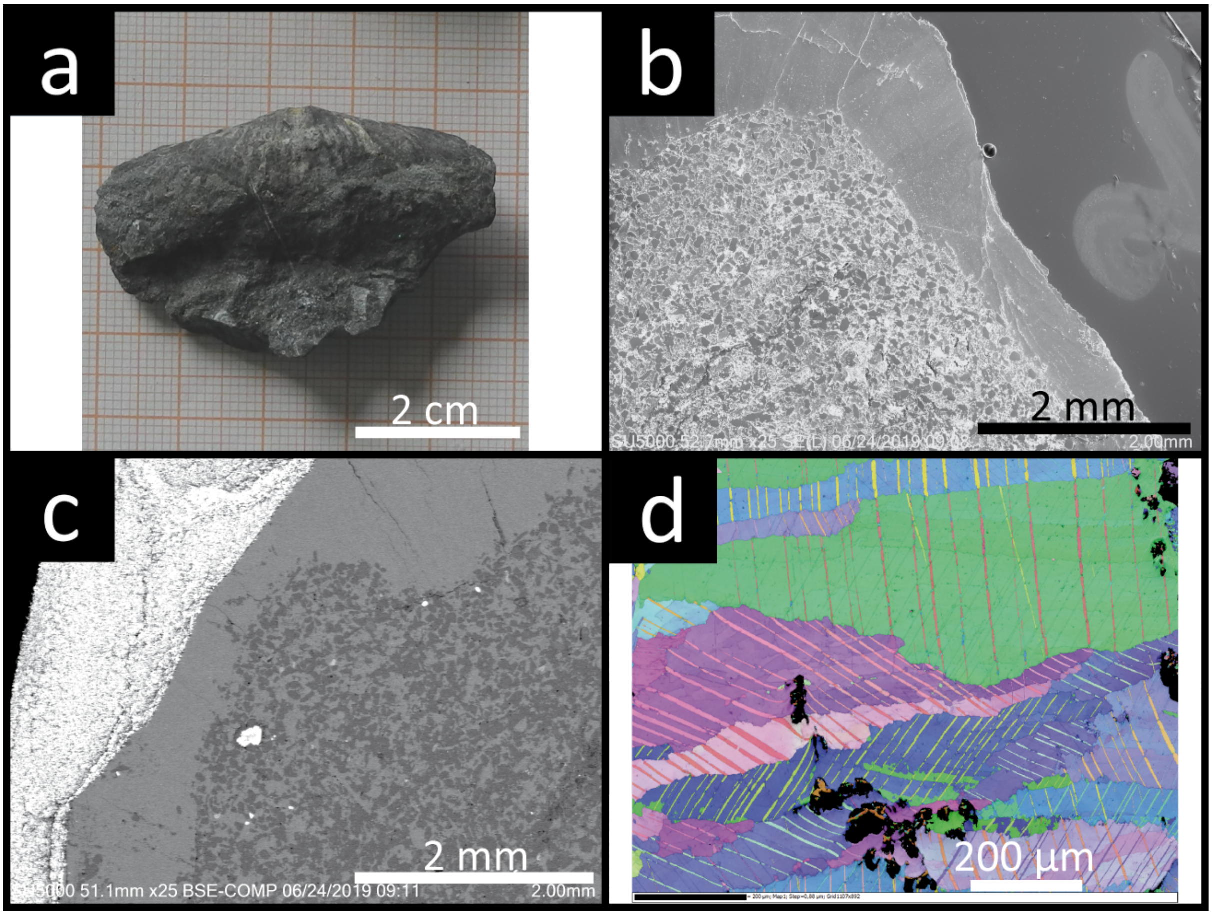

Figure 4.2.8: Photo and microscopic analyses of fossil *Gypospirifer* sp. (V42): a) photo showing the preserved material around the umbo of a ventral valve, b) SEM image as an overview showing the shell interlocked with the rock matrix on the inside of the shell, c) SEM image showing frequent fractures perpendicular to the shell´s surface, d) EBSD orientation map (IPF colour code z-axis) showing a columnar ultrastructure with extensive pressure twinning.

4.2.9 *Afghanospirifer* sp. (V46)

General overview: The specimen is a fraction of a ventral valve with shell material preserved in most places so that the overall shape and the ridges are discernible. On the inside the shell is attached to a rock matrix (figure 4.2.9.a).

SEM: The SEM images show that the preserved shell material is composed of the large mineral units of a columnar layer (figure 4.2.9.b) presenting a very fine porosity and excessive twinning (figure 4.2.9.c). On the inner side the shell material is interlocked with the attached rock matrix. Breakage is common with the frequent fractures going in all directions.

EBSD: The EBSD measurements present a variety of details. Firstly, two ultrastructures were found: next to the columnar layer a thin band of a presumable fibrous layer can be seen (indicated in figure 4.2.9.d). The fibrous layer is only maximally 50 µm thick and the fibres´ shapes are strongly disturbed. Secondly, strong fracturing is present throughout the material.

Thirdly, excessive and multi-directional pressure twinning (e-twins) is present within the larger grains (figure 4.2.9.e). Fourthly, recrystallization of the pre-existing material through secondary calcite can be found as singular small crystals, but also large clusters; even in the columnar layer.

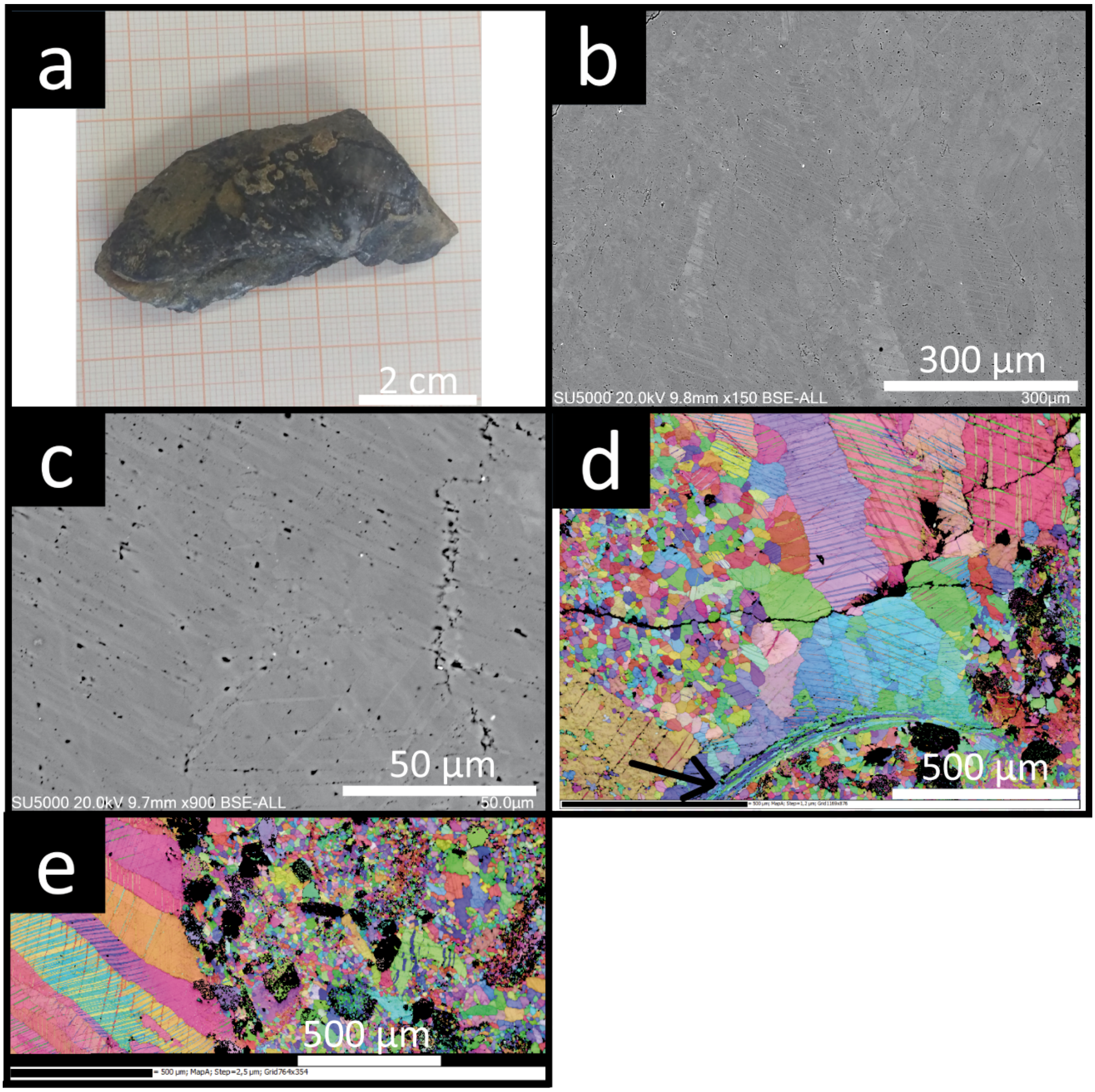

Figure 4.2.9: Photo and microscopic analyses of fossil *Afghanospirifer* sp. (V46): a) photo showing the part of the preserved ventral valve showing an umbo and ridges, b) SEM image of a columnar ultrastructure, c) SEM image of the fine porosity and extensive twinning within the columnar layer, d) EBSD orientation map (IPF colour code z-axis) of the columnar layer with fractures and large patches of secondary calcite, but also showing a second preserved ultrastructure, a presumable fibrous layer (arrow), e) EBSD orientation map (IPF colour code x-axis) showing the extensive twinning within the large grains of the columnar ultrastructure.

4.2.10 *Alispirifer* cf. *middlemissi* (V50)

General overview: The sample was received as a small cut-off irregular fraction in a cuboid of rock matrix of roughly 15 x 10 x 5 mm. The intense fracturing of the material points to a strong diagenetic impact, but a further determination of the state of preservation is not possible without analytical methods (figure 4.2.10.a).

SEM: As the SEM images disclose, the shell material has a maximal thickness of about 1.4 mm. The little shell material preserved is broken in two pieces and presents a multitude of fissures (figure 4.2.10.b). Dissolution is present and very extensive in some areas in conjunction with the fissures. The majority of the preserved material seems to consist of a columnar layer showing twinning (figure 4.2.10.c) and fine fissures (figure 4.2.10.d). In one place a very small (~ 0.2 x 1 mm) remnant with a different ultrastructure is attached to the columnar layer (indicated in figure 4.2.10.b). This second ultrastructure consists of elongate, slightly wavy mineral units, appearing to be fibres but not unequivocally determinable in the SEM images (figure 4.2.10.e).

EBSD: The EBSD maps reveal a high co-orientation within the columnar layer (figures 4.2.10.f and g). Pressure twins (e-twins) are present within this ultrastructure, but the columnar mineral units do not show any other obvious disturbance. The second type of ultrastructure shows the much smaller and elongate grains of the presumable fibrous layer (figure 4.2.10.h). Compared to the columnar layer, this ultrastructure is strongly disturbed and altered through amalgamation.

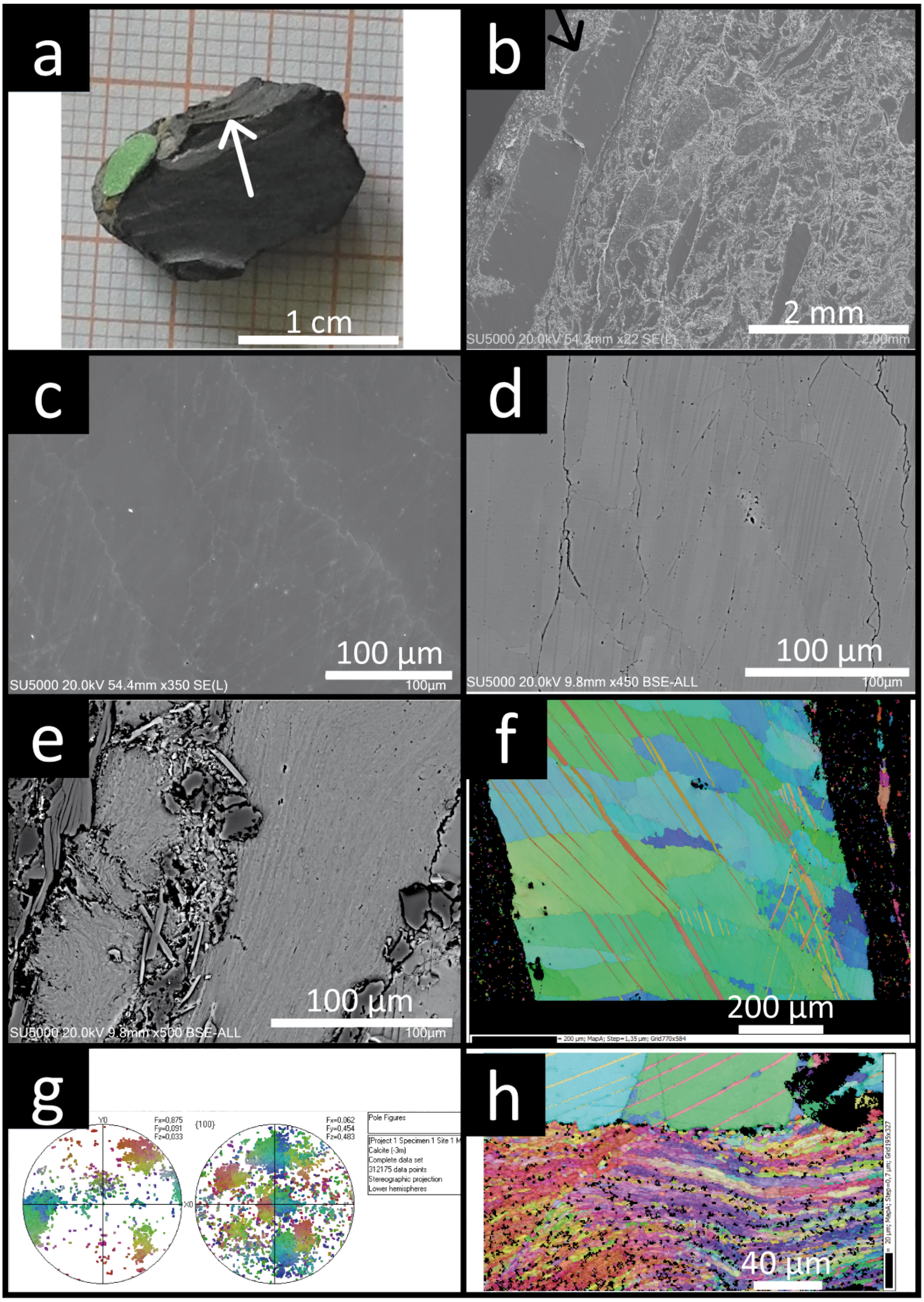

Figure 4.2.10: Photo and microscopic analyses of fossil *Alispirifer* cf. *middlemissi* (V50): a) photo showing the small fraction of the preserved shell material, b) SEM image showing the strong breakage and dissolution, arrow indicating the small remnant of a second ultrastructural unit, c) SEM image of the columnar layer with extensive pressure twinning, d) SEM image showing frequent very fine fissures, e) SEM image of the second ultrastructure of presumable fibres, f) EBSD orientation map (IPF colour code y-axis) of the columnar layer presenting a still very high co-orientation, g) calcite pole figure belonging to the map in image f, showing the bundling of the orientations for the columns (green/ blue) and pressure twins (red/ yellow), h) EBSD orientation map (IPF colour code y-axis) of the presumable fibrous, but certainly strongly overprinted ultrastructure attached to the columnar layer.

5 Discussion

As it is always the case in nature, there are a myriad of factors that play into these processes of diagenetic alteration. Not all can be heeded. For one, the environment in which the diagenetic overprint occurs can be extremely complex and parameters can change repeatedly. But also in the laboratory experiments there are sources for discrepancies. For one, the work material has been taken from nature and therefore shows natural variations, but also the experimental setup or the machines can be subjected to irregularities.

Natural variation is an important building block of evolution and, luckily, can not be removed. Therefore, it is a scientist´s objective to, although not measurable, consider these factors when evaluating results.

5.1 Alteration series project

5.1.1 Sequence

Despite the numerous differing types of ultrastructures from the many species, a generally valid succession of occurrences can be observed in all alterations. The changes follow the same order (figure 5.1), but they can overlap and slightly vary in strength and scope due to the different factors such as thickness of the shell, fluid chemistry, duration, organic content, mineralogy, or pore system.

This succession of occurrences can be categorized into three levels.

Level 1 takes place nearly instantly after the beginning of overprint. The organic matter, like the organic sheath hemming the fibres in the bivalve *Mytilus edulis*, or the extensive network of biopolymer fibrils in the prismatic ultrastructure of the extant gastropod *Haliotis ovina*, disintegrates and leaves an interconnected web of secondary porosity, expanding the pre-existing primary porosity. Also at this stage, fissures and breakage can occur (mechanical disintegration), depending on the pressure conditions and a possible susceptibility of some features. One according example of such a feature is the highly organic sheath at the interface of the two ultrastructures of *Mytilus edulis,* which, with the disintegration of the organics, leaves such a wide gap, so that the material regularly separates along this line.

Level 2 comprises the amalgamation and consequential distortion of the mineral units of the various ultrastructures, while the primary phase principally remains preserved. Both processes are based on the dissolution and reprecipitation of the mineral phase in contact with the alteration fluid. With the expanded pore system comes an increase of the surface area and the percolation of the alteration fluid, leading to an upsurge in dissolution. After and during dissolution, the process of reprecipitation takes place in the cavital space, leading to the amalgamation of the primary mineral units of the existing ultrastructure. A consequence of amalgamation is the distortion of the characteristic shape of the pristine biogenic mineral units. Through the ongrowth of the new material the outline of the biogenic mineral units becomes more rounded. In further process of the merging of two or several mineral units with a similar orientation, larger compounds develop that mostly show no resemblance to the primary material. Additionally, with the physical amalgamation of the mineral units, their crystallographic orientations gradually assimilate until the compound presents one singular orientation. An in-depth breakdown of the process of amalgamation is given in the following chapter 5.1.2.

Level 3 begins with the nucleation of secondary calcite. The newly nucleated secondary calcite grows independently to the pre-existing mineralogy as an inorganically formed calcite. If given the right conditions and enough space, it can form relatively large grains with a high crystallinity. The nucleation process begins predominantly in the remaining cavital space and after a notable amalgamation. This secondary calcite phase denotes the start of calcitization of the pre-existing material through the progressive growth of the secondary calcite pending the replacement of the primary mineralogy, resulting in the loss of primary ultrastructural features. Additionally, through the spreading of the new mineral grains, the cavities are being filled out, leading to a decrease in porosity. Hence, the maximally overprinted shell presents a dense material consisting of large secondary calcite grains presenting a relatively high crystallinity (Shearman and Fuller 1969) (figure 5.2).

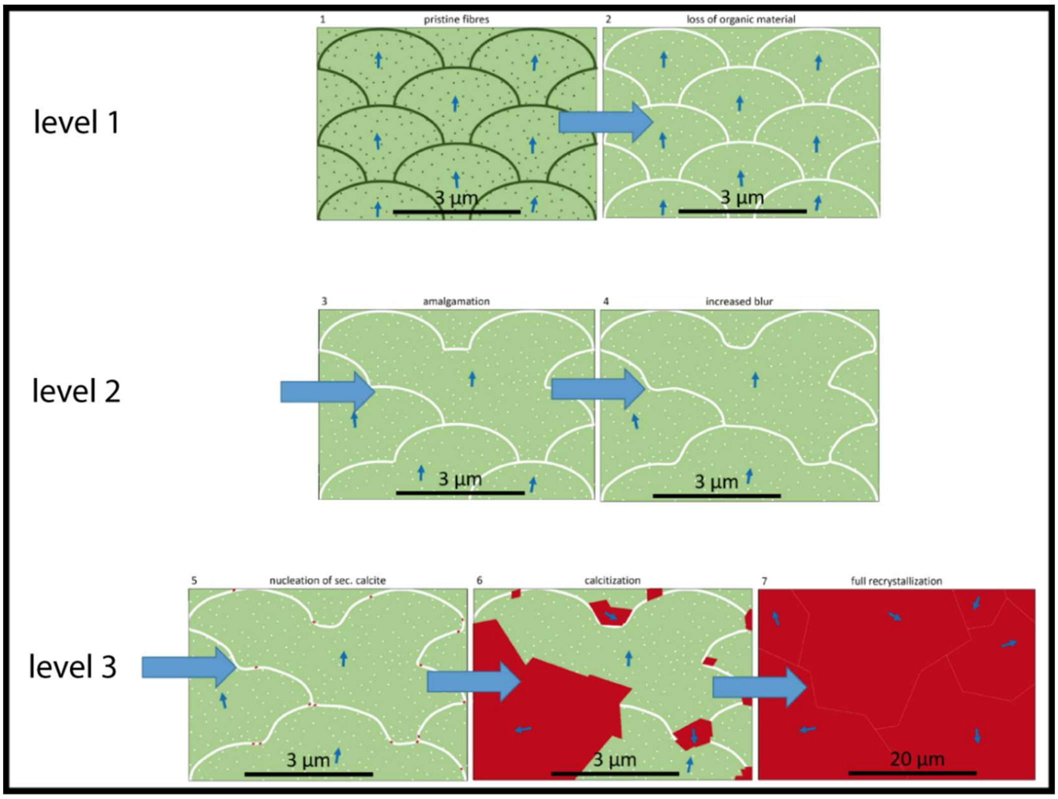

Figure 5.1: Schematic sketch of the typical sequence of the diagenetic impact as observed in the alteration series as well as the fossil material on the example of a fibrous ultrastructure.

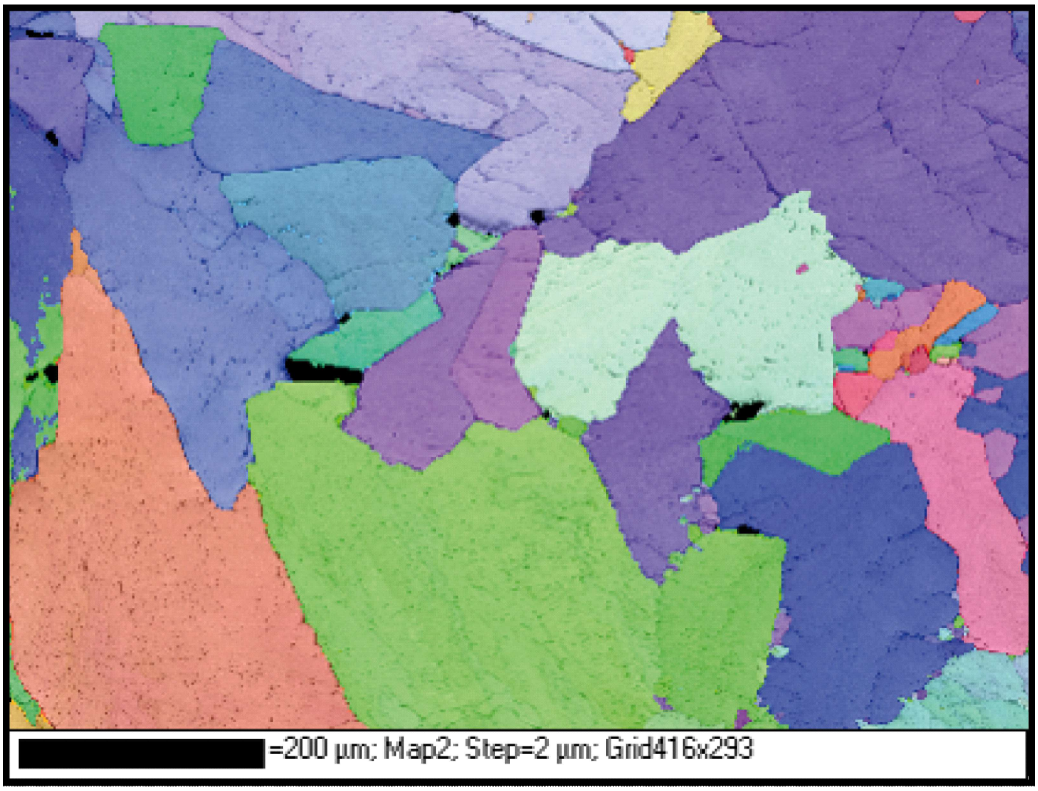

Figure 5.2: EBSD orientation map (IPF colour code x-axis) showing how a typical completely overprinted biogenic material could look like, example of *Haliotis ovina* altered for 14 d in marine fluid.

5.1.2 Amalgamation

In this work the term „amalgamation“ is used to describe the process of biogenic mineral units merging with neighbouring biogenic mineral units during natural diagenesis or laboratory-based hydrothermal alteration (mimicking of natural diagenesis). This process begins after the loss of the organic matter and the subsequent expansion of the pore network along with the enhanced percolation of the alteration fluid. The underlying principles are the dissolution of the primary material in contact with the alteration fluid and the reprecipitation of the dissolved material onto the surface of the biogenic mineral units while adapting its crystallographic orientation (homoepitactic ongrowth) (Casella et al. 2018a). This leads to a minimization or elimination of grain boundaries and complies with the principle for minimal Gibbs free energy.

The dissolution and reprecipitation leads to a change of textural intricacies. The characteristic primary shape of the biogenic mineral unit becomes more rounded and distorted until, with the connection of two or more mineral units, larger compounds form, which are even more unequal to the primary texture. It is also to note that, due to the addition of the secondary inorganically grown material and the change of the texture, and despite the retention of the mineral phase and crystallographic orientation, a material impacted by amalgamation has to be considered secondary.

5.1.3 Calcitization

Typically, after the process of organic disintegration and amalgamation starts the process of calcitization. It begins with the nucleation of secondary calcite grains, chiefly in the open cavital space where the flux of the supersaturated fluid is high and space is abundant. Especially for aragonitic starting material space is an important factor, for calcite (density of calcite: 2.71 g/cm^3) has a lower density as aragonite (density of aragonite: 2.93 g/cm^3) and hence needs more space for the same amount of material (Northwood and Lewis 1968).

With ongoing growth, the secondary inorganic calcite starts to replace the pre-existing, often amalgamated material. Unlike amalgamation, calcitization can engender a change in mineralogy, in addition to changes in crystallographic orientation and the loss of ultrastructural features (Casella 2018).

There is still some debate on the designation of this process, for sometimes the pre-existing material already contains calcite. This pre-existing calcite, however, is of biogenic origin while the secondary calcite which forms in the course of a diagenetic overprint is inorganic and thus more stable. Tucker and Wright (1990) and others (e.g. Rabier et al. 2008) apply the more general term “neomorphism”, which has been introduced by Folk (1965), for this “process of replacement and recrystallization” with a “change in mineralogy”, but include calcitization, including the biogenic calcite to inorganic calcite transformation, as a process of neomorphism. Middleton defines the term “calcitization” in the Encyclopedia of Sediments and Sedimentary Rocks (Middleton et al. 2003) as follows: “Calcitization is the transformation of any mineral to calcite and as such can be a type of recrystallization (calcite to calcite), replacement (e.g. anhydrite to calcite) or neomorphism (aragonite to calcite)”. This is the definition applied in this work.

5.1.4 Resistance

There are four factors of the biogenic material that affect the response of the material to alteration, that were established in the course of this work. One of these factors is the organic matter. Its content and distribution have an influence on the formation of the secondary porosity, but also of fissures and larger cracks, up to the separation of parts of the shell. The experiments on the bivalve *Mytilus edulis* are an excellent example for that, for in every experimental setup the shell separated along the organic-rich shift between the nacreous layer and the fibrous layer (figure 5.3). These breakages allow the flow of the alteration fluid and provide ample additional surface area for the fluid to expedite the overprint process. Furthermore, it supplies free space for the nucleation and growth of secondary calcite. As seen in the experiments on the gastropod *Haliotis ovina*, the organic rich layer between the two ultrastructural units was always the region of the first nucleation of secondary calcite (figure 4.1.4). A contrary example would be the alteration experiments on the stony coral *Porites* sp. as well as the inorganic monocrystals. In this material there is overall minimal or no organic content, effectuating a high resistance to alteration.

Closely interlinked to the organic matter is the factor porosity. It acts similarly to the breakage described in the last chapter. Interconnected, open pore space increases the percolation rate of the fluid and allows the penetration into the material. The result is an enhanced and broadly distributed overprint. In the fibrous layer of *Mytilus edulis* this effect shows in the rapid amalgamation of the fibres after the loss of the organic sheath enveloping the singular fibre strands. Within the inorganic monocrystals that possess no organic matter and hence form no pore system, the overprint proceeds from the only surface area exposed to the alteration fluid, the external side, while the inner areas are mainly unaffected in that way.

The third factor is the mineralogy. The underlying principles of this is the solubility of the different phases. An aragonitic starting material possesses a higher solubility as the arising calcite phase. In the process of dissolution of the aragonitic phase, the alteration fluid becomes undersaturated with regard to aragonite while supersaturated with regard to calcite (Casella 2018, Morse et al. 2007).

The texture is the fourth factor. The organically guided growth of the fibres, nacre tablets, prisms and other various ultrastructural units is not in accordance with the principle of Gibbs free energy, especially after the loss of the organic matter (Casella 2018). During the life of the organism it can uphold the texture, but after death and induced through diagenesis the material becomes subjected to the environmental influences and reshapes into its ideal form of minimal free energy.

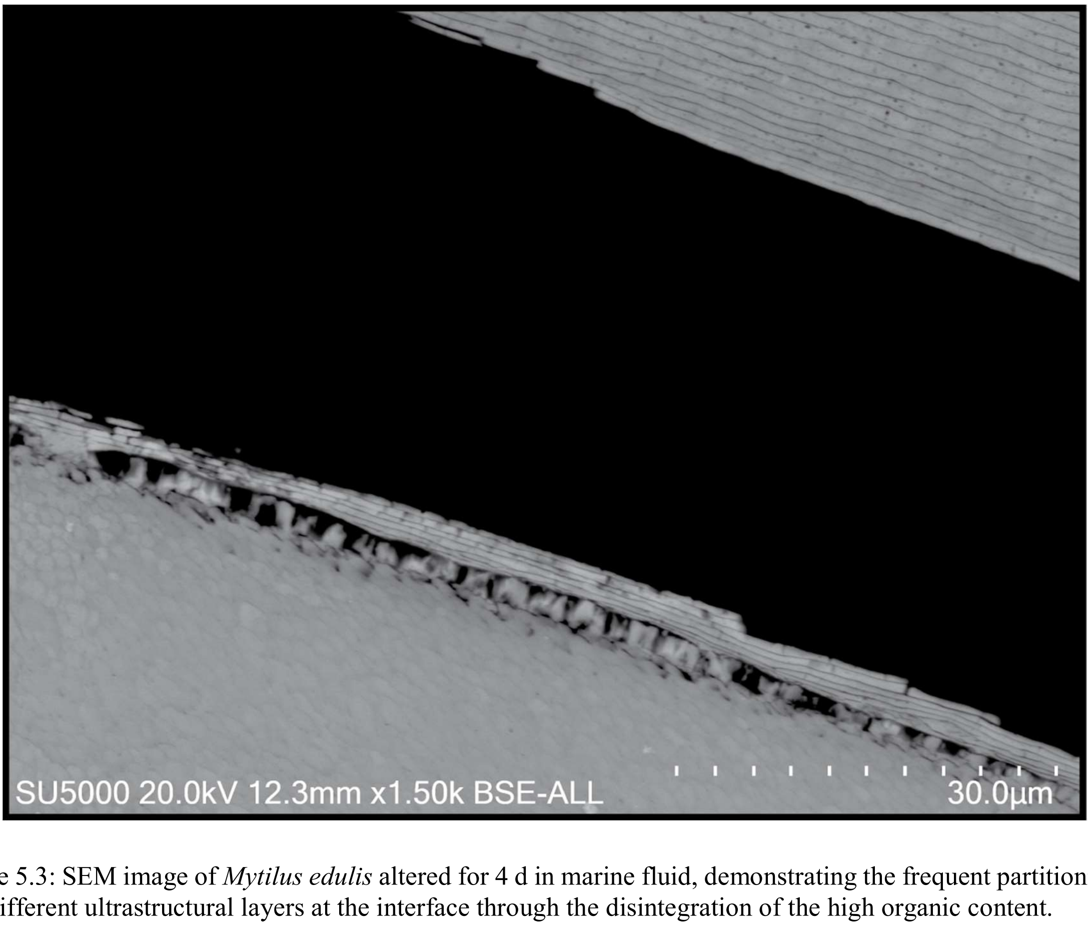

Figure 5.3: SEM image of *Mytilus edulis* altered for 4 d in marine fluid, demonstrating the frequent partitioning of two different ultrastructural layers at the interface through the disintegration of the high organic content.

5.1.5 Fluid chemistry

One portion of this work was the comparison of burial alteration fluid to marine alteration fluid. For this, inorganic aragonite and calcite monocrystals as well as three biogenic materials have been adduced: the bivalve *Arctica islandica*, the sea snail *Haliotis ovina*, and the coral *Porites* sp..

The data of the biogenic materials that have been altered with burial fluid have been acquired from the dissertation of and by Dr. Laura Casella (Casella 2018), all other results stem from this dissertation´s work. To assure maximal comparability, all materials and alteration fluids originate from the same batch. The applied methods are XRD measurements for the determination of the aragonite to calcite ratio, as well as SEM imaging to evaluate the influence on the texture.

For all alterations two things hold true: For one, the alterations performed with burial alteration fluid show an earlier rise of calcite concentration, indicating an earlier begin of calcitization compared to the materials altered with marine fluid. Secondly, the alterations performed with burial alteration fluid present an overall higher calcite content throughout all the time ranges of the alterations (figure 5.4).

While with these XRD results the burial alteration fluid proves to be more accelerating for the calcitization process, SEM imaging presents further details, particularly apparent in the inorganic materials. Samples altered with marine fluid present a very rough and tattered surface on the planes open to the fluid, while samples altered with burial fluid present more and larger grains of secondary calcite.

The fact that burial fluid facilitates an earlier and more rapid growth of secondary calcite could be explained by the high content of inhibitors within the marine alteration fluid, such as Mg. The burial fluid contains 10 mM of Mg, which equals 10 mmol/litre. The marine fluid was prepared with a synthetic sea salt that contained 46 mmol/litre, so a nearly 5 times higher content of Mg.

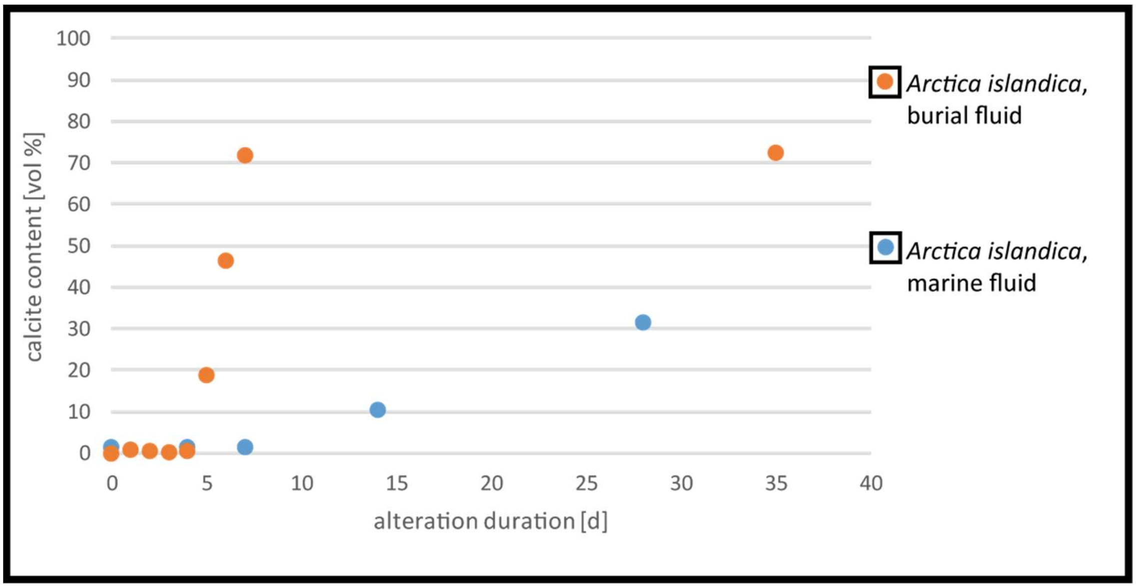

Figure 5.4: Graph presenting the rising calcite content through calcitization, comparing burial to marine fluid on the example of the bivalve *Arctica islandica*, showing the much earlier and higher increase in calcite content in alterations done with burial fluid.

5.2 Fossil project

In the alteration experiments, different levels of overprint are attained through the different durations of the experiments, while in the fossil material the various geothermal gradients of the respective basins led to various levels of overprint. The four basins come with four temperature ranges: basin 1) Castell'Arquato Basin with up to 50 °C, basin 2) Pennine Basin with 100 – 120 °C, basin 3) Lombardian Basin with 150 – 200 °C, and basin 4) Karakoram Basin with 300 – 350 °C. As described in chapter 2.1, all fossil specimens are of the phylum brachiopoda with varying combinations of the following ultrastructures: primary layer, fibrous layer, and columnar layer.

Materials from the basin 1 possess the characteristics of a beginning of level 2 of overprint, as described in chapter 5.1.1 above. The fibrous texture is well preserved, but shows amalgamation (figure 4.2.1.d). A band of heavy distortion runs through the fibrous layer, pointing to a singular event such as a local pressure event or an increased overprint aided by the percolation of the alteration fluid through a fissure (figure 4.2.1.c). However, no calcitization (in the form of secondarily nucleated calcite) is present, not even in the frequent punctae of the shell.

The materials from basin 2 feature the characteristics of level 2, plus, but only locally, level 3. The materials from this basin are all from the genus *Gigantoproductus*, presenting a thick columnar ultrastructure and a thin primary layer. The primary layer shows strong merging and distortion. Additionally, along the interface to the columnar ultrastructure as well as along fractures running through the primary layer runs a band of recrystallized material (figure 4.2.2.e), strongly suggesting the previous presence of a thick organic layer that, through its degradation, presented ample open pore space for the percolation of the alteration fluid and the following nucleation of secondary calcite.

The materials of basin 3 show the features of a level 3 of overprint. The fibrous ultrastructure is still discernible, but it exhibits amalgamation, which is very pronounced in most areas (figure 4.2.3.c). Furthermore, extensive areas of secondary calcite and frequent fissures are present in the shell material.

The ample materials from basin 4 present all the signs of an intensive level 3 of overprint, resulting from high temperatures and high pressure conditions. There is strong breakage, strong amalgamation within the fibrous layer, and patches of secondary calcite within the columnar layer. Additionally, the material from this basin shows very frequent pressure twinning within the larger grains of the columnar layer (figure 4.2.9.d).

5.3 Comparability of altered and fossil specimen

As seen in the previous chapters, the characteristic events and their sequential steps (levels) within the alteration experiments coincide with the findings in the fossil material. After the loss of the organic matter with the accompanying surge in porosity comes the amalgamation, followed by the calcitization with the substitution of pre-existing material by secondary calcite.

Naturally, also some differences lie between the laboratory experiments and natural diagenesis. The complexity of nature, as briefly mentioned above, does not only have to be considered in regard to the diagenetic processes the fossil material experiences, but also in context with the laboratory based alteration experiments. The aim of these experiments was to mimic the environmental conditions that are found during diagenesis, in order to analyze the small individual steps through the variation of some influencing factors, and to investigate the importance of these individual influencing factors that are known to introduce a diagenetic overprint. Here, some limitations arise in the setup of the alteration experiments. The circumstances that are found in nature can not be copied 1:1 to the laboratory environment. For example, natural processes, such as orogenesis, never present only one temperature or one fluid chemistry in its development. It presents a beginning phase, followed by an increase, and has possibly several peak phases before its ending. It may even be reactivated after a dormancy period. These constant changes could not be applied to the laboratory experiments. Here, one temperature frame and one alteration fluid was decided on and utilized for one experiment. This, however, is not a detriment of the experiments, they in fact allow to investigate the effect of one single factor through the aimed variation of the latter while maintaining the same adjustments of the other factors. One implementation of this procedure was the comparison of the alteration fluids that is described in chapter 5.1.

Now another obvious and extensive difference is the duration of the influence. While natural diagenesis happens in geological time frames, the individual laboratory experiments were conducted with a maximal duration of just 28 days each, due to the time limitations of a human life, or rather, a doctorate. The comparison of the findings of the alteration experiments to the findings of the fossil material, however, shows that despite the large dimension of this discrepancy, the sequence of occurrences still corresponds.

A further difference to be addressed separately is the pressure. While it is a part of any diagenetic environment, in the experiments, the pressure arises in form of water vapour pressure from the heating and expansion of the gas and fluid in the sealed crucible, but unlike geologic environments the specimens were not exposed to lithostatic pressure or tectonic stress. An experimental setup that includes a specifically added and regulated pressure could surely yield interesting and valuable results.

Another difference lies in the material that has been investigated. The samples for the alteration experiments were recent taxa belonging to the bivalves, gastropods, and corals. The fossil specimen on the other hand are all extinct taxa belonging to the brachiopods. The reasoning behind this is that the fossil taxa are extinct and, hence, no extant (in order to be pristine) specimen of these taxa could be obtained for the alteration experiments. Furthermore, the alteration experiments were performed to, inter alia, compare the effect of different alteration fluids. For this the results of another doctoral research were consulted for comparison. Therefore, the same species as utilized in this other doctoral research were chosen for this work´s hydrothermal experiments. Still, the results of this dissertation show that the two groups of the alteration series project and the fossil project are clearly comparable. Systematic differences of the various taxa, such as ultrastructural units are not restricted to one species, but may occur in systematically quite distantly related groups, as it is the case with fibres, which frequently occur in brachiopods as well as bivalves.

Despite these differences, the discrepancies are rather minor in comparison to the many commonalities that lead to an overall accordance. Also my doctoral predecessor came to the conclusion, that „laboratory-based, simulated diagenetic alteration discloses microstructural and geochemical features that are comparable to those in fossil specimen“ (Casella 2018, see also Casella et al. 2017, Ritter et al. 2017).

6 Conclusions

One of the most important findings of this doctoral work is that the relatively simple setup of the hydrothermal alteration experiments produces results that are highly relevant for the comparison to, and understanding of the naturally altered fossils that experienced the complex and prolonged process of diagenesis. This conclusion encourages to carry out additional experiments to further decode the intricacies of diagenesis and its effect on the materials adduced for palaeoenvironmental reconstructions.

The comparison of the alteration series project to the fossil project shows that the alteration of calcium carbonatic material proceeds in a specific sequence, regardless of the specific ambient conditions. This sequence can be categorized into three levels. However, the individual events may overlap or vary in intensity, depending on many factors. The external factors are temperature or geothermal gradient, duration, pressure conditions, and the fluid chemistry. The internal factors are the ultrastructure, organic matter, porosity and mineralogy. Level 1 is characterized by the disintegration of the organic matter, an enhanced porosity, and an elevated fragility. Level 2 shows a distortion of the primary mineral units through amalgamation. This amalgamation presents itself as larger clusters of mineral units that merged together and adopted the same or a similar crystallographic orientation. Level 3 is accompanied by the beginning of calcitization with the nucleation of secondary calcite, which in further course leads to the replacement of the primary biogenic phase by the inorganic calcite grains and a loss of the primary ultrastructure. A graphic depiction of this sequence and the levels of overprint by the example of a fibrous ultrastructure can be found in figure 5.1 above (see chapter 5.1.1). This classification of the alteration process allows a preliminary insight into the level of overprint, for which no lengthy EBSD measurements are necessary, but only SEM images.

This sequence of an overprint process was found in the alteration series project, as well as the fossil project. Within the fossil project, the material was categorized by the originating four basins, which underwent different thermal gradients. Basin 1, the Castell’Arquato Basin with a thermal gradient of up to 50 °C, presents a beginning level 2 of overprint: slight amalgamation was found within the fibrous layer, but no fractures nor secondary calcite. Basin 2, the Pennine Basin with a thermal gradient of 100 to 120 °C, presents a level 2 plus locally a level 3: the primary ultrastructure presents strong amalgamation and even recrystallization along its interface to the columnar layer, which however presented no obvious signs of overprint. Basin 3, the Lombardian Basin with a thermal gradient of 150 to 200 °C, presents a level 3 of overprint: the fibrous ultrastructure shows strong amalgamation, frequent fissures, and patches of recrystallized secondary calcite. Basin 4, the Karakoram Basin with a thermal gradient of 300 to 350 °C, presents an intensive level 3 of overprint: very strong amalgamation and distortion can be found within the fibrous ultrastructure, while strong breakage, large clusters of secondary calcite, and even extensive pressure twinning can be found within the columnar ultrastructure.

Despite this general consensus, some factors lead to a variance in strength of the different aspects of the overprint. Herein, these are referred to as the influencing factors. The extensive alteration experiments that have been conducted in the course of this doctoral research presented a detailed insight into these factors that have a relevant influence on the process of overprint. This insight helps to interpret and evaluate the analytical results of the material a future scientist strives to investigate. Next to the obvious factors, such as the temperature and duration, the factors that were unambiguously detected are the quantity and distribution of the organic matter, the pore system, the ultrastructure, the mineralogy of the specimen, and the chemical composition of the alteration fluid.

The quantity and distribution of the organic matter determines the quantity and distribution of the cavital space that results from the disintegration of the organic matter, which is the secondary porosity. The extent and interconnection of the porosity, primary and secondary, controls the flux of the alteration fluid through the material and the amount of surface area that comes in contact with the alteration fluid. A high flux and a large surface area both lead to a significantly stronger overprint on the material.

The type of ultrastructure has a rather complex effect, for it includes the factors organic matter, porosity, and mineralogy, as well as the size and shape of the biogenic mineral units. Most of these factors are looked at separately and in detail, but it has been found that a prismatic ultrastructure, through its extensive network of interconnected biopolymer fibrils leading to an equally extensive network of porosity, tends to allow a very early beginning of calcitization. A characteristic of a fibrous ultrastructure, on the other hand, is a relatively early and strong amalgamation of the individual fibres. Here, the fibrous mineral units can form large clusters of slightly distorted fibres that also adapted one crystallographic orientation. A nacreous ultrastructure, however, presents a very strong resistance to overprint. Amalgamation in a nacreous ultrastructure is characterized by the adaptation of the crystallographic orientation of neighbouring nacre tablets, while the individual nacre tablets tend to retain their characteristic shape. Calcitization intrudes a nacreous ultrastructure at a very late stage.

The chemical composition of the alteration fluid stands in complex interrelation with the mineralogy of the material. Density, stability, and inhibitors are factors within this division that determine the dissolution and reprecipitation patterns. The evaluation of the results from the series of hydrothermal alteration experiments, where the effects of a burial alteration fluid was compared to the effects of a marine alteration fluid, shows that the usage of a burial alteration fluid leads to an earlier onset of the various stages of overprint, especially the nucleation of secondary calcite (see figure 5.4 above). The marine alteration fluid, on the other hand, presents a more aggressive dissolution pattern on the material (see figure 4.1.6.f and o above).

These very detailed findings are an invaluable guidance for the interpretation of the findings within a diagenetically overprinted fossil and allow a very accurate and comprehensive understanding of the state of preservation of the material at hand. Because, when choosing fossil material for the utilization in palaeoenvironmental reconstructions, its aptitude for this application has to be established. As described in chapter 1, during its long dwell time after death (for some of this work´s materials that was hundreds of millions of years) the material experienced many alterations that affected the primary signatures of the period of its life. If signs of overprint are found in the strata of the fossil´s origin, a detailed analysis of the fossil material is necessary in order to assess the level and characteristic of overprint and, as a result, the suitability of the fossil for its purpose. This work shows that the application of EBSD analysis is a very comprehensive and detailed method to determine the usability of the material. It enables an analysis of details such as porosity, amalgamation, fracturing, and calcitization, which allows the determination of the type and strength of overprint. The meaning of my results is unique for each specimen, because it considers a multitude of factors and unfolds its ultimate value only in conjunction with further investigations in the approach for palaeoenvironmental reconstruction, as applied by my CHARON colleagues.

7 Outlook

Although this research together with the work of co-workers from the CHARON project provide a wide base of alteration experiments, additional experimental series would be hugely beneficial. An additional information pool with variation of the external impact factors would allow a more in-depth analysis of the kind and strength of the influence the individual factors bring about the material. The existing data shows that the most important factors would be the alteration fluid chemistry, duration of the experiments, and ultrastructure. Hydrothermal alteration experiments that also present a pressure environment, for example, could be hugely beneficial to create a laboratory environment that is even more similar to the natural conditions during diagenesis.

A different detail that is very worth investigating more in depth is the organic content and the thereto relating porosity. As the analyses herein show, these are crucial factors when it comes to the strength of overprint. Numerical measurements on these details set into context with the results of an alteration series would allow a more thorough understanding of the effect and importance of the organic content, and the primary and secondary porosity during diagenetic overprint.

Another variation of the experimental setup that could further assimilate the conditions of the laboratory experiments to the ones present in natural diagenesis is adding a percolation of the alteration fluid through pressuring it through the sample material. In nature, when a tectonic plate is being subducted the fluids would be pressed towards the earth´s surface, adding a heightened percolation of the fluid through the open pore system of the material. Another doctoral student of the CHARON project, Dr. Dongmei Yu from the Ruhr-University in Bochum, carried out such an experimental setup on a small scale and the results proved a much higher rate of secondary calcite formation. An alteration series with this experimental setup could lead to a higher comparability of the laboratory experiments and the natural material. Additionally, through the heightened effects, the differences of the alteration fluids (burial, meteoric, and marine) could be discerned easier and clearer.

Although EBSD analysis has proven to cover all the important niches to decipher the processes of diagenetic overprint, and the addition of XRD as well as AFM analysis added some crucial details, the application of TEM measurements could be a valuable complement. TEM is a frequent method applied in the field of diagenesis for it is able to simultaneously identify a mineral while revealing crystal defects. These defects are known to be the primary site for recrystallization processes (Frisia-Bruni and Wenk 1985), so a look into this detail could yield interesting information.

Bibliography

Abdolmaleki J. and Tavakoli V. 2016. Anachronistic facies in the early Triassic successions of the Persian Gulf and its palaeoenvironmental reconstruction. Palaeogeography, Palaeoclimatology, Palaeoecology, vol. 446, pp. 213-224.

Addadi L. Raz S., Weiner S. 2003. Taking Advantage of Disorder: Amorphous Calcium Carbonate and Its Roles in Biomineralization. Advanced Materials, vol. 15(12), pp. 959-970.

Aitkenhead N. and Chrisholm J.I. 1982. A standard nomenclature for the Dinantian formations of the Peak District of Derbyshire and Staffordshire. Institute of Geological Sciences, London.

Aitkenhead N., Chrisholm J.I. and Stevenson I.P. 1985. Geology of the country around Buxton, Leek and Bakewell. Memoir for 1:50 000 geological sheet 111 (England and Wales). HMSO Publications, London.

Aizenberg J., Addadi L., Weiner S., Lambert G. 1996. Stabilization of amorphous calcium carbonate by specialized macromolecules in biological and synthetic precipitates. Advanced Materials, vol. 8(3), pp. 222-226.

Allen P.A. and Allen J.R. 2005. Basin analysis: principles and applications. 2nd ed. Blackwell Publishing. 350 Main Street, Malden, Ma 02148-5020, USA.

Altree-Williams A., Pring A., Ngothai Y., Brugger J. 2015. Textural and compositional complexities resulting from coupled dissolution-reprecipitation reactions in geomaterials. Earth-Science Reviews, vol. 150, pp. 628-651.

Anderson T.F., Bender M.L., Broecker W.S. 1973. Surface areas of biogenic carbonates and their relation to fossil ultrastructure and diagenesis. Journal of Sedimentary Petrology, vol. 43(2), pp. 471-477.

Andrews I.J. 2013. The Carboniferous Bowland Shale gas study: geology and resource estimation. London, UK, British Geological Survey for Department of Energy and Climate Change, pp. 1-56.

Angiolini L. 1993. Ultrastructure of some Permian and Triassic Spiriferida and Athyridida (Brachiopoda). Rivista italiana di Paleontologia a Stratigrafia, vol. 99(3), pp. 283-306.

Angiolini L. 1995. Pemian brachiopods from Karakorum (Pakistan). Pt. 1. Rivista Italiana di Paleontologia e Stratigrafia, vol. 101(2), pp. 165-211.

Angiolini L. 1996. Permian brachipods from Kararorum (Pakistan). Pt. 2. Rivista Italiana di Paleontologia e Stratigrafia, vol. 102(1), pp. 3-26.

Angiolini L., Brunton H., Zanchi A. 1999. Late Carboniferous brachiopods form Karakorum, Pakistan. Rivista Italiana di Paleontologia e Stratigrafia, vol. 105(1), pp. 3-22.

Angiolini L. 2001. Permian brachiopods from Karakorum (Pakistan). Pt. 3. Rivista Italiana di Paleontologia e Stratigrafia, vol. 107(3), pp. 307-344.

Angiolini L., Brunton H., Gaetan M. 2005. Early Permian (Asselian) Brachiopods from Karakorum (Pakistan) and their palaeobiogeographical significance. Palaeontology, vol. 48(1), pp. 69-86.

Angiolini L., Stephenson M., Leng M.J., Jadoul F., Millward D., Aldridge A., Andrews J., Chenery S., Williams G. 2011. Heterogeneity, cyclicity and diagenesis in a Mississippian brachiopod shell of palaeoequatorial Britain. Terra Nova, vol. 24(1), pp. 16-26.

Angiolini L., Zanchi A., Zanchetta S., Nicora A., Vezzoli G. 2013. The Cimmerian geopuzzle: new data from South Pamir. Terra Nova, vol. 25, pp. 352-360.

Archbold N.W. and Thomas G.A. 1986. Neospirifer and Trigonotreta (Spiriferida, Brachiopoda) from the Permian of Western Australia. Alcheringa, vol. 10, pp. 125-161.

Arvidson R.S., Collier M., Davis K.J., Vinson M.D., Amonette J.E., Luttge A. 2006. Magnesium inhibition of calcite dissolution kinetics. Geochimica et Cosmochimica Acta, vol. 70(3), pp. 583-594.

Atkinson M.J. and Bingman C. 1996. Elemental composition of commercial seasalts. Journal of Aquariculture and Aquatic Sciences, vol. 8(2), pp. 39-42.

Bally A.W., and Snelson S. 1980. Realms of subsidence. Facts and Principles of World Petroleum Occurrence, Memoir 6, pp. 9-94.

Bathurst R.G.C. 1975. Carbonate sediments and their diagenesis. Elsevier Science B.V., Amsterdam, The Netherlands.

Bauwens M., Ohlsson H., Barbé K., Beelaerts V., Dehairs F., Schoukens J. 2009. On Climate Reconstructions using Bivalve Shells: Three Methods to Interpret the Chemical Signature of a Shell. IFAC Proceedings Volumes, vol. 42(12), pp. 407-412.

Beaumont C., Keen C., Boutilier R. 1982. A comparison of foreland and rift margin sedimentary basins. Philosophical Transactions of the Royal Society London, vol. A305, pp. 295-317.

Beck R. and Andreassen J.-P. 2010. The onset of spherulitic growth in crystallization of calcium carbonate. Journal of Crystal Growth, vol. 312, pp. 2226-2238.

Becker R. and Döring W. 1935. Kinetische Behandlung der Keimbildung in übersättigten Dämpfen. Annalen der Physik, vol. 416(8), pp. 719-752.

Beniash E., Aizenberg J., Addadi L., Weiner S. 1997. Amorphous calcium carbonate transforms into calcite during sea urchin larval spicule growth. Proceedings of the Royal Society of London, Series B, vol. 264, pp. 461-465.

Bennett C.E., Williams M., Leng M.J., Siveter D.J., Davies S.J., Sloane H.J., Wilkinson I.P. 2011. Diagenesis of fossil ostracods: Implications for stable isotope based palaeoenvironmental reconstruction. Palaeogeography, Palaeoclimatology, Palaeoecology, vol. 305(1-4), pp. 150-161.

Birkeland C. 1997. Life and death of coral reefs. Chapman and Hall, International Thomson Publishing, USA.

Bittner A. 1890. Brachiopoden der alpinen Trias. Abhandlungen der Kaiserlich-Königlichen Geologischen Reichsanstalt, vol. 14, pp. 1-325.

Bjørlykke K. 1994. Fluid-flow processes and diagenesis in sedimentary basins. Geological Society, London, Special Publications, vol. 78(1), pp. 127-140.

Bodine M.W., Holland H.D., Borcsik M. 1965. Co-precipitation of manganese and strontium with calcite. Problems of Postmagmatic Ore Deposition - Proc. Symposium 2, Prague, pp. 401-406.

Boggs Jr.S. and Boggs S. 2009. Petrology of sedimentary rocks. Cambridge University Press.

Bostick N.H. and Alpern B. 1977. Principles of sampling, preparation and constituent selection for microphotometry in measurement of maturation of sedimentary organic matter. Journal of Microscopy, vol. 109(1), pp. 41-47.

Bostick N.H. 1979. Microscopic measurement of the level of catagenesis of solid organic matter in sedimentary rocks to aid exploration for petroleum and to determine former burial temperatures — a review. The Society of Economic Paleontologists and Mineralogists, vol. 26, pp. 17-43.

Brand U. and Veizer J. 1980. Chemical diagenesis of a multicomponent carbonate system – 1: trace elements. Journal of Sedimentary Research, vol. 50(4), pp. 1219-1236.

Brand U. and Veizer J. 1981. Chemical diagenesis of a multicomponent carbonate system – 2: stable isotopes. Journal of Sedimentary Research, vol. 51(3), pp. 987-997.

Brand U. 1994. Morphochemical and replacement diagenesis of biogenic carbonates. Developments in Sedimentology, vol. 51, pp. 217-282.

Breislin C.J. 2018. Basin-Scale Mineral and Fluid Processes at a Platrofm Margin, Lower Carboniferous, UK. Doctoral Thesis, University of Manchester, Faculty of Science and Engineering, School of Earth and Environmental Sciences.

Burke W.H., Denison R.E., Heatherington E.A., Koepnick R.B., Nelson H.F., Otto J.B. 1982. Variation of seawater ^{87}Sr/^{86}Sr throughout Phanerozoic time. Geology, vol. 10, pp. 516-519.

Burley S. and Worden R. 2009. Sandstone diagenesis: recent and ancient. Volume 24. John Wiley & Sons.

Burnham A.K. and Sweeney J.J. 1989. A chemical kinetic model of vitrinite maturation and reflectance. Geochimica et Cosmochimica Acta, vol. 53(10), pp. 2649-2657.

Campbell K.A., Farmer J.D., Des Marais D. 2002. Ancient hydrocarbon seeps from the Mesozoic convergent margin of California: carbonate geochemistry, fluids and palaeoenvironments. Geofluids, vol. 2(2), pp. 63-94.

Casella L.A., Griesshaber E., Yin X., Ziegler A., Mavromatis V., Müller D., Ritter A.-C., Hippler D., Harper E.M., Dietzel M., Immenhauser A., Schöne B.R., Angiolini L., Schmahl W.W. 2017. Experimental diagenesis: insights into aragonite to calcite transformation of *Arctica islandica* shells by hydrothermal treatment. Biogeosciences, vol. 14(6), pp. 1461-1492.

Casella L.A. 2018. Nano- and microstructural transformation processes during diagenesis of biogenic carbonates. Dissertation at the Ludwig-Maximilians University, Munich, Germany.

Casella L.A., He S., Griesshaber E., Fernández Diaz L., Greiner M., Harper E.M., Jackson D.J., Ziegler A., Mavromatis V., Dietzel M., Eisenhauer A., Veintemillas-Verdaguer S., Brand U., Schmahl W.W. 2018a. Hydrothermal alteration of aragonitic biocarbonates: assessment of micro- and nanostructural dissolution–reprecipitation and constraints of diagenetic overprint from quantitative statistical grain-area analysis. Biogeosciences, vol. 15, pp. 7451-7484.

Casella L.A., Griesshaber E., Simonet Roda M., Ziegler A., Mavromatis V., Henkel D., Laudien J., Häusserman V., Neuser R.D., Angiolini L., Dietzel M., Eisenhauer A., Immenhauser A., Brand U., Schmahl W.W. 2018b. Micro- and nanostructures reflect the degree of diagenetic alteration in modern and fossil brachiopod shell calcite: A multi-analytical screening approach (CL, FE-SEM, AFM, EBSD). Palaeogeography, Palaeoclimatology, Palaeoecology, vol. 502, pp. 13-30.

Chapman R.E. 1987. Fluid flow in sedimentary basins: a geologist´s perspective. Geological Society, London, Special Publications, vol. 34, pp. 3-18.

Checa A.G., Esteban-Delgado F.J., Rodrìguez-Navarro A.B. 2007. Crystallographic structure of the foliated calcite of bivalves. Journal of Structural Biology, vol. 157, pp. 393-402.

Coan E.V., Valentich-Scott P., Sadeghian P.S. 2012. Bivalve seashells of tropical West America: marine bivalve mollusks from Baja California to Northern Peru. Museum of Natural History, Peru.

Compston W. 1960. The carbon isotopic compositions of certain marine invertebrates and coals from the Australian Permian. Geochimica et Cosmochimica Acta, vol. 18(1-2), pp. 1-22.

Compton R.G. and Brown C.A. 1994. The Inhibition of Calcite Dissolution/Precipitation: Mg^{2+} Cations. Journal of Colloid and Interface Science, vol. 165(2), pp. 445-449.

Crippa G., Angiolini L., Bottini C., Erba E., Felletti F., Frigerio C., Hennissen J.A.I., Leng M.J., Petrizzo M.R., Raffi I., Raineri G., Stephenson M.H. 2016. Seasonality fluctuations recorded in fossil bivalves during the early Pleistocene: Implications for climate change. Palaeogeography, Palaeoclimatology, Palaeoecology, vol. 446, pp. 234-251.

Deming D., Nunn J., Evans D. 1990. Thermal effects of compaction-driven groundwater flow from overthrust belts. Journal of Geophysical Research, vol. 95(B5), pp. 6669-6683.

Dhondt A. 1971. Systematic revision of Entolium, Propeamussium (Amusiidae) and Syncyclonema (Pectinidae, Bivalvia, Mollusca) of the European Boreal Cretaceous. Institut royal des Sciences naturelles de Belgique, vol. 32.

Dickson J.A.D. 2003. Neomorphism and Recrystallization. In: Middleton G.V., Church M.J., Coniglio M., Hardie L.A., Longstaffe F.J. (eds.) Encyclopedia of Sediments and Sedimentary Rocks. Kluwer Academic Publishers, PO Box 17, 3300 AA Dordrecht, The Netherlands.

Dove P.M. and Hochella M.F.Jr. 1993. Calcite precipitation mechanisms and inhibition by orthophosphate: In situ observations by Scanning Force Microscopy. Geochimica et Cosmochimica Acta, vol. 57(3), pp. 705-714.

Dow W.G. and O'Connor D.I. 1982. Kerogen maturity and type by reflected light microscopy applied to petroleum exploration. The Society of Economic Paleontologists and Mineralogists. How to Assess Maturation and Paleotemperatures (SC7).

Ewbank G., Manning D.A.C., Abbott G.D. 1995. The relationship between bitumens and mineralization in the South Pennine Orefield, central England. Journal of the Geological Society, London, vol. 152, pp. 751-765.

Finch A.A., Shaw P.A., Weedon G.P., Holmgren K. 2001. Trace element variation in speleothem aragonite: potential for palaeoenvironmental reconstruction. Earth and Planetary Science Letters, vol. 186(2), pp. 225-267.

Folk R.L. 1965. Some aspects of recrystallization in ancient limestones. Special Publications of The Society of Economic Paleontologists and Mineralogists.

Fossen H. 2010. Structural Geology. Cambridge University Press.

Frenkel J. 1939. A General Theory of Heterophase Fluctuations and Pretransition Phenomena. The Journal of Chemical Physics, vol. 7(7), pp. 538-547.

Frei R., Gaucher C., Døssing L.N., Sial A.N. 2011. Chromium isotopes in carbonates – A tracer for climate change and for reconstructing the redox state of ancient seawater. Earth and Planetary Science Letters, vol. 312(1-2), pp. 114-125.

Frimmel H.E. 2009. Trace element distribution in Neoproterozoic carbonates as palaeoenvironmental indicator. Chemical Geology, vol. 258(3-4), pp. 338-353.

Frisia-Bruni S. and Wenk H.R. 1985. Replacement of aragonite by calcite in sediments from the San Cassiano Formation (Italy). Journal of Sedimentary Petrology, vol. 55(2), pp. 159-170.

Fürsich F.T., Singh I.B., Joachimski M., Krumm S., Schlirf M., Schlirf S. 2005. Palaeoclimate reconstructions of the Middle Jurassic of Kachchh (western India): an integrated approach based on palaeoecological, oxygen isotopic, and clay mineralogical data. Palaeogeography, Palaeoclimatology, Palaeoecology, vol. 217(3-4), pp. 289-309.

Gaetani M. and Sacca D. 1985. Brachipodi Neogenici e Pleistocenici della provincia di Messina e della Calabria meridionale. Geologica Romana, vol. 22, pp. 1-43.

Gaetani M., Gnaccolini M., Poliani G., Grignani D., Gorza M., Martellini L. 1992. An anoxic intraplatform basin in the Middle Triassic of Lombardy (Southern Alps, Italy): anatomy of a hydrocarbon source. Rivista Italiana di Paleontologia e Stratigrafia, vol. 97(3-4), pp. 329-252.

Gaetani M., Angiolini L., Garzanti E., Jadoul F., Leven E.Y.A., Nicora A., Sciunnach D. 1995. Permian Stratigraphy in the Northern Karakorum, Pakistan. Rivista Italiana di Paleontologia e Stratigrafia, vol. 101(2), pp. 107-152.

Gaetani M. 1997. The Karakorum Block in Central Asia, from Ordovician to Cretaceous. Sedimentary Geology, vol. 109, pp. 339-359.

Gaetani M. 2010. From Permian to Cretaceous: Adria as pivotal between extensions and rotations of Tethys and Atlantic Oceans. In: Marco Beltrando, Angelo Peccerillo, Massimo Mattei, Sandro Conticelli, and Carlo Doglioni, The Geology of Italy: tectonics and life along plate margins, Journal of the Virtual Explorer, Electronic Edition, ISSN 1441-8142, volume 36, paper 6, doi:10.3809/jvirtex.2010.00235.

Gaetani M., Nicora A., Henderson C., Cirilli S., Gale L., Rettori R., Vuolo I., Atudorei V. 2013. Refinements in the Upper Permian to Lower Jurassic stratigraphy of Karakorum, Pakistan. Facies, vol. 59(4), pp. 915-948.

Ghielmi M., Minervini M. Nini C., Rogledi S., Rossi M., Vignolo A. 2010. Sedimentary and tectonic evolution in the eastern Po-Plain and northern Adriatic Sea area from Messinian to Middle Pleistocene (Italy). Rendiconti Lincei, vol. 21(1), pp. 131-166.

Ghielmi M., Minervini M., Nini C. 2013. Late Miocene-Middle Pleistocene sequences in the Po Plain – Northern Adriatic Sea (Italy): The stratigraphic record of modification phases affecting a complex foreland basin. Marine and Petroleum Geology, vol. 42, pp. 50-81.

Giuffre A.J., Gagnon A.C., De Yoreo J.J., Dove P.M. 2015. Isotopic tracer evidence for the amorphous calcium carbonate to calcium transformation by dissolution-reprecipitation. Geochimica et Cosmochimica Acta, vol. 165, pp. 407-417.

Greiner M., Fèrnandez-Diaz L., Griesshaber E., Zenkert M.N., Yin X., Ziegler A., Veintemillas-Verdaguer S., Schmahl W.W. 2018. Biomineral Reactivity: The Kinetics of the Replacement Reaction of Biological Aragonite to Apatite. Minerals, vol. 8(315), pp. 1-31.

Grossman E.L., Mii H.-S., Yancey T.E. 1993. Stable isotopes in Late Pennsylvanian brachiopods from the United States: Implications for Carboniferous paleoceanography. Geological Society of Americal Bulletin, vol. 105(10), pp. 1284-1296.

Grotzinger J., Jordan T.H., Press F., Siever R. 2008. Allgemeine Geologie. 5. Auflage. Springer Verlag, Berlin Heidelberg.

Guo Y., Deng W., Wei G., Lo L., Wang N. 2019. Clumped isotopic signatures in land-snail shells revisited: Possible palaeoenvironmental implications. Chemical Geology, vol. 519, pp. 83-94.

Gutteridge P. 1983. Sedimentological study of the Eyam Limestone formation of the east-central part of the Derbyshire Dome. Unpublished PhD thesis, University of Manchester, UK.

Gutteridge P. 1987. Dinantian sedimentation and the basement structure of the Derbyshire Dome. Geological Journal, vol. 22, pp. 25-41.

Gutteridge P. 1991. Revision of the Monsal Dale/Eyam Limestone boundary (Dinantian) in Derbyshire. Mercian Geologist, vol. 12, pp. 71-78.

Gutteridge P. 1995. Late Dinantian (Brigantian) carbonate mud-mounds of the Derbyshire carbonate platform. In: Monty C.L.V, Bosence D.W.J., Bridges P.H. and Pratt B.R. (eds) Carbonate mud-mounds: their origin and evolution. International Association of Sedimentologists Special Publications, vol. 23, pp. 289-307.

Gutteridge P. 2003. A record of the Brigantian limestone succession in the partly infilled dale quarry, Wirksworth. Mercian Geologist, vol. 15, pp. 219-224.

Helwig J.A. 1985. Origin and Classification of Sedimentary Basins. Offshore Technology Conference 4843, pp. 21-25.

Hertlein L.G. and Grant U.S. 1972. The geology and paleontology of the marine Pliocene of San Diego, California (Paleontology: Pelecypoda).

Hollis C. and Walkden G. 1996. The use of burial diagenetic calcite cements to determine the controls upon hydrocarbon emplacement and mineralization on a carbonate platrorm, Derbyshire, England. Geological Society, London, Special Publications, vol. 107(1), pp. 35-49.

Hollis C. 1998. Reconstructing fluid history: an integrated approach to timing fluid expulsion and migration on the Carboniferous Derbyshire Platform, England. Geological Society, London, Special Publications, vol. 144(1), pp. 153-159.

Hollis C. and Walkden G. 2002. Reconstructing fluid expulsion and migration north of the Variscan Orogen, northern England. Journal of Sedimentary Research, vol. 72(5), pp. 700-710.

Hubbard R.J., Pape J., Roberts D.G. 1985. Depositional sequences mapping as a technique to establish tectonic and stratigraphic framework and evaluate hydrocarbon potential on a passive continental margin. In: Berg O.R., Wolverton D.G., Seismic Stratigraphy 11; An Integrated Approach to Hydrocarbon Exploration. American Association of Petroleum Geologists Memoir, Tulsa vol. 39, pp. 79-92.

Hunt G.R. 1979. Near-infrared (1.3–2.4) μm spectra of alteration minerals—Potential for use in remote sensing. Geophysics, vol. 44(12), pp. 1974-1986.

Ichikuni M. 9173. Partition of strontium between calcite and solution: Effect of substitution by manganese. Chemical Geology, vol. 11(4), pp. 315-319.

Immenhauser A., Nägler T.F., Steuber T., Hippler D. 2005. A critical assessment of mollusk $^{18}O/^{16}O$, Mg/Ca, and $^{44}Ca/^{40}Ca$ ratios as proxies for Cretaceous seawater temperature seasonality. Palaeogeography, Palaeoclimatology, Palaeoecology, vol. 215(3-4), pp. 221-237.

Immenhauser A., Schöne B.R., Hoffmann R., Niedermayer A. 2015. Mollusc and brachiopod skeletal hard parts: intricate archives of their marine environment. Sedimentology, vol. 63(1), pp. 1-59.

Iordan M. 1993. Triassic brachiopods of Romania. In: Palfy J., Voros A. (eds.) Mesozoic Brachiopods of Alpine Europe, pp. 49-58.

James N.P. and Jones B. 2015. Origin of carbonate sedimentary rocks. John Wiley & Sons, Chichester, West Sussex, U.K.

Jarosch D. and Heger G. 1986. Neutron diffraction refinement of the crystal structure of aragonite. Tschermaks mineralogische und petrographische Mitteilungen, vol. 35(2), pp. 127-131.

Short J.W. and Potter D.G. 1987. Shells of Queensland and the Great Barrier Reef: marine gastropods. Brown R.

Johnson A.L., Hickson J.A., Bird A., Schöne B.R., Balson P.S., Heaton T.H., Williams M. 2009. Comparative sclerochronology of modern and mid-Pliocene (c. 3.5 Ma) Aequipecten opercularis (Mollusca, Bivalvia): an insight into past and future climate change in the north-east Atlantic region. Palaeogeography, Palaeoclimatology, Palaeoecology, vol. 284(3-4), pp. 164-179.

Kafanov A.I. 2003. Neogene and Paleogene mulluscan (Bivalvia) cenozones of Sakhalin and Kuril Islands. Science Reports, Institut of Geosciences, University of Tsukuba, Section B. 24, pp. 45-79.

Kamhi S.R. 1963. On the Structure of Vaterite, $CaCO_3$. Acta Crystallographica, vol 16, pp. 770-772.

Kawano J., Shimobayashi N., Miyake A., Kitamura M. 2009. Precipitation diagram of calcium carbonate polymorphs: its construction and significance. Journal of Physics: Condensed Matter, vol. 21, pp. 1-6.

Khim B.K., Kyung S.W., Suk H.Y. 2000a. Comparison of oxygen isotope profile of a fossil bivale with the modern hydrographic condition: case study of the Seoguipo Formation (Korea). Geosciences Journal, vol. 4(1), pp. 15-24.

Khim B.K., Kyung S.W., Je J.G. 2000b. Stable isotope profiles of bivalve shells: seasonal temperature variations, latitudinal temperature gradients and biological carbon cycling along the east coast of Korea. Continental Shelf Research, vol. 20(8), pp. 843-861.

Kingston D.R., Dishroon C.P., Williams P.A. 1983. Hydrocarbon plays and global basin classification. AAPG bulletin, vol. 67(12), pp. 2194-2198.

Kinsman D.J.J. 1969. Interpretation of Sr^{2+} concentrations in carbonate minerals and rocks. Journal of Sedimentary Petrology, vol. 39, pp. 486-508.

Klemme H.D. 1980. Petroleum basins-classifications and characteristics. Journal of petroleum geology, vol. 3(2), pp. 187-207.

Korte C., Kozur H.W., Veizer J. 2005. $\delta^{13}C$ and $\delta^{18}O$ values of Triassic brachiopods and carbonate rocks as proxies for coeval seawater and palaeotemperature. Palaeogeography, Palaeoclimatology, Palaeoecology, vol. 226(3-4), pp. 287-306.

Krumbein W.C. 1942. Physical and Chemical Changes in Sediments after Deposition. Journal of Sedimentary Petrology, vol. 12, pp. 111-117.

Ladd H.D. 1966. Chitons and Gastropods (Haliotidae through Adeorbidae) from Western Pacific Islands. United States Geological Survey Professional Paper, vol. 531, pp. 1-98.

Lahann R.W. 1978. A chemical model for calcite crystal growth and morphology control. Journal of Sedimentary Research, vol. 48(1), pp. 337-347.

Land L.S. 1967. Diagenesis of skeletal carbonates. Journal of Sedimentary Research, vol. 37(3), pp. 914-930.

Lee T., Chen J. 2009. Biomimetic gallstone formation: Crystallization of calcium carbonate by the evolving taurocholate-lecithin-cholesterol complex lipid system. Crystal Growth and Design, vol 9(8), pp. 3737-3748.

Li J., Cai Z., Chen H., Cong H., Wang L., Wei Q., Luo Y. 2018. Influence of differential diagenesis on primary depositional signals in limestone-marl alternations: An example from Middle Permian marine successions, South China. Palaeogeography, Palaeoclimatology, Palaeoecology, vol. 495, pp. 139-151.

Linnaeus C. 1758. Systema Naturae per Regna Tria Naturae, Secundum Classes, Ordines, Genera, Species, cum Characteribus, Differentiis, Synonymis, Locis. Editio Decima, vol. 1, pp. 1-824.

Lippmann F. 1973. Crystal Chemistry of Sedimentary Carbonate Minerals. In: Sedimentary Carbonate Minerals. Minerals, Rocks and Inorganic Materials (Monograph series of Theoretical and Experimental Studies), vol. 6. Springer, Berlin, Heidelberg.

Lopatin N.V. 1971. Time and temperature as factors in coalification. Izvestiya Akademii SSSR, Seriya Geologicheskaya, vol. 3, pp. 95-106.

López-Pérez R.A. 2005. The Cenozoic hermatypic corals in the eastern Pacific: history of research. Earth-Science Reviews, vol. 72(1-2), pp. 67-87.

Lüttge A. and Arvidson R.S. 2010. Reactions at surfaces: a new approach integrating inferometry and kinetic simulations. Journal of the American Ceramic Society, vol. 93, pp. 3519-3530.

Ma Y., Cohen S.R. Addadi L., Weiner S. 2008. Sea Urchin Tooth Design: An "All-Calcite" Polycrystalline Reinforced Fiber Composite for Grinding Rocks. Advanced Materials, vol. 20(8), pp. 1555-1559.

Markgraf S.A. and Reeder R.J. 1985. High-temperature structure refinements of calcite and magnesite. American Mineralogist, vol. 70(5-6), pp. 590-600.

Marquet R. and Dijkstra H.H. 2000. Pliocene species of Aequipecten (Mollusca, Bivalvia, Pectinidae) from the North Sea Basin. Contributions to Tertiary and Quaternary Geology, vol. 37(3-4), pp. 39-55.

Mantovani N. 2002. The genus Tetractinella Bittner, 1890: morphology, ultrastructure, and 3D reconstruction. Rivista Italiana di Paleontologia e Stratigrafia, vol. 108(1), pp. 37-50.

McKenzie D. 1978. Some remarks on the development of sedimentary basins. Earth and Planetary science letters, vol. 40(1), pp. 25-32.

Middleton G.V., Church M.J., Coniglio M., Hardie L.A., Longstaffe F.J. 2003. Encyclopedia of Sediments and Sedimentary Rocks. Kluwer Academic Publishers, PO Box 17, 3300 AA Dordrecht, The Netherlands.

Milke R., Neusser G., Kolzer K., Wunder B. 2013. Very little water is necessary to make a dry solid silicate system wet. Geology, vol. 41(2), pp. 247-250.

Mineralienatlas (1999-2021). URL: https://mineralienatlas.de/

Monegatti P., Raffi S., Roveri M., Taviani M. 2001. A one day trip in the outcrops of the Castell'Arquato Plio-Pleistocene Basin: from the Badlands of Monte Giogo to the Stirone River. Paleobiogeography and Paleoecology, International Conference, Piacenza and Castell'Arquato, Italy, pp. 1-22.

Moore C. and Wade W. 2013. Chapter 9 Summary of early diagenesis and porosity modification of carbonate reservoirs in a sequence stratigraphic and climatic framework. In: Developments in Sedimentology. Elsevier Science B.V., Amsterdam, pp. 207-238.

Morse J.W. 1983. The kinetics of calcium carbonate dissolution and precipitation. In: Carbonates: Mineralogy and Chemistry (ed. Reeder R.J.). Reviews in Mineralogy and Geochemistry, vol. 11, pp. 227-264.

Morse J.W. 2003. Formation and diagenesis of carbonate sediments. In: Mackenzie F.T., Holland H.D., Turekian K.K. Sediments, diagenesis, and sedimentary rocky: treatise on Geochemistry, Elsevier Science B.V., Amsterdam, pp. 67-85.

Morse J.W., Arvidson R.S., Lüttge A. 2007. Calcium Carbonate Formation and Dissolution. Chemical Reviews, vol. 107(2), pp. 342-381.

Mukkamala S., Anson C., Powell A. 2006. Modelling calcium carbonate biomineralization processes. Journal of Inorganic Biochemistry, vol. 100(5-6), pp. 1128-1138.

Müller A., Gagan M.K., McCulloch M.T. 2001. Early marine diagenesis in corals and geochemical consequences for paleoceanographic reconstructions. Geophysical Research Letters, vol. 28, pp. 4471-4474.

Nakamura M. and Watson E.B. 2001. Experimental study of aqueous fluid infiltration into quartzite: implications for the kinetics of fluid redistribution and grain growth driven by interfacial energy reduction. Geofluids, vol. 1(2), pp. 73-89.

Nolan L.S.P., Angiolini L., Jadoul F., Della Porta G., Davies S.J., Banks V.J., Stephenson M.H. and Leng M.J. 2017. Sedimentary context and palaeoecology of *Gigantoproductus* shell beds in the Mississippian Eyam Limestone Formation, Derbyshire carbonate platform, central England. Proceedings of the Yorkshire Geological Society, vol. 61, pp. 239-257.

Northwood D.O. and Lewis D. 1968. Transformation of vaterite to calcite during grinding. American Mineralogist, vol. 53(11-12), pp. 2089-2092.

Ogino T., Suzuki T., Sawada K. 1987. The formation and transformation mechanism of calcium carbonate in water. Geochimica et Cosmochimica Acta, vol 51(10), pp. 2757-2767.

Paleobiology Database Fossilworks (no year). URL: http://fossilworks.org/.

Palfy J. 2003. The Pelsonian brachiopod fauna of the Balaton Highland. Geologica Hungarica, Series Palaeontologica, vol. 55, pp. 139-158.

Palmer T.J. and Wilson M.A. 2004. Calcite precipitation and dissolution of biogenic aragonite in shallow Ordovician calcite seas. Lethaia, vol. 37, pp. 417-427.

Parkinson D. and Cusack M. 2007. Stable oxygen and carbon isotopes in extant brachiopod shells: keys to deciphering ancient ocean environments. In: Kaesler R. (ed.) Treatise on Invertebrate Palaeontology, Part H. Geological Society of America, pp. 2522-2531. ISBN: 9780813731360.

Pederson C., Mavromatis V., Dietzel M., Rollion-Bard C., Nehrke G., Jöns N., Jochum K.P., Immenhauser A. 2019a. Diagenesis of mollusc aragontite and the role of fluid reservoirs. Earth and Planetary Science Letters, vol. 514, pp. 130-142.

Pederson C.L., Weiss L., Mavromatis V., Rollion-Bard C., Dietzel M., Neuser R., Immenhauser A. 2019b. Significance of fluid chemistry throughout diagenesis of aragonitic *Porites* corals – An experimental approach. The Depositional Record, vol. 5(3), pp. 592-612.

Pederson C., Mavromatis V., Dietzel M., Rollion-Bard C., Breitenbach S.F.M., Yu D., Nehrke G., Immenhauser A. 2020. Variation in the diagenetic response of aragonite archives to hydrothermal alteration. Sedimentary Geology, vol. 406, 105716.

Perrin C., Smith D.C. 2007. Earliest Steps of Diagenesis in Living Scleractinian Corals: Evidence from Ultrastructural Pattern and Raman Spectroscopy. Journal of Sedimentary Research, vol. 77(6), pp. 495-507.

Peterman Z.E., Hedge C.E., Tourtelot H.A. 1970. Isotopic composition in seawater throughout the Phanerozoic time. Geochimica et Cosmochimica Acta, vol. 34(1), pp. 105-120.

Pina C.M., Becker U., Risthaus P., Bosbach D., Putnis A. 1998. Molecular-scale mechanisms of crystal growth in barite. Nature, vol. 395, pp. 483-486.

Pingitore Jr.N.E., Eastman M.P., Sandidge M., Oden K., Freiha B. 1988. The coprecipitation of manganese(II) with calcite: an experimental study. Marine Chemistry, vol. 25(2), pp. 107-120.

Plummer L. and Busenberg E. 1982. The solubilities of calcite, aragonite and vaterite in CO_2-H_2O solutions between 0 and 90 °C, and an evaluation of the aqueous model for the system $CaCO_3$-CO_2-H_2O. Geochimica et Cosmochimica Acta, vol 46(6), pp. 1011-1040.

Poitevin P., Thébault J., Siebert V., Donnet S., Archambault P., Doré J., Chauvaud L., Lazure P. 2019. Growth Response of Arctica islandica to North Atlantic Oceanographic Conditions Since 1850. Frontiers in Marine Science, vol. 6, art. 483.

Politi Y., Arad T., Klein E., Weiner S., Addadi L. 2004. Sea urchin spine calcite forms via a transient amorphous calcium carbonate phase. Science, vol. 306(5699), pp. 1161-1164.

Politi Y., Metzler R.A., Abrecht M., Gilbert B., Wilt F.H., Sagi I., Addadi L., Weiner S., Gilbert P.U.P.A. 2008. Transformation mechanism of amorphous calcium carbonate into calcite in the sea urchin larval spicule. Proceedings of the National Academy of Sciences of the United States of America, vol. 105(45), pp. 17362-17366.

Popp B.N., Podosek F.A., Brannon J.C., Anderson T.F., Pier J. 1986. 87Sr/86Sr ratios in Permo-Carboniferous sea water from the analyses of well-reserved brachiopod shells. Geochimica et Cosmochimica Acta, vol. 50(7), pp. 1321-1328.

Price R.A. 1973. Large-scale gravitational flow of supracrustal rocks, southern Canadian Rockies. In: Gravity and Tectonics. deJong K.A. and Scholten R. (ed.), John Wiley, New York.

Putnis C.V., and Ruíz-Agado E. 2013. The mineral-water-interface: where minerals react with the environment. Elements, vol. 9, pp. 177-182.

Rabier C., Anguy Y., Cabichon G., Genthon P. 2008. Characterization of various stages of calcitization in *Porites* sp corals from uplifted reefs – Case studies from New Caledonia, Vanuatu, and Futuna (South-West Pacific). Sedimentary Geology, vol. 211, pp. 73-86.

Radha A.V. and Navrotsky A. 2013. Thermodynamics of carbonates. Reviews in Mineralogy and Geochemistry, vol. 77(1), pp. 73-121.

Raz S., Weiner S., Addadi L. 2000. Formation of high-magnesian calcites via an amorphous precursor phase: possible biological implications. Advanced Materials, vol. 12(1), pp. 38-42.

Reddy M.M., and Wang K.K. 1980. Crystallization of calcium carbonate in the presence of metal ions: I. Inhibition by magnesium ion at pH 8.8 and 25 C. Journal of Crystal Growth, vol. 50(2), pp. 470-480.

Reeder R.J. (ed.) 2018. Carbonates: mineralogy and chemistry. Vol. 11. Walter de Gruyter GmbH & Co KG.

Richards, H.G. 1962. Studies on the marine Pleistocene: The marine Pleistocene of the Americas and Europe; the marine Pleistocene molluscs of Eastern North America. Transactions of the American Philosophical Society, vol. 52(3), pp. 1-141.

Richardson C.A. 2001. Molluscs as archives of environmental change. Oceanography and Marine Biology, vol. 39, pp. 103-164.

Ritter A.-C., Mavromatis V., Dietzel M., Kwiecien O., Wiethoff F., Griesshaber E., Casella L.A., Schmahl W.W., Koelen J., Neuser R.D., Leis A., Buhl D., Niedermayr A., Breitenbach S.F.M., Bernasconi S.M., Immenhauser A. 2017. Exploring the impact of diagenesis on (isotope) geochemical and microstructural alteration features in biogenic aragonite. Sedimentology, vol. 64(5), pp. 1354-1380.

Roberts D. and Bally A. 2012. Some remarks on basins and basin classification and tectonostratigraphic megasequences. Regional Geology and Tectonics: Principles of Geologic Analysis, Elsevier, pp. 76-92.

Rodriguez-Navarro C., Jimenez-Lopez C., Rodriguez-Navarro A., Gonzalez-Muñoz M.T., Rodriguez-Gallego M. 2007. Bacterially mediated mineralization of vaterite. Geochimica et Cosmochimica Acta, vol. 71(5), pp. 1197-1213.

Rozanski K., Johnsen S.J., Schotterer U., Thompson L.G. 1997. Reconstruction of past climates from stable isotope records of palaeo-precipitation preserved in continental archives.

Ruhr-University Bochum 2017. Accessed 15.07.2020. URL: https://www.ruhr-uni-bochum.de/charon/charon2/index.html.

Ruhr-University Bochum 2020. Accessed 02.02.2021. URL: https://www.ruhr-uni-bochum.de/charon/charon2/team.html.

Ruíz-Agudo E. and Putnis C.V. 2012. Direct observations of mineral-fluid reactions using atomic force microscopy: the specific example of calcite. Mineralogical Magazine, vol. 76, pp. 227-253.

Ruíz-Agudo E., Putnis C.V., Rodriguez-Navarro C., Putnis A. 2012. Mechanism of leached layer formation during chemical weathering of silicate minerals. Geology, vol. 40, pp. 947-950.

Ruíz-Agudo E., Putnis C.V., Putnis A. 2014. Coupled dissolution and precipitation at mineral-fluid interfaces. Chemical Geology, vol. 383, pp. 132-146.

Sawada K. 1997. The mechanisms of crystallization and transformation of calcium carbonates. Pure and Applied Chemistry, vol. 69(5), pp. 921-928.

Schneider R.R., Schulz H.D., Hensen C. 2006. Marine Carbonates: Their Formation and Destruction. In: Schulz H.D., Zabel M. (eds) Marine Geochemistry. Springer, Berlin, Heidelberg.

Schroeder J.H. 1969. Experimental dissolution of calcium, magnesium, and strontium from Recent br., Houk s.D., Freyre Castro A.S., Fiebig Jiogenic carbonates; a model of diagenesis. Journal of Sedimentary Research, vol. 39(3), pp. 1057-1073.

Schöne B.R., Houk S.D., Freyre Castro A.D., Fiebig J., Oschmann W. 2005. Daily Growth Rates in Shells of *Arctica islandica*: Assessing Subseasonal Environmental Controls on a Long-lived Bivalve Mollusk. Palaios, vol. 20, pp. 78-92.

Searle M.P. and Tirrul R. 1991. Structural and thermal evolution of the Karakoram crust. Journal of the Geological Society, London, vol. 148, pp. 65-82.

Sepkoski J.J. 2002. A compendium of fossil marine animal genera. Bulletins of American paleontology, vol. 363, pp. 1-560

Serra O. 1986. Chapter 7 Information on Diagenesis (Transformation of rocks and sediments). In: Developments in Petroleum Science. Elsevier, vol. 15(B), pp. 341-336.

Shearman D.J. and Fuller J.G. 1969. Anhydrite diagenesis, calcitization, and organic laminites, Winnipegosis Formation, Middle Devonian, Saskatchewan. Bulletin of Canadian Petroleum Geology, vol. 17(4), pp. 496-525.

Smyth J.R. and Ahrens T.J. 1997. The crystal structure of calcite III. Geophysical Research Letters, vol. 24(13), pp. 1595-1598.

St. John B., Bally A.W., Klemme H.D. 1984. Sedimentary Provinces of the world – hydrocarbon productive and nonproductive. American Association of Petroleum Geologists, Catalogue 645.

Stach E., Mackowsky M.T., Teichmüller M., Taylor G.H., Chandra D., Teichmüller R. 1982. Stachs Textbook on Coal Petrology, 3rd edn. Gebrüder Borntraeger, Berlin.

Sutor D.J. and Wooley S.E. 1968. Gallstone of Unusual Composition: Calcite, Aragonite, and Vaterite. Science, vol. 159(3819), pp. 1113-1114.

Sweeney J.J. and Burnham A.K. 1990. Evaluation of a simple model of vitrinite reflectance based on chemical kinetics. American Association of Petroleum Geologists (AAPG bulletin), vol. 74(10), pp. 1559-1570.

Taddei Ruggiero E. and Annunziata G. 2002. Bioerosion on a *Terebratula scillae* population from the Lower Pleistocene of Lecce area (Southern Italy). Acta Geologica Hispanica, vol. 37(1), pp. 43-51.

Taddei Ruggiero E. and Taddei R. 2006. I brachiopodi delle Calcareniti di Marina (Lecce). Thalassia Salentina, vol. 29 suppl., pp. 301-307.

Tissot B.P. and Welte D.H. 1984. From kerogen to petroleum. In: Petroleum formation and occurrence. Springer, Berlin, Heidelberg, pp. 160-198.

Torti V. and Angiolini L. 1997. Middle Triassic Brachiopods from Val Palina, Bergamasc Alps, Italy. Rivista Italiana di Paleontologia e Stratigrafia, vol. 103(2), pp. 149-172.

Tucker M.E. and Wright V.P 1990. Chapter 7 Diagenetic processes, products and environments. In: Carbonate Sedimentology. Blackwell Science Ltd, pp. 314-362.

Van Gijzel P. 1982. Characterization and identification of kerogen and bitumen and determination of thermal maturation by means of qualitative and quantitative microscopical techniques. The Society of Economic Paleontologists and Mineralogists. How to Assess Maturation and Paleotemperatures (SC7).

Vinson M.D., Arvidson R.S., Luttge A. 2007. Kinetic inhibition of calcite (1 0 4) dissolution by aqueous manganese (II). Journal of Crystal Growth, vol. 307(1), pp. 116-125.

Wang D., Wallace A.F., De Yoreo J.J., Dove P.M. 2009. Carboxylated molecules regulate magnesium content of amorphous calcium carbonates during calcification. Proceedings of the National Academy of Sciences of the United States of America, vol. 106(51), pp. 21511-21516.

Waterhouse J.B. 2004. Permian and Triassic stratigraphy and fossils of the Himalaya in northern Nepal. Volume 6. Oamaru, New Zealand, Earthwise.

Weiner S., Levi-Kalisman Y., Raz S., Addadi L. 2003. Biologically Formed Amorphous Calcium Carbonate. Connective Tissue Research, vol. 44(1), pp. 214-218.

Weiss I.M., Tuross N., Addadi L., Weiner S. 2002. Mollusc larval shell formation: amorphous calcium carbonate is a precursor phase for aragonite. Journal of Experimental Zoology, vol. 293(5), pp. 478-491.

Williams A., Brunton C.H.C., Carlson S.J., Baker P.G., Carter J.L., Curry G.B., Dagys A.S., Gourvennec R., Hou H.F., Jin Y.G., Johnson J.G., Lee D.E., MacKinnon D.I., Pacheboeuf P.R., Smirnova T.N., Sun D.L. 2006. Treatise on Investebrate Paleontology, Part H, Brachiopoda. Volume 5: Rhynchonelliformea, pp. 1689-2320.

Wilson B.R., Wilson C., Baker P. 1993. Australian Marine Shells: Prosobranch Gastropods, part one, vol. 1. Uwa Pub.

Woodring W.P. 1982. Geology and paleontology of canal zone and adjoing parts of Panama: Description of Tertiary mollusks (Pelecypods: Propeamussiidae to Cuspidariidae). United States Geological Survey Professional Paper, vol. 306.

Wood S.V. 1848. A Monograph of the Crag Mollusca, Or Descriptions of Shells from the Middle and Upper Tertiaries of the East of England: Univalves. Pte. 1. Palaeontographical society.

World Register of Marine Species WoRMS (no year). Accessed 02.02.2021. URL: http://marinespecies.org/aphia.php?p=taxdetails&id=445340.

Xu A.-W., Antionietti M., Cölfen H., Fang Y.-P. 2006. Uniform Hexagonal Plates of Vaterite $CaCO_3$ Mesocrystals Formed by Biomimetic Mineralization. Advanced Functional Minerals, vol. 16(7), pp. 903-908.

Yamamoto K., Takizawa M., Takayanagi H., Asami R., Iryu Y. 2017. Nonlinear relationship between preservation of microstructure and geochemical composition of Pleistocene brachiopod shells from the Ryukyu Islands, southwestern Japan. Island Arc, vol. 26(6).

Zanchi A. and Gaetani M. 2011. The geology of the Karakoram range, Pakistan: the new 1:100,000 geological map of Central-Western Karakoram. Italian Journal of Geosciences (Bollettino della Società geologica italiana), vol. 130(2), pp. 161-262.

Zhang J. and Lin J. 2004. Vaterite-type $YBO_3:EU^{3+}$ crystals: Hydrothermal synthesis, morphology and photoluminescence properties. Journal of Crystal Growth, vol. 271(1-2), pp. 207-215.